

Functional role of the Synaptic Adhesion Molecule N-cadherin in Synaptic Vesicle Exo- and Endocytosis

Inaugural-Dissertation

zur Erlangung des Doktorgrades
der Mathematisch-Naturwissenschaftlichen Fakultät
der Heinrich-Heine-Universität Düsseldorf

vorgelegt von

Sushma Dagar
aus Sakatpur

Düsseldorf, October 2019

aus dem Institut für Neuro-und Sinnesphysiologie
der Heinrich-Heine-Universität Düsseldorf

Gedruckt mit der Genehmigung der
Mathematisch-Naturwissenschaftlichen Fakultät der
Heinrich-Heine-Universität Düsseldorf

Referent: Prof. Dr. K. Gottmann

Korreferent: Prof. Dr. H. Aberle

Tag der mündlichen Prüfung: 29.01.2020



तमसो मा ज्योतिर्गमय ।

From darkness, lead me to light.

- (Bhadaranyaka Upanisad 1.3.28)

Dedicated to the two most important women in my life

Mom & Grandma

Summary

Neurotransmission at chemical synapses is initiated by fusion of neurotransmitter filled synaptic vesicles to the presynaptic membrane. This fusion process called exocytosis is followed subsequently by vesicle endocytosis. The compensatory endocytosis of the synaptic vesicle membrane newly added to the presynaptic plasma membrane during exocytosis is necessary for maintaining the size and proper functioning of synapses.

N-cadherin, a Ca^{2+} dependent homophilic cell adhesion protein, is well known to play an important postsynaptic role in long-term-potential and spine stabilization. It has also been described to influence presynaptic function at mammalian CNS synapses. However, the specific roles of N-cadherin in presynaptic vesicle exo- and endocytosis remain to be clarified. In this work, the functional role of N-cadherin at cortical synapses was examined, with a keen focus on synaptic vesicle endocytosis. To understand the role of N-cadherin in synaptic vesicle cycling at cortical synapses, synaptophysin-pHluorin (SypHy) fluorescence imaging was performed in cultured mouse cortical neurons during and directly following extracellular stimulations. N-cadherin expression and function were manipulated by either a Cre mediated conditional knockout approach or by overexpression of a mutant N-cadherin protein lacking the extracellular domains (Ncad Δ E). SypHy imaging results in N-cadherin knockout neurons at room temperature showed no significant changes in vesicle exo- and endocytosis. However, synaptic vesicle endocytosis is known to be highly temperature-sensitive. Therefore, I repeated the SypHy experiments in N-cadherin knockout neurons at physiological temperature, which resulted in significantly reduced vesicle endocytosis. However, vesicle exocytosis seemed not to be affected by N-cadherin knockout. We reasoned that N-cadherin knockout might reduce the availability of readily releasable vesicles in response to single action potentials, but the stimulation paradigm used in our experimental setup might be too long-lasting and due to short-term plasticity phenomena might result in a similar total number of vesicles released. To test this hypothesis, the effect of N-cadherin knockout on exocytosis was additionally studied using a stimulation protocol with less action potentials and indeed, vesicle exocytosis was now found to be reduced.

To further investigate a potential specific role of N-cadherin in different modes of vesicle endocytosis, N-cadherin knockout cortical neurons were co-stained with FM1-43 to stain all endocytosed vesicles and with tetramethylrhodamine–dextran (TMR-dextran, 40 kDa) to stain vesicles endocytosed via bulk endocytosis. Different stimulations paradigms were used to activate the different modes of endocytosis. N-cadherin knockout neurons showed a significant reduction in clathrin-mediated endocytosis of individual vesicles. Most interestingly, FM1-43 stained puncta co-localizing with TMR-dextran were also reduced in N-cadherin knockout neurons indicating also impaired bulk endocytosis.

As a first step in investigating the molecular mechanisms of regulation of endocytosis by N-cadherin, the role of actin was tested. Jasplakinolide, an actin polymerizing drug, rescued vesicle endocytosis defects in N-cadherin knockout neurons suggesting that N-cadherin regulates endocytosis via actin. During strong vesicle release, clathrin-mediated endocytosis is too slow to compensate for the newly added presynaptic vesicle membrane. Therefore to maintain the structural and functional integrity of the synapses, neurons need an additional mode of endocytosis, and they are suggested to undergo vesicle membrane retrieval via large invaginations in the form of bulk endosomes at the peri-active zone. Since N-cadherin is also located at the peri-active zone, a role of N-cadherin in regulating bulk endocytosis was proposed. To address this hypothesis, structured illumination microscopy (SIM) imaging was performed during strong synaptic vesicle release. SIM imaging was done on immunocytochemically stained synapses and N-cadherin clusters were quantitatively analysed for their spatial relation to pre- (VGLUT1) and postsynaptic (PSD95) sites. SIM imaging results suggested that during strong vesicle release N-cadherin is recruited to the peri-active zone of the synapses largely devoid of N-cadherin prior to stimulation. These findings indicate that synapses may need additional N-cadherin during strong synaptic vesicle release to undergo efficient compensatory bulk endocytosis.

This work also investigated the influence of N-cadherin on the functioning of other synaptic cell adhesion molecules (SCAMs) like Neuroligin1 and LRRTM2. Neuroligin1 and LRRTM2 were compared for their synaptogenic activity using an overexpression approach during the differentiation of mouse cortical neurons *in vitro*.

The presynaptic vesicle cluster inducing effect of overexpressed Neuroligin1 and LRRTM2 was quantified by immunostaining VAMP2 positive puncta in the contacting axon. The vesicle cluster inducing activity of Neuroligin1 was developmentally downregulated, while LRRTM2 was found to exhibit synaptogenic activity in both immature and mature neurons. The N-cadherin dependence of the vesicle cluster inducing activities was examined by Cre mediated conditional knockout of N-cadherin from postsynaptic sites. Intriguingly, the synaptogenic effect of Neuroligin1 was found to be dependent on N-cadherin expression in immature neurons. In contrast, LRRTM2's synaptogenic effect was independent of N-cadherin expression both in immature and mature neurons.

In summary, the major finding of this work is that N-cadherin plays important regulatory roles in both vesicle exocytosis and endocytosis at central synapses under physiological temperature conditions.

Zusammenfassung

Die Neurotransmission an chemischen Synapsen wird durch Fusion von mit Neurotransmittern gefüllten synaptischen Vesikeln mit der präsynaptischen Membran initiiert. Diesem als Exozytose bezeichneten Fusionsprozess folgt eine Vesikelendozytose. Die kompensatorische Endozytose der synaptischen Vesikelmembran, die der präsynaptischen Plasmamembran während der Exozytose neu hinzugefügt wurde, ist erforderlich, um die Größe und Funktion der Synapsen aufrechtzuerhalten.

N-Cadherin, ein Ca^{2+} -abhängiges homophiles Zelladhäsionsprotein spielt bekanntermaßen eine wichtige postsynaptische Rolle bei der langfristigen Potenzierung und Stabilisierung der Synapsen. Es wird auch vermutet, dass es die präsynaptische Funktion an ZNS-Synapsen von Säugetieren beeinflusst. Die spezifischen Funktionen von N-Cadherin bei der präsynaptischen Vesikel Exo- und Endozytose müssen jedoch noch geklärt werden. In dieser Arbeit wurde die funktionelle Rolle von N-Cadherin an kortikalen Synapsen untersucht, wobei der Schwerpunkt auf der Endozytose synaptischer Vesikel lag. Um die Rolle von N-Cadherin beim Zyklus der synaptischen Vesikel an kortikalen Synapsen zu verstehen, wurde die Fluoreszenzbildgebung von Synaptophysin-pHluorin (SypHy) in kultivierten kortikalen Mausneuronen während, und direkt nach, extrazellulären Stimulationen durchgeführt. Expression und Funktion von N-Cadherin wurden entweder durch einen Cre-vermittelten konditionalen Knockout-Ansatz oder durch Überexpression eines mutierten N-Cadherin-Proteins ohne die extrazellulären Domänen (Ncad NE) manipuliert. Die Ergebnisse der SypHy-Bildgebung in N-Cadherin-Knockout-Neuronen bei Raumtemperatur zeigten keine signifikanten Veränderungen der Vesikel-Exo- und -Endozytose. Es ist jedoch bekannt, dass die Endozytose der synaptischen Vesikel sehr temperaturempfindlich ist. Daher wiederholte ich die SypHy-Experimente in N-Cadherin-Knockout-Neuronen bei physiologischer Temperatur, was zu einer signifikant verringerten Vesikelendozytose führte. Die Vesikelexozytose schien jedoch nicht durch N-Cadherin-Knockout beeinträchtigt zu werden. Ich stellte die Hypothese auf, dass ein N-Cadherin-Knockout die Verfügbarkeit leicht freisetzbarer Vesikel als Reaktion auf einzelne Aktionspotentiale verringern könnte, das in meinem Versuchsaufbau verwendete

Stimulationsparadigma jedoch möglicherweise zu langanhaltend ist und aufgrund von kurzfristigen Plastizitätsphänomenen zu einer ähnlichen Gesamtzahl der freigesetzten Vesikel führen könnte. Um diese Hypothese zu testen, wurde der Effekt von N-Cadherin-Knockout auf die Exozytose zusätzlich unter Verwendung eines Stimulationsprotokolls mit weniger Aktionspotentialen untersucht, und tatsächlich wurde nun eine Verringerung der Vesikelexozytose registriert.

Um eine mögliche spezifische Rolle von N-Cadherin bei verschiedenen Arten der Vesikelendozytose weiter zu untersuchen, wurden die kortikalen N-Cadherin-Knockout-Neuronen mit FM1-43 angefärbt, um alle endozytierten Vesikel darzustellen und simultan mit Tetramethylrhodamin-Dextran (TMR-Dextran, 40 kDa) zur Färbung von Vesikeln, die über Bulk-Endozytose endozytiert wurden. Verschiedene Stimulationsparadigmen wurden verwendet, um die verschiedenen Arten der Endozytose zu aktivieren. N-Cadherin-Knockout-Neuronen zeigten eine signifikante Reduktion der Clathrin-vermittelten Endozytose einzelner Vesikel. Am interessantesten ist, dass FM1-43-gefärbte Synapsen, die gleichzeitig mit TMR-Dextran langefärbt waren, auch bei N-Cadherin-Knockout-Neuronen reduziert waren, was auf eine beeinträchtigte Bulk-Endozytose hinweist.

Als ersten Schritt zur Untersuchung der molekularen Mechanismen der Regulation der Endozytose durch N-Cadherin wurde die Rolle von Aktin getestet. Jasplakinolid, eine aktinpolymerisierende Substanz, verbesserte Vesikelendozytosedefekte in N-Cadherin-Knockout-Neuronen, was darauf hindeutet, dass N-Cadherin die Endozytose über Aktin reguliert. Während einer starken Vesikelfreisetzung ist die Clathrin-vermittelte Endozytose zu langsam, um die neu hinzugefügte präsynaptische Vesikelmembran zu kompensieren. Um die strukturelle und funktionelle Integrität der Synapsen aufrechtzuerhalten benötigen Neuronen einen zusätzlichen Endozytosemodus, und es wird vorgeschlagen, dass sie über große Invaginationen in Form von Bulk-Endosomen an der periaktiven Zone erfolgt. Da sich N-Cadherin auch in der periaktiven Zone befindet, wurde eine Rolle von N-Cadherin bei der Regulierung der Bulk-Endozytose vermutet. Um diese Hypothese zu belegen, wurde während der Freisetzung synaptischer Vesikel eine strukturierte Beleuchtungsmikroskopie (SIM) durchgeführt. Die SIM-Bildgebung wurde an immunzytochemisch gefärbten Synapsen durchgeführt, und die N-Cadherin-Cluster

wurden quantitativ auf ihre räumliche Beziehung zu prä- (VGLUT1) und postsynaptischen (PSD95) Stellen analysiert. Die Ergebnisse der SIM-Bildgebung deuteten darauf hin, dass während einer starken Vesikelfreisetzung N-Cadherin in die periaktive Zone der Synapsen rekrutiert wird, die vor der Stimulation weitgehend frei von N-Cadherin ist. Diese Befunde deuten darauf hin, dass Synapsen während einer starken Freisetzung synaptischer Vesikel möglicherweise zusätzliches N-Cadherin benötigen, um eine effiziente kompensatorische Bulk-Endozytose durchzuführen.

Diese Arbeit untersuchte auch den Einfluss von N-Cadherin auf die Funktion anderer synaptischer Zelladhäsionsmoleküle (SCAMs) wie Neuroligin1 und LRRTM2. Neuroligin1 und LRRTM2 wurden hinsichtlich ihrer synaptogenen Aktivität unter Verwendung eines Überexpressionsansatzes während der Differenzierung von kortikalen Mausneuronen *in vitro* verglichen. Der präsynaptische Vesikelcluster induzierende Effekt von überexprimiertem Neuroligin1 und LRRTM2 wurde durch Immunfärbung von VAMP2-positiven Puncta im kontaktierenden Axon quantifiziert. Die Vesikelcluster-induzierende Aktivität von Neuroligin1 wurde in der Entwicklung herunterreguliert, während LRRTM2 sowohl in unreifen als auch in reifen Neuronen synaptogene Aktivität zeigte. Die N-Cadherin-Abhängigkeit der Vesikelcluster-induzierenden Aktivitäten wurde durch einen Cre-vermittelten konditionalen Knockout von N-Cadherin an postsynaptischen Stellen untersucht. Interessanterweise zeigte sich, dass die synaptogene Wirkung von Neuroligin1 in unreifen Neuronen von der N-Cadherin-Expression abhängt. Im Gegensatz dazu war die synaptogene Wirkung von LRRTM2 sowohl in unreifen als auch in reifen Neuronen unabhängig von der N-Cadherin-Expression.

Zusammenfassend ist das wichtigste Ergebnis dieser Arbeit, dass N-Cadherin sowohl bei der Vesikelexozytose als auch bei der Endozytose an zentralen Synapsen unter physiologischen Temperaturbedingungen eine wichtige regulatorische Rolle spielt.

1.0 INTRODUCTION	1
1.1 Presynaptic vesicle cycling at chemical synapses.....	2
1.1.1 Exocytosis of synaptic vesicles.....	4
1.1.2 Endocytosis processes	6
1.2 Cadherins	9
1.2.1 N-cadherin	9
1.2.2.1 Structure.....	9
1.2.2.1 Expression pattern	11
1.2.2.1 Presynaptic functions	13
1.2.2.1 Postsynaptic functions	13
1.3 Other cell adhesion molecules	14
1.3.1 Neuroligins	14
1.3.2 LRRTMs	17
1.4 Aims of the study.....	19
 2.0 Materials and Methods	21
2.1 Materials (Solutions and chemicals).....	21
2.1.1 Cell culture medium.....	21
2.1.2 Buffers for immunocytochemical stainings.....	22

2.1.3 Extracellular Solutions	23
2.1.4 Plasmids	25
2.1.5 Antibodies	26
2.2 Cell Culture	27
2.2.1 Cleaning of Coverslips	27
2.2.2 PO coating	27
2.2.3 Mouse	28
2.2.4 Culturing primary dissociated cortical neurons	28
2.2.5 Glial culture	29
2.2.6 Glial microisland cultures	29
2.3 Transfection of primary cortical neurons	31
2.2.1 Magnetofection™ for neuronal transfection	31
2.2.2 Conditional N-cadherin knockout	32
2.4 Fluorescence microscopy	32
2.4.1 Imaging Setup	32
2.4.1.1 Immunocytochemistry (ICC).....	33
2.4.1.2 SypHy Fluorescence Imaging	34
2.4.1.3 FM1-43 and TMR-dextran Co-staining	36
2.4.2 SIM imaging	39
2.4.2.1 ELYRA setup	40

2.4.2.2 SIM imaging of N-cadherin during neuronal differentiation and upon strong synaptic activity	40
2.5 Data analysis	41
2.5.1 SypHy signal analysis	41
2.2.2 FM1-43 and TMR-dextran signal analysis	42
2.2.3 Analysis of SIM Images	42
2.6 Statistical Analysis	43
3.0 Results	44
3.1 Functional role of N-cadherin in synaptic vesicle cycling	44
3.1.1 Recording synaptic vesicle exo- and endocytosis using SypHy in autaptic glial microisland cultures	44
3.1.2 Effects of N-cadherin knockout on vesicle exo- and endocytosis at room temperature	47
3.1.3 Effect of N-cadherin knockout on vesicle exo- and endocytosis at near physiological temperature (34°C)	49
3.1.4 Effects of NcadΔE mediated inhibition of N-cadherin functions on vesicle cycling at near physiological temperature	52
3.1.5 Effects of N-cadherin knockout on vesicle exocytosis in weak stimulation condition	54

3.2 Monitoring the functional role of N-cadherin in synaptic vesicle endocytosis using FM1-43 and tetramethylrhodamine (TMR)-dextran uptake	57
3.2.1 Stimulation and temperature dependent characteristics of FM1-43 and TMR-dextran uptake	58
3.2.2 Functional role of N-cadherin in regulating clathrin-mediated endocytosis and bulk endocytosis	61
3.2.2.1 Effects of N-cadherin knockout on clathrin-mediated endocytosis (CME)	61
3.2.2.2 Effect of N-cadherin knockout on bulk endocytosis	63
3.2.2.3 Effect of Ncad Δ E overexpression on clathrin-mediated endocytosis	65
3.2.2.5 Effect of Ncad Δ E overexpression on bulk endocytosis	67
3.3 Mechanisms of the regulation of synaptic vesicle endocytosis by N-cadherin.....	69
3.3.1 N-cadherin regulates synaptic vesicle endocytosis via actin	70
3.3.2 Mechanisms of regulation of bulk endocytosis by N-cadherin	73
3.3.2.1 Structured illumination microscopy (SIM) of N-cadherin and pre- and postsynaptic markers	74
3.3.2.2 Comparison of wide field imaging with SIM imaging	74

3.2.2.3 Spatial correlation of N-cadherin expression to pre-and postsynaptic molecules	75
3.2.2.4 Developmental changes in synaptic localization of N-cadherin	78
3.2.2.5 Effects of strong synaptic stimulation on N-cadherin synaptic localization	81
3.2.2.6 Redistribution of N-cadherin induced by strong release (K ⁺ stimulation).....	82
3.2.2.7 Spatial distribution of N-cadherin at synapses after strong K ⁺ stimulation	84
3.4 Comparative analysis of the synaptogenic activities of Neuroligin1 and LRRTM2 in cortical neurons	86
3.4.1 Synptogenic activities of Neuroligin1 and LRRTM2	87
3.4.1.1 Synptogenic activities of Neuroligin1 and LRRTM2 in immature neurons	87
3.4.1.2 Synptogenic activities of Neuroligin1 and LRRTM2 in mature neurons (12-13 DIV)	90
3.4.2 Regulation of the synptogenic properties of NLG1 and LRRTM2 by N-cadherin	93
3.4.2.1 Effect of N-cadherin knockout on the synptogenic activities of Neuroligin1 and LRRTM2 in immature neurons (6-7 DIV)	94

3.4.2.2 Effect of Ncad Δ E mediated inhibition of N-cadherin function on the synaptogenic activities of NLG1 and LRRTM2 in immature neurons (6-7 DIV)	96
3.4.2.3 Effect of N-cadherin knockout on the synaptogenic activity of LRRTM2 in mature neurons (14-15 DIV)	98

4.0 Discussion101

4.1 SybHy imaging as a tool to study vesicle exo- and endocytosis	102
4.2 Role of N-cadherin in regulating synaptic vesicle exocytosis	103
4.3 Role of N-cadherin in regulating synaptic vesicle endocytosis	104
4.4 Role of N-cadherin in regulating clathrin-mediated endocytosis	105
4.5 Role of N-cadherin in regulating activity-dependent bulk endocytosis ..	106
4.6 Regulation of vesicle endocytosis by actin	107
4.7 SIM imaging based analysis of the mechanism of regulation of endocytosis by N-cadherin	108
4.8 Regulation of the synaptogenic properties of LRRTM2 and Neuroigin1 by N-cadherin	111

5.0 References114

6.0 Appendix132

6.1 Abbreviations	132
6.2 List of figures	135
6.3 Curriculum vitae	137

6.4 Publications and conferences	137
6.4.1 Publications	137
6.4.2 Conferences	138

7.0 Acknowledgement

01-

Introduction

1. Introduction

Human brain during development is thought to contain approximately 10^{11} neurons which interact and form 10^{15} synapses in precise neuronal network to finally establish a complex brain. Synapses are specialized intercellular contacts between two different neurons. Based on of the different types of information processing, synapses can be categorized into two types: electrical and chemical synapses. At electrical synapses, the information transfer occurs in a bidirectional manner via gap junctions in the form of potential shifts between two neurons while chemical synapses transmit information unidirectionally by releasing neurotransmitter molecules at specialized asymmetric junctions. Chemical Synapses are composed of two compartments: 1) presynaptic terminal and 2) postsynaptic region. The presynaptic compartment contains neurotransmitter filled synaptic vesicles, specialized sites (active zone) and protein machinery needed for neurotransmitter release while postsynaptic region has transmitter reception apparatus in the form of special protein receptors. Action potential (electrical signal) is converted into a chemical signal by the release of neurotransmitter at presynaptic terminal. The neurotransmitters bind to the specific receptors present on the postsynaptic site and can transmit information further. For example, binding of neurotransmitter can open ion channels thus allowing the flow of ions inside the postsynaptic cell which can lead to depolarization. This finally converts the chemical signal back to electrical signal. Cell adhesion molecules (CAMs) are known to transsynaptically control the formation of these chemical synapses and more recently CAMs have been suggested to be involved in the synaptic vesicle cycling.

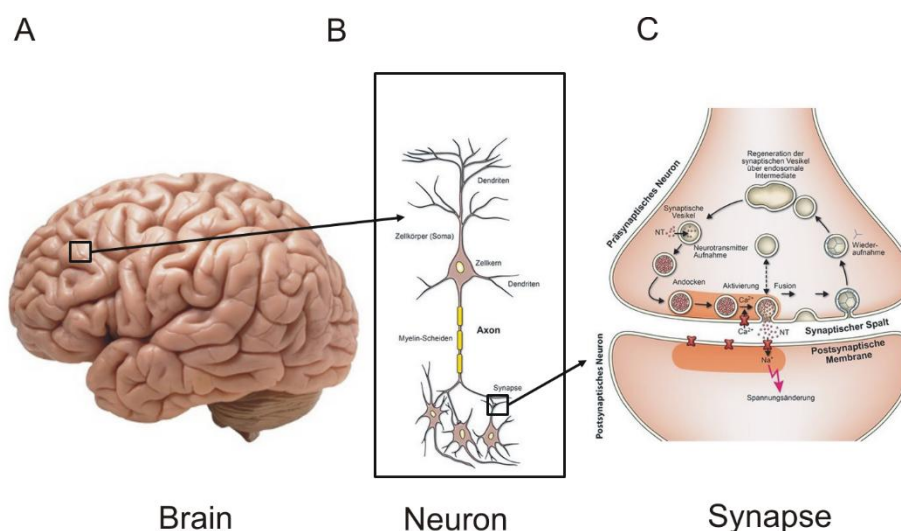


Figure 1.1 An illustration depicting an overview from brain to synapse

A diagram showing a cartoon of brain (A), neuron (B) and a synapse (C). Brain contains thousands of neurons that interact with each other at special contact sites called synapses. The information transfer occurs at synapses.

1.1 Presynaptic vesicle cycling at chemical synapses

One of the crucial features of the chemical synapses within the central nervous system (CNS) is their ability to adapt to the changes in neuronal activity. The chemical synapses process information in the form of signal transmission (Fig. 1.1). The strength of the presynaptic signal during synaptic transmission is determined by the neurotransmitter release. Neurotransmitters are packed inside the synaptic vesicles (SVs). These vesicles can be categorized into three different groups with different spatial localization and release kinetics (reviewed by Rizzoli and Betz, 2005). The first group of vesicles which are available for exocytosis upon stimulation is called readily releasable pool (RRP). The readily releasable pool (RRP) is the smallest group of vesicles that is docked and primed at the presynaptic membrane (Südhof, 2004). This pool has 5-20 vesicles and is required to be refilled by another pool, named recycling vesicle pool. The recycling pool makes up to 20 % of the total vesicle cluster and refills the RRP whenever needed (during longer stimulation, Schikorski and Stevens, 1997; for review see Harata et al., 2001). Reserve pool is the largest pool of synaptic vesicles also known as resting vesicle pool. The function of this vesicle pool has not been clarified yet. For example, during physiological conditions, this vesicle pool is very difficult to release in hippocampal neurons

(Harata et al., 2001). Therefore, these observations suggest that RRP and recycling vesicle pool are working together to maintain the functioning of the synapses during prolonged synaptic transmission. The specific function of the reserve pool is not yet clear, but it might play a key role during strong synaptic activity. During information transfer, neurotransmitter filled vesicles fuse with the presynaptic membrane via exocytosis and this extra added membrane is recycled via compensatory endocytosis. On the postsynaptic site, different types of receptors (ionotropic and metabotropic) gets modulated in response to the released neurotransmitters and further transmit information. The main focus of this work was the evaluation of the functional role of the cell adhesion molecule, N-cadherin in regulating the presynaptic vesicle cycling (exo- and endocytosis) and gain further insights into the mechanism of activity-dependent regulation of endocytosis.

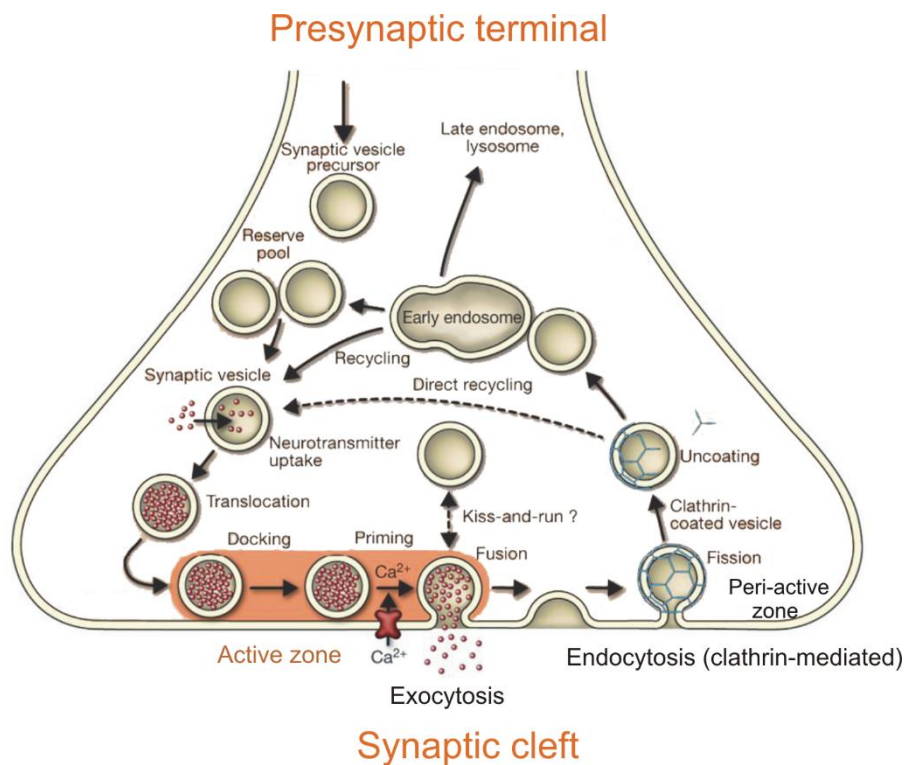


Figure 1.2 The presynaptic vesicle cycle

(modified after Jahn and Fasshauer, 2012)

Synaptic vesicle cycling in a nerve terminal. Synaptic vesicles are filled with neurotransmitter inside the presynaptic terminal. Neurotransmitter-filled vesicles get translocated to the active zone in the presynaptic plasma membrane where they undergo docking and priming. These steps enable the vesicles to be ready for release. During an action potential, influx of Ca^{2+} -ions through voltage-gated Ca^{2+} channels triggers the rapid fusion of synaptic vesicle with the membrane of the presynaptic terminal, finally leading to the release of neurotransmitters. After exocytosis, small parts of the plasma

membrane are retrieved by various modes endocytosis. One common form of endocytosis shown here is clathrin-mediated endocytosis. The newly retrieved vesicles further gets reacidified and probably joins the vesicle pool again.

1.1.1 Exocytosis of synaptic vesicles

During synaptic transmission, presynaptic terminals release neurotransmitters. Transmitter-filled vesicles undergo exocytosis at the presynaptic active zone. The active zone is a well-characterized area in the presynaptic membrane and it has clusters of proteins called cytomatrix of the active zone (CAZ). The exocytosis initiation step involves an ATP-dependent docking and priming of synaptic vesicles. This enables them to quickly respond to Ca^{2+} influx. Two protein complexes, the SNARE (soluble N-ethylmaleimide-sensitive factor (NSF) attachment protein receptor) protein complex and the SM (Sec1/Munc18-like) protein complex, are involved in this process. SNARE-complex is composed of three different SNARE proteins, synaptobrevin, syntaxin and synaptosomal-associated protein 25 (SNAP-25). SNAP-25 contributes two SNARE motifs whereas synaptobrevin and syntaxin provide one SNARE motif each, finally resulting in a four-helix bundle which is essential for Ca^{2+} triggered synaptic transmission (Söllner et al., 1993; Poirier et al., 1998; Sutton et al., 1998). The essential role of these proteins in vesicle fusion was established using neurotoxins like tetanus or botulinum. These neurotoxins are substrate specific proteases and were shown to block synaptic vesicle fusion to the presynaptic membrane by cleaving synaptobrevin (Link et al., 1992; Schiavo et al., 1992), SNAP-25 (Blasi et al., 1993a) or syntaxin (Blasi et al., 1993b). Upon Ca^{2+} -influx, the *trans*-SNARE complex connects the synaptic vesicle membrane with the presynaptic plasma membrane and enables the opening of fusion pore (Südhof and Rizo, 2011; Rizo and Xu, 2015). Synaptotagmin is a Ca^{2+} sensor which contains two Ca^{2+} ion binding sites (C2A and C2B) and is anchored at synaptic vesicle membrane via its transmembrane domain. Two Ca^{2+} ions can bind to C2A and three Ca^{2+} ions bind to C2B (Geppert et al., 1994; Ubach et al., 1998; reviewed in Südhof, 2013). Synaptotagmin also binds to syntaxin via its C2 domain (Lai et al., 2011). The binding of Ca^{2+} to synaptotagmin leads to conformational changes in the SNARE-complex and initiates the fusion of the synaptic vesicle membrane with the presynaptic membrane. Complexins are small molecules that bind to *trans*-SNARE complexes

and modulates the vesicle fusion process (McMahon et al., 1995; Südhof, 2004; Trimbuch and Rosenmund, 2016; Courtney et al., 2019). Several SM proteins like Munc-18 or Munc-13 catalyze the membrane fusion event (Verhage et al., 2000; Varoqueaux et al., 2002). Munc-13 is an active zone protein that is involved in vesicle priming (Brose et al., 1995; Augustine et al., 1999). At rest, Munc-18 blocks the assembly of SNARE-complex by interacting with syntaxin through high affinity binding. Munc-13, on the other hand, interferes with the Munc-18/syntaxin-complex by activating a protein kinase (PKC) thus promoting the open configuration of syntaxin. This syntaxin, in turn, participates in SNARE assembly (Fujita et al., 1996; Betz et al., 1997; Brose et al., 2000; Burkhardt et al., 2008; Südhof and Rothman, 2009; Hu et al., 2011). Along with SM proteins, two chaperon systems also support the SNARE-complex assembly. A trimeric complex consists of CSP α (cysteine string protein α), the heat shock protein 70 (Hsc70) and SGT (glutamate and threonine-rich protein) has been shown to be essential for proper synaptic function (Tobaben et al., 2001; Sharma et al., 2012). Synucleins are the other presynaptic chaperons that have been shown to compensate CSP α -knockout induced neurodegeneration in vertebrates (Chandra et al., 2005; Burré et al., 2010). Several other active zone proteins have also been identified which regulate the SNARE-complex formation and fusion pore opening. For example, vesicle docking and priming are facilitated by RIM (Rab3-interacting molecules) proteins. RIM proteins have also been shown to be important in the recruitment of Ca²⁺-channels (VDCCs) to the active zone (Koushika et al., 2001; Deng et al., 2011; Han et al., 2011; Kaeser et al., 2012) and can affect short-term plasticity (Castillo et al., 2002; Schoch et al., 2002; Uriu et al., 2010; Kaeser et al., 2012). RIM-binding proteins (RIM-BP) facilitate the recruitment of Ca²⁺-channel by binding with RIM (Kaeser et al., 2012). Several other proteins like α -Liprins, piccolo and bassoon are known to be important for vesicle clustering and therefore are indirectly important for proper synaptic vesicle exocytosis (Dai et al., 2006; Mukherjee et al., 2010). After the opening of the fusion pore, the two membranes completely merge, and SNARE- complexes are converted from *trans*- to *cis*- form which is finally dissociated into monomers by NSF (N-ethylmaleimide sensitive factor) and SNAPs ("soluble NSF-attachment proteins) (Pang and Südhof, 2010). SNARE-complex proteins and synaptic vesicles are recycled after the release of neurotransmitters. There are compensatory mechanisms which involve uptake of small parts of the presynaptic membrane that contain all the machinery of exocytosis

(Hayashi et al., 2008). This local recycling of synaptic vesicles and exocytosis machinery enables synapses to undergo continuous signal transmission.

1.1.2 Endocytosis processes

To maintain the availability of vesicles during synaptic transmission, synapses need a compensatory mechanism which comes in the form of synaptic vesicle endocytosis. First, the SNARE-complex is disassembled with the help of the ATPase NSF and this process is controlled by α -SNAP. Subsequently, parts of the lipid bilayer and specific vesicular molecules get endocytosed to maintain synaptic transmission. Dynamin, a GTPase pinches off the newly formed vesicles from the presynaptic membrane (Ferguson et al., 2007; Raimondi et al., 2011; Ferguson and De Camilli, 2012). Until now, four different forms of synaptic vesicle endocytosis have been described.

Kiss-and-run: Kiss-and-run is the most disputed form of endocytosis (Rizzoli and Jahn, 2007). It is thought to occur directly at the active zone. In this, synaptic vesicles do not fuse completely with the presynaptic plasma membrane, instead they form a small (~ 5 nm) fusion pore to release neurotransmitters into the synaptic cleft and then quickly get recycled (~ 1 -2sec) (Stevens and Williams, 2000).

Clathrin-mediated endocytosis: The most common and arguably the best characterized form of endocytosis is clathrin-mediated endocytosis (CME). CME is the dominant form of endocytosis during low intensity stimulation (Granseth et al., 2006) and involves the formation of clathrin coats around the presynaptic membrane invaginations (or vesicles) of a certain size (~ 40 – 50 nm in diameter) budding from the plasma membrane. These clathrin-coated vesicles are finally pinched off with the help of dynamin, a GTPase (Brodin et al., 2000; Royle and Lagnado, 2010). Clathrin coated pits were first reported in the frog neuromuscular junction (NMJ) by electron microscopy (Heuser et al., 1974). Several clathrin-adaptor proteins like AP-2, AP-180 or stonin2 helps to recruit clathrin-coat thus ensuring the recycling of vesicular membrane and its protein components (Haucke and De Camilli, 1999; Saheki and De Camilli, 2012). This form of endocytosis is generally believed to be relatively slow (τ = several to tens of seconds). The full-collapse of vesicular membrane during exocytosis may lead to lateral diffusion of synaptic vesicular proteins, thus creating a high demand for these diffused vesicular proteins to be recycled. This implies that the

vesicles are generated through this pathway at the peri-active zone (adjacent to active zone) and these vesicles either directly join the releasable vesicle pool or indirectly via early endosomes (Heuser and Reese, 1973; Hoopmann et al., 2010). The peri-active zone that surrounds the active zone and is thought to be the major site for clathrin-mediated endocytosis and bulk endocytosis (Gad et al., 1998; Roos and Kelly, 1999; Teng and Wilkinson, 2000; Hua et al., 2011).

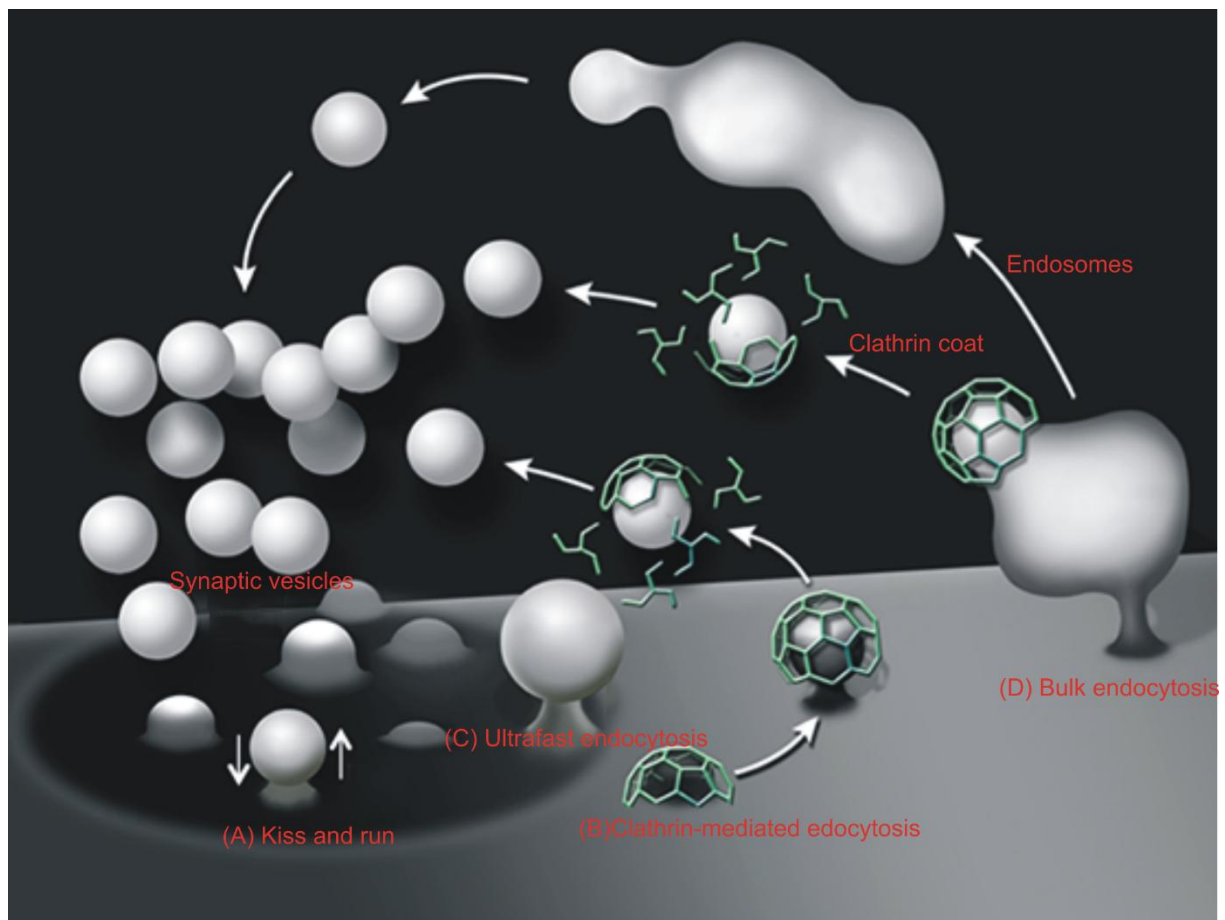


Figure 1.3 Different modes of synaptic vesicle endocytosis

(modified from Saheki and De Camilli, 2012)

Schematic diagram of synaptic vesicle cycling in the presynaptic terminals illustrating various modes of synaptic vesicle (SV) membrane retrieval. (A) Kiss-and-run, (B) clathrin-mediated endocytosis, (C) ultrafast endocytosis, and (D) bulk endocytosis.

Activity-dependent bulk endocytosis (ADBE): Another form of vesicle retrieval is bulk endocytosis. During intense neuronal activity, large pieces of presynaptic membrane is internalized in the form of endosomes (Miller and Heuser, 1984; Holt et al., 2003; Wu and Wu, 2007; Hayashi et al., 2008; Clayton and Cousin, 2009; Wenzel et al., 2012; Kittelmann et al., 2013). High intensity stimulation leads to increased calcium concentration in the synaptic terminal. This results in the fusion of a lot of synaptic vesicles with the presynaptic membrane, thus increasing the area of the presynaptic terminal. Increased calcium activates a phosphatase, calcineurin. Calcineurin dephosphorylates and thus, in turn, activates many endocytic proteins including Syndapin-I and dynamin (Cheung and Cousin, 2013). Bulk endocytosis may also occur in the absence of dynamin (Wu et al., 2014), suggesting the existence of multiple pathways for the formation of large endosomes (for ADBE).

Ultrafast endocytosis: Recently, a new pathway for rapid vesicle recovery has been identified using an innovative electron microscopy technique in *C. elegans* motor neurons (Watanabe et al., 2013a) and mouse hippocampal neurons (Watanabe et al., 2013b; Brockmann and Rosenmund, 2016). In the flash-and-freeze approach, synaptic transmission is induced by stimulating neurons using single optogenetic stimulation and the subsequent membrane dynamics are captured by freezing neurons at defined time intervals (Watanabe S, 2016). After a single stimulus, the presynaptic vesicle membrane undergoes recovery at the sites lateral to the fusion sites within 100 ms. This endocytic pathway is independent of clathrin but clathrin is needed later to generate individual synaptic vesicles from endosomes (Watanabe et al., 2013a; b; Watanabe et al., 2014). The molecular mechanism of ultrafast endocytosis is not well understood due to its recent discovery. However, initial studies have described a few key factors. First, calcium influx itself is not sufficient but the fusion of SVs to the presynaptic membrane is the pre-requisite to induce ultrafast endocytosis (Watanabe et al., 2013a, b). Second, filamentous actin, F-actin, is needed for initializing the membrane curvature (Watanabe et al., 2013b). Third, the dynamin function is required to pinch off the endocytic vesicles formed during this pathway (Watanabe et al., 2013a, b). Fourth, ultrafast endocytosis takes place at physiological temperature and at the lateral site to the active zone (typically within 200 nm) (Watanabe and Boucrot, 2017). Delvendahl et al., 2016 have also reported a temperature-sensitive, clathrin-independent endocytosis activated by a single

action potential at hippocampal mossy fiber synapses. This endocytic pathway is rapid ($\tau = \sim 1$ s) and is sensitive to actin perturbation thus likely represents ultrafast endocytosis (Delvendahl et al., 2016). A more recent study showed that the endocytic processes happening after 10 Hz stimulation are formin-dependent and are clathrin-independent. This paper used rapid acid quenching of pHluorins to suggest that all these actin-dependent endocytosis events occur on multiple time-scales ($\tau_{\text{fast}} = 760$ ms and $\tau_{\text{slow}} = 26$ s; Soykan et al., 2017; Gan and Watanabe 2018, review).

1.2 Cadherins

Cadherins (Ca^{2+} -dependent adhesion molecule) are one of the most prominent synaptic cell adhesion molecule family present at the synapses (Arikkath and Reichardt, 2008). This synaptic adhesion molecules family consists of three different groups: classic cadherins (e.g. N-, R- and E-cadherin), protocadherins and the cadherin-related neuronal receptors (CNR). The most common classical cadherin in the mammalian CNS is neuronal (N)-cadherin. N-cadherin proteins are present at both sides of the synapses, the pre- and postsynaptic site and bind to each other via homophilic interactions within the synaptic cleft. The homophilic interactions of N-cadherin are known to be Ca^{2+} -dependent (for review see Pokutta and Weis, 2007; Brigidi and Bamji, 2011).

1.2.1 N-cadherin

1.2.1.1 Structure

Neural (N)-cadherin is the most abundantly expressed classic cadherin in the brain representing a type I cadherin. N-cadherin has 5 extracellular tandemly repeated domains (EC1-EC5) with 110 amino acids each, a single-pass transmembrane domain and a cytoplasmic tail (100 amino acids) (Hata et al., 1988). The extracellular domains are proposed to play distinct roles. The first two domains (EC1 and EC2) were suggested to be important for adhesive properties, while the other domains are suggested to help in promoting adhesive efficiency by positioning the essential domains relatively far from the cell surface (Shan et al., 2004). Extracellular (EC) domain contains special motifs with an amino acid sequence of histamine, alanine and valine (HAV motif). HAV motif has been proposed to be important for homophilic interactions of N-cadherin (Yap et al., 1997; Williams et al., 2000; Pokutta and Weis, 2007; Brasch et al., 2012). The extracellular domains are separated by Ca^{2+} -binding

sites that enable homophilic interactions in *cis*- and *trans*- (Nagar et al., 1996; Patel et al., 2006; Pokutta and Weis, 2007; Brasch et al., 2012). For *cis*- interactions, EC1 domain of one N-cadherin interacts with EC2 domain of another N-cadherin on the same side of the synapse whereas for *trans*- interaction, EC1 domain of one N-cadherin binds with EC1 domain of another N-cadherin on the other side of the synapses (Pokutta and Weis, 2007). *Cis*- interactions are known to be stronger as compared to weak *trans*- interactions. Therefore, N-cadherin is suggested to form *cis*- dimers first and then have *trans*- interactions (Shapiro et al., 1995; Brasch et al., 2012). On the C-terminal side, N-cadherin has been shown to interact with actin cytoskeleton via beta-catenin and alpha-catenin (Drees et al., 2005; Brigidi and Bamji, 2011). N-cadherin is synthesized from a precursor protein, Pro-N-cadherin (Ozawa and Kemler 1990).

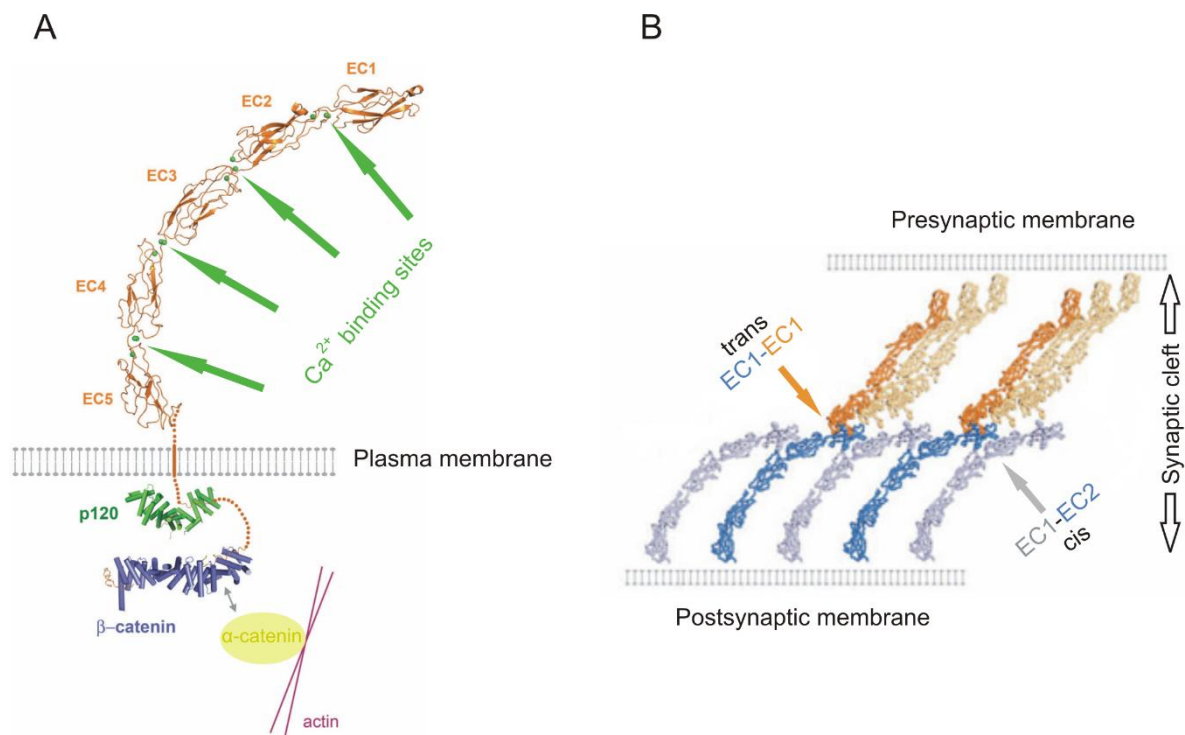


Figure 1.4 Homophilic adhesion of classical cadherins

(modified after Brasch et al., 2012)

Complete structure of classical cadherins. Cadherins contain 5 extracellular domains (EC1-EC5). These extracellular domains have Ca²⁺ binding sites which are important for its homophilic interactions. The cytoplasmic domain have binding sites for p120 and β-catenin. Interaction of c-terminal domain of β-catenin with α-catenin connects cadherins to the actin-cytoskeleton. (B) *Cis*- and *trans*- interactions of cadherin. Cadherin achieve extracellular adhesion by two types of interactions. *Cis*- interaction is mediated by EC1-EC2 binding while *trans*- interaction happens via EC1-EC1 binding.

1.2.1.2 Expression patterns

In vivo, N-cadherin has been shown to be expressed in specific patterns, indicating its possible role in target recognition via axon outgrowth and the establishment of functional connections (Redies et al., 1993; Obst-Pernberg et al., 2001). Jontes et al., 2004 showed for the first time that N-cadherin is expressed very early at nascent synapses by co-localization with synaptic markers and suggested the potential role of extracellular domains in N-cadherin trafficking and targeting. *In vitro*, N-cadherin is expressed at both excitatory and inhibitory synapses in young hippocampal neurons but later it is found to be localized only at mature excitatory synapses (Benson and Tanaka, 1998). Thus during development, N-cadherin disappears from inhibitory synapses suggesting the presence (possibility) of another member of the cadherin family at inhibitory synapses. Additionally, N-cadherin is also found to undergo changes in its synaptic localization within excitatory synapses during development. More specifically, N-cadherin is shown to be present in the centre of the active zone at immature synapses (*in vivo* & *in vitro*) and is suggested to move to the perisynaptic zone upon synapse maturation (Elste and Benson, 2006). Uchida et al., 1996 showed that in the mouse brain, N-cadherin along with α N- and β -catenin is localized at the border of neurotransmitter release site (active zone).

N-cadherin knockout mouse is lethal as the mutant embryos die around embryonic day 10 because of dramatic abnormalities in the development of heart tissue (Radice et al., 1997). Therefore, various alternative approaches have been developed to investigate the role of N-cadherin at synapses. These approaches includes a pan-cadherin block of function by either expressing a dominant-negative truncated cadherin (Togashi et al., 2002; Andreyeva et al., 2012), by application of antibodies and peptides that block the interaction of extracellular N-cadherin domains (Tang et al., 1998; Bozdagi et al., 2000), embryonic stem cells (ES) derived N-cadherin knockout neurons (Jüngling et al., 2006; Stan et al., 2010), and cre-mediated conditional knockout approach (Bozdagi et al., 2010; van Stegen et al., 2017).

Interfering with the N-cadherin function is known to affect both pre- and postsynaptic sites. On the presynaptic site, interfering with N-cadherin led to the reduction in the presynaptic vesicle accumulation in immature neurons and decreased vesicle cycling

in both immature as well as mature hippocampal neurons (Togashi et al., 2002; Stan et al., 2010).

A conditional knockout of N-cadherin in the cerebral cortex resulted in the random organization of cytoarchitecture or failure in the proper organization of the cytoarchitecture (Kadowaki et al., 2007). N-cadherin was proposed to play an important role in axon guidance towards the selection of appropriate synaptic partners enabling the formation of specific connections. Strong homophilic binding properties of N-cadherin seems to be important for this. Huntley and Benson, 1999 demonstrated that blocking N-cadherin by specific antibodies resulted in the abnormal growth of thalamic fibers into the cortical layer II of the somatosensory cortex. These fibers are known to physiologically grow until (terminate in) layer IV of the somatosensory cortex.

NMDA (N-methyl-D-aspartate) receptor (NMDAR) activity has been shown to control the endocytosis of N-cadherin. More precisely, the rate of endocytosis of N-cadherin is suggested to be reduced upon activation of NMDA receptors (NMDAR), which in turn results in increased levels of membrane-associated N-cadherin (Tai et al., 2007). In contrast, Marambaud et al., 2003 described an activity-driven reduction in N-cadherin adhesion. This study showed that NMDA receptor activity resulted in enhancement of presenilin-1 (PS1) and presenilin-1, in turn, cleaves N-cadherin at its transmembrane domain to generate Ncad/CTF2 cytoplasmic fragment (Marambaud et al., 2003). ADAM10 is also known to cleave N-cadherin and generate Ncad/CTF1 membrane fragment (Reiss et al., 2005; Uemura et al., 2006). Ncad/CTF1 fragment is subsequently cleaved by PS1 to produce Ncad/CTF2 (Uemura et al., 2006). N-cadherin is known to dimerize in response to high K^+ induced depolarization and attain protease-resistant properties indicating enhanced cadherin-mediated intercellular adhesion. This data suggest that N-cadherin mediated synaptic adhesion is dynamically modulated by synaptic activity (Tanaka et al., 2000). In line with the above results, Yam et al., 2013 showed that transient synaptic stimulation modulates N-cadherin localization within the synapse.

1.2.1.3 Presynaptic functions

N-cadherin has been proposed to play a crucial structural role in the organization of presynaptic compartment like presynaptic vesicle clustering (Murase et al., 2002; Togashi et al., 2002; Bamji et al., 2003; Bozdagi et al., 2004; Stan et al., 2010). More recent studies have shown the functional cooperation of N-cadherin with other cell adhesion molecules. N-cadherin postsynaptically recruited Neuroligin1 via S-SCAM (synaptic scaffolding molecule), and Neuroligin1 in turn, enhanced vesicle clustering, thereby regulating vesicle clustering effect of Neuroligin1 at the presynaptic site (Stan et al., 2010; Aiga et al., 2011; van Stegen et al., 2017). N-cadherin also plays a crucial role in the functionality of mature synapses. Synaptic functions were examined after interfering with postsynaptic N-cadherin and the results revealed reduced presynaptic release (Jüngling et al., 2006; Vitureira et al., 2011). N-cadherin has also been suggested to play an important role in synaptic plasticity. In mouse embryonic stem (ES) cells derived N-cadherin null neurons, the short-term plasticity at glutamatergic synapses were dramatically altered (Jüngling et al., 2006). Overexpression of N-cadherin has been shown to enhance vesicle exo- and endocytosis in cultured cortical neurons. Most intriguingly, enhancement of synaptic vesicle endocytosis by N-cadherin was shown to be release dependent at room temperature (van Stegen et al., 2017).

1.2.1.4 Postsynaptic functions

Postsynaptically, N-cadherin has been shown to be involved in spine formation. Knockdown of N-cadherin resulted in decreased spine number and formation of filopodia-like dendritic spines demonstrating its pivotal role in spine formation (Togashi et al., 2002; Saglietti et al., 2007). Moreover, N-cadherin has been shown to be required for synapse stabilization and functional maturation (Bozdagi et al., 2004). N-cadherin knockout from adult mice led to a significant impairment in LTP persistence, but not induction. Short term disruption of N-cadherin function using blocking peptide is shown to enhance spine motility and reduced spine length (Mysore et al., 2007).

N-cadherin is synthesized during the late phase of LTP and newly formed synapses recruit N-cadherin where it may function initially as a synapse stabilizer and later help in functional maturity (Bozdagi et al., 2000). N-cadherin couples spine structural modification with LTP. The deletion of N-cadherin has a profound effect on the

stability of coordinated spine enlargement and LTP at mature CA1 synapses (Bozdagi et al., 2010). Conditional knockout of N-cadherin from the forebrain and Hippocampus of adult mice resulted in reduced beta-catenin levels and GluA1 and PSD were also diminished. Loss of N-cadherin also led to an increase in inhibitory synapses and decreased the severity of hippocampal seizures. Knockout mice showed impaired spatial memory (hippocampal-dependent memory of spatial episodes, Nikitczuk et al., 2014). N-cadherin has also been shown to regulate synapses in a negative manner. A short term mis-match expression of N-cadherin selectively on the postsynaptic site resulted in impaired synaptic function while long term expression of N-cadherin on the postsynaptic site led to axon retraction and synapse elimination (Pielarski et al., 2013). Bian et al., 2015 showed the role of cadherin/catenin cell adhesion system in coordinated spine pruning and maturation in the mouse somatosensory cortex.

1.3 Other cell adhesion molecules

Neuroligins and LRRTMs are postsynaptic adhesion molecule and both are known to interact presynaptically with Neurexins. Recent studies have identified the role of N-cadherin in regulating the functions of Neuroigin1 (Stan et al., 2010; Aiga et al., 2011). Since LRRTM2 and Neuroigin1 have similar functions (synaptogenic, de Wit et al., 2009; Ko et al., 2009) and bind with Neurexins, I asked whether LRRTM2 function is also regulated by N-cadherin.

1.3.1 Neuroligins

Neuroligins are heterophilic cell adhesion molecules located on the postsynaptic site and are known to interact with presynaptic neurexins (Ichtchenko et al., 1995). Structurally, Neuroligins have a single extracellular domain, a transmembrane region, and a cytoplasmic part. Neuroligins are type 1 transmembrane proteins and there are four Neuroigin genes in mouse, Neuroigin1-4 (NLG1-4) (Ichtchenko et al., 1996). Neuroigin1 is well known to be expressed exclusively at excitatory synapses (Song et al., 1999) while Neuroigin2 is localized to inhibitory synapses (Varoqueaux et al., 2004). Neuroigin3 is shown to be present both at excitatory glutamatergic synapses and inhibitory GABAergic synapses (Budreck and Scheiffele, 2007). NLG4 is expressed at relatively low levels in the adult mouse brain.

N-terminal side of Neuroligin1 can bind to various isoforms of neurexins but the most common binding partners are β -neurexins (irrespective of the insert at splice site 4). Neuroligin1/ β -neurexin interactions are Ca^{2+} -dependent and have been shown to be involved in synapse formation and synapse maturation in central nervous system. Cytoplasmic part of Neuroligins have PDZ-domain recognition motif and can bind to several proteins in the postsynaptic terminal like PSD9 or S-SCAM (Irie et al., 1997; Chen et al., 2000).

Scheiffele et al., 2000 showed that postsynaptic overexpression of Neuroligin1 in non-neuronal cells induced presynaptic vesicle clustering in the contacting axons and this effect disappeared when soluble neurexins were added to block the neuroligin/neurexin interaction (Scheiffele et al., 2000). Overexpression of Neuroligins in cultured neurons leads to an increase in the synapse number, confirming the synaptogenic activity for Neuroligins (Chih et al., 2005; Boucard *et al*, 2005). Functionally, NLG1 overexpression has been shown to increase mEPSC and mIPSC frequency indicating an increase in the number of functional synapses (Prange et al., 2004). Other studies have confirmed these findings and extended these observations in other cultures systems for various Neuroligin isoforms (Chih et al., 2005; Levinson and El-Husseini, 2005; Varoqueaux et al., 2006; Wittenmayer et al., 2009). Knock-out mice for neuroligin1-3(triple knockout) die within 24 hour after birth possibly due to respiratory failure. Loss of NLG1-3 results in a dramatic decrease in spontaneous inhibitory and excitatory activities without having any effect on the total number of synapses (Varoqueaux et al., 2006). Different neuroligins are found to be involved in specifying and validating different types of synapses via an activity-dependent mechanism (Chubykin et al., 2007). Calmodulin kinase II (CaMKII) has been shown to phosphorylate the intracellular domain (T739) of Neuroligin1 in response to synaptic activity in cultured neurons and sensory experiences in vivo (Bemben et al., 2014). Conditional genetic deletion of Neuroligins strongly impaired synapse functions without affecting the synapse number. This impairment in synaptic function was suggested to be caused by the decrease in the synaptic levels of neurotransmitter receptors (Chanda et al., 2017).

Neuroligin1 has also been found to be accumulated by N-cadherin via a linkage through the scaffolding molecule S-SCAM leading to presynaptic vesicle clustering (Stan et al., 2010, Aiga et al., 2011). To induce synapse formation in contacting

neurons, Neuroligin1 seems to also work in a neurexin-independent way (Ko et al., 2009). In the recent paper from our lab, we showed the functional role of Neuroligin1 in synaptic vesicle exocytosis at mature synapses (van Stegen et al., 2017). Mutant alleles of *Drosophila* Neuroligin 1 (DNlg1) lead to the reduced synaptic transmission at neuromuscular junctions (NMJs) and bouton number is severely reduced while an increase in DNlg1 triggers the postsynaptic differentiation at glutamatergic NMJs (Banovic et al., 2010).

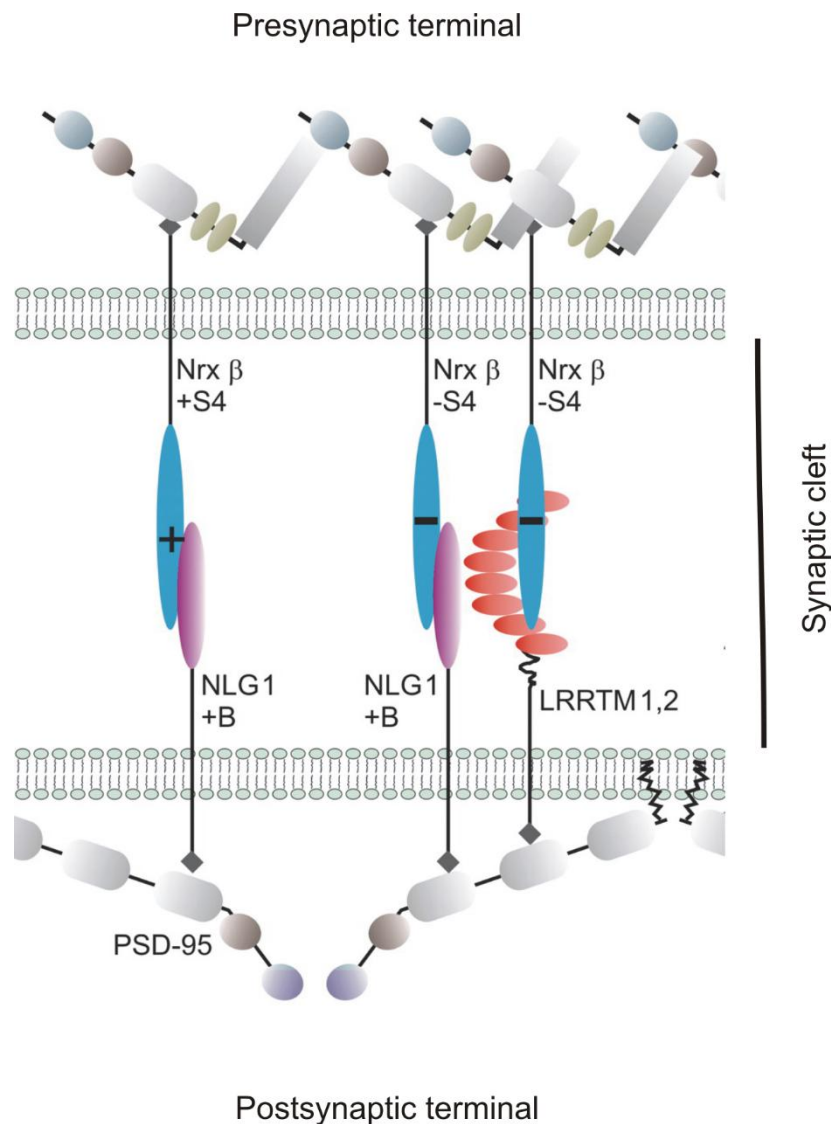


Figure 1.5 Model of Neuroligin1, LRRTM2 and Neurexin interactions at central synapses

(modified after Siddiqui et al., 2010)

Diagram of a synapse containing the postsynaptic LRRTMs (LRRTM1 and LRRTM2), Neuroligin1 (NLG1+B), and presynaptic Neurexins. Neurexins have two common splice variants, α - and β -Neurexins. Neuroligin1 interacts with β -neurexins (irrespective of the insert at splice site 4) while LRRTM2 interacts with β -neurexins which is lacking the splice site #4 insert (neurexin-1 β -S4).

LRRTM2 can also interact with α -neurexin-1 β -S4 (not shown here). LRRTMs and NLG1 also interact with PSD-95 and related scaffold proteins via different PDZ domains.

1.3.2 Leucine-rich repeat transmembrane proteins (LRRTMs)

LRRTMs were initially identified using bioinformatics tools. In vertebrates, four LRRTM (LRRTM1-4) genes are found. They are primarily localized to the postsynaptic site of excitatory synapses. Structurally, they comprise of the extracellular region with 10 LRRs domains, a single transmembrane region, and a short cytoplasmic domain. The cytoplasmic tail has a type I PDZ-binding motif that has been shown to interact with postsynaptic scaffolding protein, PSD-95 in heterologous cells (Lauren et al., 2003; de Wit et al., 2009; Linhoff et al., 2009).

All the LRRTMs are highly expressed in the developing and adult brain. They show strikingly different neural expression patterns and have overlapping distributions in various brain regions (Lauren et al., 2003). For example, LRRTM1 is expressed in the olfactory bulb and cortex whereas LRRTM2 is expressed mainly in the deep layers of the cortex.

A recent unbiased expression screen identified the synaptogenic properties of LRRTM proteins in artificial synapse formation assays (Linhoff et al., 2009). All the LRRTM proteins display synaptogenic properties in these assays, although LRRTM2 is the strongest (de Wit et al., 2009; Ko et al., 2009; Linhoff et al., 2009; Ko J, 2012) and is specifically localized in excitatory synapses (Linhoff et al., 2009). Overexpression of LRRTM1 or LRRTM2 specifically increases the excitatory synapse number and they are known to interact with neurexins on the presynaptic side. LRRTM2 only interacts with neurexins lacking an insert in splice site #4 (neurexin-1 β -S4) and forms a trans-synaptic cell adhesion complex (Ko et al., 2009; Siddiqui et al., 2010). LRRTM2 has been shown to interact with PSD-95 and recruits glutamate receptors to the postsynaptic site. The knockdown of LRRTM2 led to the decreased surface density of AMPA (α -amino-3-hydroxy-5-methyl-4-isoxazole propionic acid) and NMDA (N-methyl-D-aspartate) receptor subunits. Functionally, loss of LRRTM2 resulted in reduced strength of AMPA and NMDA receptor-mediated postsynaptic currents in hippocampal cultured neurons (de Wit et al., 2009). shRNA-mediated knockdown (KD) of both LRRTM1 and LRRTM2 at P0 selectively reduced AMPA receptor-mediated postsynaptic currents without affecting NMDA receptor-mediated

synaptic currents while it did not have any effect when the KD was induced at P21. However, LTP was blocked in CA1 pyramidal neurons of both newborn and adult mice after KD of LRRTM1 and LRRTM2 (Soler-Llavina et al., 2011, Soler-Llavina et al., 2013). Bhourri et al., 2018 recently generated double conditional knockout mice of LRRTM1 and LRRTM2 in hippocampal CA1 pyramidal neurons. Long-term potentiation (LTP) was dramatically impaired in double knockout neurons and selective LRRTM2 expression was able to rescue this effect, but not LRRTM4. To rescue LTP, its presynaptic interaction with Neurexin is required. KO of both these proteins also resulted in reduced AMPA receptor-mediated synaptic currents. All these findings suggest that both LRRTM1 and LRRTM2 help in stabilizing synaptic AMPA receptors at mature hippocampal spines during synaptic transmission and LTP (Bhourri et al., 2018).

LRRTM1 gene has been reported to be associated with left-handedness and schizophrenia and knockout mice demonstrated impaired behaviours, reduced size of hippocampus and deficits in synapse density (Francks et al., 2007; Takashima et al., 2011).

1.3 Aims of the study

The major aim of this work was to evaluate the functional roles of the synaptic adhesion protein N-cadherin in synaptic vesicle exo- and endocytosis and to elucidate the mechanisms involved in the regulation of endocytosis. This work was divided into three parts.

The first part of this study focused on the functional roles of N-cadherin in synaptic vesicle cycling. A previous study from our lab had indicated a potential role of N-cadherin in activity induced compensatory endocytosis (van Stegen et al., 2017). However, this paper used in part an N-cadherin overexpression strategy and the experiments were done only at room temperature. Several reports from other labs also indirectly indicated a role of N-cadherin in vesicle cycling (Togashi et al., 2002; Bozdagi et al., 2004; Jüngling et al., 2006; Vitureira et al., 2011). These papers either used the activity induced uptake of FM dyes or electrophysiological measurements, which both do not allow for a monitoring of the time course of endocytosis. Therefore a differential analysis of the exo- and endocytosis effects of N-cadherin in differentiated neurons still needed to be done. To study the functional roles of N-cadherin, I used a conditional knockout approach (based on Cre transfection), because constitutive N-cadherin knockout mice are lethal and die at E10 due to a failure of heart development. Synaptophysin-pHluorin (SypHy) imaging was used to quantitatively study synaptic vesicle cycling. SypHy imaging is based on fluorescence changes induced by changes in the intravesicular pH during vesicle cycling. It provides a direct measurement of both vesicle exocytosis and vesicle endocytosis + reacidification upon electrical field stimulations within one experiment. DsRed2 was co-expressed to visualize transfected neurons. In an additional experimental approach, N-cadherin functions were inhibited by overexpressing a dominant negative construct (Ncad Δ E). Autaptic cultures of mouse cortical neurons enabled the deletion of N-cadherin from both pre- and postsynaptic sites.

Potential specific roles of N-cadherin in different modes of synaptic vesicle endocytosis were further elaborated. At central synapses, clathrin-mediated endocytosis (CME) is the main mode of vesicle retrieval during single vesicle release. In addition, during strong synaptic release synapses undergo bulk endocytosis to compensate for the increase in presynaptic membrane area. By inducing activity-

dependent uptake of FM dyes and TMR-dextran, clathrin-mediated endocytosis (CME) and bulk endocytosis were examined upon conditional knockout of N-cadherin.

The second part of this work addressed the molecular mechanisms involved in N-cadherin dependent regulation of endocytosis. N-cadherin is known to influence actin organization via β - and α -catenins. Involvement of actin in the regulation of synaptic vesicle endocytosis was examined using SypHy imaging. Jasplakinolide, an actin polymerizing drug was used to rescue the effects of conditional N-cadherin knockout. To specifically understand the mechanisms of bulk endocytosis, intense synaptic activity was induced by high $[K^+]$ stimulation and N-cadherin was immunostained. Structured illumination microscopy (SIM) imaging was performed to analyse the changes in N-cadherin localization upon intense synaptic activity. The spatial distribution of N-cadherin was also analysed in relation to pre- and postsynaptic molecules at synapses.

The final part of this study was focused on the comparative analysis of synaptogenic activities of two postsynaptic adhesion molecules, Neuroligin1 and LRRTM2. The presynaptic receptors for both, Neuroligin1 and LRRTM2 are Neurexins. Neuroligin1 is well known to induce synaptic vesicle clusters and this synaptogenic effect is controlled by N-cadherin (Stan et al., 2010; Aiga et al., 2011). However, it was not known whether N-cadherin also regulates the synaptogenic activity of LRRTM2. To study this, the synaptogenic properties of both, Neuroligin1 and LRRTM2 were compared in cultured cortical neurons using an overexpression strategy. Synaptogenic effects were studied by immunostaining for the synaptic vesicle protein VAMP2 to quantify presynaptic vesicle clustering effects. A potential N-cadherin dependence was evaluated by Cre mediated conditional N-cadherin knockout and by inhibiting N-cadherin functions using a dominant negative construct (Ncad Δ E).

In summary, this work describes detailed analyses of the functional roles of N-cadherin in synaptic vesicle exo- and endocytosis and provides potential clues for the molecular mechanisms involved.

02-

**Materials
&
Methods**

2. Materials and Methods

2.1 Materials (Solutions and chemicals)

2.1.1 Cell culture medium

Basal Medium Eagle (BME medium) Gibco; Cat. No. 1010-02

+ FBS	50 ml	Gibco; Cat. No. 10500-64
+ L-Glutamin (200 mM)	5 ml	Gibco; Cat. No. 25030-24
+ Glucose (40%)	3 ml	J.T. Baker; Cat. No.0114
+ Insulin-Transferrin- Selenium solution	5 ml	Gibco; Cat. No. 51300-44
+ Penicillin- Steptomycin solution	5 ml	Gibco; Cat. No. 15140-22

NeuroBasal (NB) medium Gibco; Cat. No. 21103-049

+ B27- Supplement 50x	10 ml	Gibco; Cat. No. 17504-36
+ GlutaMAX-I-Supplement	2.5 ml	Gibco; Cat. No. 35050-38
+ Pencillin-Streptomycin solution 100X	5 ml	Gibco; Cat. No. 15140-122

Following solutions were also used for culturing cells:

PBS Dulbecco's phosphate buffered saline (PBS+/+)	Gibco; Cat. No. 14040-091
PBS Dulbecco's phosphate buffered saline without Ca ²⁺ , Mg ²⁺ (PBS-/-)	Gibco; Cat. No. 14190-094
1x Trypsin-EDTA (0.05%)	Gibco; Cat. No. 25300-054
Trypsin (0.25%)	Gibco; Cat. No. 25050-014

Poly-L-Ornithine (PO)	1mg/ml	Sigma-Aldrich; Cat. No. P-655
Boric acid	0.15 M	Sigma-Aldrich; Cat. No.083K0055

Solutions used for transfection

NeuroMag	OZ Biosciences; Cat. No. NM51000
----------	----------------------------------

2.1.2 Buffers for immunocytochemical stainings

Blocking buffer I

FBS (heat-inactivated)	10%	Gibco; Cat No. 10500-064
Sucrose	5%	Merck; Cat No. 1076871000
BSA	2%	Sigma-Aldrich; Cat. No. A4919
TritonX100	0.3%	Sigma-Aldrich; Cat. No.X100
...in PBS Dulbecco's phosphate-buffered saline (PBS+/+)	82.7%	Gibco; Cat. No. 14040-091

Blocking buffer II

Equivalent to blocking buffer I but without FBS. Equal replacement of FBS with PBS+/+

4%PFA

2.1.3 Extracellular Solutions

Solutions for Synaptophysin-pHluorin (SypHy) experiments

Extracellular solutions (SypHy)

NaCl	136 mM	J.T.Baker; Cat. No. 0278
KCl	2.5 mM	Sigma-Aldrich; Cat. No. 31248
CaCl ₂	2 mM	Sigma-Aldrich; Cat. No. 12074
MgCl ₂	1.3 mM	Sigma-Aldrich; Cat. No. 63068
HEPE	10 mM	AppliChem; Cat. No.A1069,0100
Glucose	10 mM	Merck; Cat. No. 1083370250
DL-AP5	50 µM	Tocris; Cat. No. 0105
DNQX	10 µM	Tocris; Cat. No. 0189

NH₄Cl solution (SypHy)

NaCl	36 mM	J.T.Baker; Cat. No. 0278
KCl	2.5 mM	Sigma-Aldrich; Cat. No. 31248
CaCl ₂	2 mM	Sigma-Aldrich; Cat. No. 12074
MgCl ₂	1.3 mM	Sigma-Aldrich; Cat. No. 63068
HEPES	10 mM	AppliChem; Cat. No. A 1069,0100
Glucose	10 mM	Merck; Cat. No. 1083370250
NH ₄ Cl	100 mM	Sigma-Aldrich; Cat. No. A0171-100

Solutions for FM & TMR-dextran experiments

NaCl	136 mM	J.T.Baker; Cat. No. 0278
KCl	2.5 mM	Sigma-Aldrich; Cat. No. 31248
CaCl ₂	2 mM	Sigma-Aldrich; Cat. No. 12074
MgCl ₂	1.3 mM	Sigma-Aldrich; Cat. No. 63068
HEPES	10 mM	AppliChem; Cat. No. A 1069,0100
Glucose	10 mM	Merck; Cat. No. 1083370250
DL-AP5	50 µM	Tocris; Cat. No. 0105
DNQX	10 µM	Tocris; Cat. No. 0189
FM1-43	10 µM	Molecular Probes; Cat. No.T-3163
ADVASEP	1 mM	Sigma-Aldrich; Cat. No.A3723
Tetramethylrhodamine-dextran555(TMR-dextran, 40 kDa)	50 µM	Invitrogen; Cat. No. D-1842

Solutions for SIM experiments**Normal extracellular solution**

NaCl	136 mM	J.T.Baker; Cat. No. 0278
KCl	2.5 mM	Sigma-Aldrich; Cat. No. 31248
CaCl ₂	2 mM	Sigma-Aldrich; Cat. No. 12074
MgCl ₂	1.3 mM	Sigma-Aldrich; Cat. No. 63068
HEPES	10 mM	AppliChem; Cat. No. A 1069,0100
Glucose	10 mM	Merck; Cat. No. 1083370250
DL-AP5	50 µM	Tocris; Cat. No. 0105
DNQX	10 µM	Tocris; Cat. No. 0189

50mM stimulation

NaCl	88.5 mM	J.T.Baker; Cat. No. 0278
KCl	50 mM	Sigma-Aldrich; Cat. No. 31248
CaCl ₂	2 mM	Sigma-Aldrich; Cat. No. 12074
MgCl ₂	1.3 mM	Sigma-Aldrich; Cat. No. 63068
HEPES	10 mM	AppliChem; Cat. No. A 1069,0100
Glucose	10mM	Merck; Cat. No. 1083370250
DL-AP5	50 µM	Tocris; Cat. No. 0105
DNQX	10 µM	Tocris; Cat. No. 0189

2.1.4 Plasmids

pEGFP-N1

Enhanced Green Fluorescent Protein; Kanamycin resistance; Clontech.

pDsRed2-N1

Discosoma sp. Red Fluorescent Protein 2; Kanamycin resistance; Clontech.

EBFP2-N1

Enhanced Blue Fluorescent Protein, Kanamycin resistant (a gift from Michael Davidson; available at addgene plasmid # 54595).

Neuroigin-1-EGFP

Neuroigin-1 (*Rattus norvegicus*) fused to multiple cloning site of pEGFP-N1; Kanamycin resistance; (gift from Dr. T. Dresbach, University of Göttingen, Germany).

pBOS-myc-LRRTM2

LRRTM2 (human) fused to myc inserted into pBOS vector; Ampicillin resistant (gift from Dr. J. de Wit, Leuven, Belgium).

pBS598EF1alpha-EGFPcre

Cre recombinase fused to EGFP inserted into pBS598 vector (addgene); Ampicillin resistance.

N-cadherin Δ E

pcDNA3.1-FLAG-NCadCTF1 (Δ E N-cadherin expression plasmid; developed in Dr. Gottmann lab; Andreyeva et al., 2012).

SypHy-A4 (Rat Synaptophysin-pHluorin)

pH sensitive pHluorin fused to rat synaptophysin inserted into pEGFP-C1; Kanamycin resistance; (gift from Dr. L. Lagnado, Cambridge, UK; available at addgene plasmid # 24478).

2.1.5 Antibodies

Primary antibodies used

Anti-VAMP2: rabbit polyclonal; 1:2000; Abcam; Cat. No. 3347; anti-N-cadherin: rabbit polyclonal; 1:2000, 1:500; Abcam; Cat. No. 18203; anti-N-cadherin: mouse; 1:500; BD Biosciences; Cat. No. 610920; anti-PSD95: mouse monoclonal; 1:500; Thermo Fisher Scientific MA1-046; anti-VGLUT1: guinea pig polyclonal; 1:500; Synaptic Systems; Cat. No. 135304; anti-Bassoon: mouse monoclonal; 1:500; EnzoLifesciences (previously Stressgen); Cat. No. ADI-VAM-PS003; anti-SAP102: guinea pig polyclonal; 1:500; Synaptic Systems; Cat. No. 124214.

Secondary antibodies used:

Alexa Fluor (AF) conjugated secondary antibodies from Invitrogen were used. AF 555 goat anti-rabbit: 1:1000, 1:500; Invitrogen; Cat. No. A21429; AF555 goat anti-mouse: 1:500; Invitrogen; Cat. No. A21147; AF488 goat anti-guinea pig: 1:500; Invitrogen; Cat. No. A11073; AF647 goat anti-mouse: 1:500; Invitrogen; Cat. No. A21241.

2.2 Cell Culture

In this study, experiments were performed on primary cortical neuronal cultures. Two different culture systems were used:-1) neuronal mass cultures and 2) autaptic cultures. In neuronal mass cultures, neocortical neurons were grown on Poly-L-Ornithine coated coverslips while autaptic cultures had clusters of neurons grown on the top of glial cells forming microislands. Neurons were dissociated from cortices of E18 fetuses from either C57/BL6 wildtype or Ncad^{flox/flox} on 15 mm glass coverslips. These coverslips were first cleaned and coated with Poly-L-Ornithine (PO), before starting the cultures. The cleaning of the coverslips enhanced the attachment of the PO-coating onto the glass surface of coverslips.

2.2.1 Cleaning of Coverslips

About 500 coverslips (15 mm; Assistant) were washed by placing them in a big glass petri dish containing freshly prepared 1M HCL on a shaker for 2 hours (h) at 200 rpm. After 2 h, HCL was removed and replaced with demineralized water for 2 minutes (min). The coverslips were subsequently rinsed two more times, 2 min each with demineralized water, before checking the pH. Next rinsing step involved Millipore water (2 x, 2 min each) on the shaker. The coverslips were then dehydrated several times with 100% ethanol (fresh ethanol during each step) and dried up for 2h at 180°C. The dried coverslips were then filled into a glass bottle and sterilized for 3h at 180°C.

2.2.2 PO coating

After cleaning, the coverslips were coated with PO to ensure the attachment of the neurons without the help of glial cells. The coverslips were incubated overnight with 70-80 µl of Poly-L-Ornithine (1mg/ml in 0.15M Borat buffer; pH 8.35) at 37°C in an incubator and subsequently washed three times with sterile aqua dest. Finally, the coverslips were dried inside the laminar flow hood overnight, before use.

2.2.3 Mouse

In this work, two different mice lines were used, wild type (C57/BL6J) and floxed N-cadherin (Ncad^{flox/flox}) mice. In Ncad^{flox/flox} mice, exon1 of N-cadherin (Cdh2) gene was flanked on both sides by loxP sites (Jackson Labs; Kostetskii et al., 2005).

2.2.4 Culturing primary dissociated cortical neurons

Dissociated primary cortical neurons were cultured from E18 or E19 fetuses on the PO coated coverslips. Based on the experiments, wildtype C57/BL6 or Ncad^{flox/flox} fetuses were used.

18 days old embryos were removed from the uterus after killing the pregnant mouse and were decapitated. They were kept on ice in a 100x20 mm tissue culture petri dish (Sarstedt). From now onwards, all the steps were done under a laminar flow hood to prevent contamination. First, the scalp was removed. The cranium was opened from the posterior side of the head using sterile forceps and the brain was carefully removed with the help of a micro scoop. The brain was then transferred to a small culture dish (Falcon; 35x10 mm) filled with ice-cold DPBS+/+ to prevent the brain tissue from drying out. The brain was dissected under a microscope with 20x magnification. Using a sterile scalpel, the cerebellum and midbrain were removed. An incision was made along the midline of the brain to separate two hemispheres and the meninges were removed. Hippocampus was removed and the cortices were chopped into smaller pieces and collected in 1 ml DPBS+/+. The tissue was digested by adding 200 µl of pre-warmed 0.25% Trypsin and 20 µl of DNase and incubated at 37° in a water bath for 5 min. After 5 minutes, trypsin was removed and BME medium (FBS containing) was added to neutralise the trypsin effect. Finally, the tissue was dissociated by mechanical trituration in the BME medium using a 1 ml pipette tip. For further dissociation, a 200 µl pipette tip was used. The cell suspension was then diluted by adding 3 ml BME medium and was centrifuged for 1 min at 400 rpm to remove big non-dissociated tissue pieces and rests of meninges. The supernatant was collected and centrifuged again for 5 min at 900 rpm. The pellet was dissolved in the BME medium and the cell concentration was determined by counting the cells with the help of Neubauer's chamber. For mass cultures, 30-40000 cells were seeded as a drop in the centre of the PO coated coverslips and

incubated for 1h at 37°C/5CO₂/90%humidity. NB medium + B27 supplement was added carefully and cultures were grown for up to 15 days.

2.2.5 Glial culture

The pups (P0-P2) from C57/BL6 mice were used for cultivating confluent monolayers of glial cells. A pup was decapitated and the brain was removed. Cortical tissue from this brain was dissociated analogous to 2.2.4. The cell pellet was dissolved in 1 ml BME medium and this cell suspension was cultivated in two cell culture flasks (Nunc, 25 cm²) for 10-14 days in the BME medium until all neurons died and the glial cells were grown to form a confluent layer. The BME medium was exchanged twice a week to support the growth of the glial cells.

2.2.6 Glial microisland cultures

Glial microisland cultures were used for synaptophysin-pHluorin (SypHy) imaging experiments. The neurons were grown in a small neuronal network on top of the glial microisland (Fig 2.1). In microisland cultures, neuronal process, especially axon growth was restricted in a smaller space leading to the formation of synapses (autapses) with the dendrites of the same neuron. The autaptic culture systems were really important for SypHy experiments as they made it possible to study synaptic vesicle cycling with the help of presynaptically expressed SypHy and at the same time manipulating any postsynaptically expressed molecule. They were of particular interest in this study as it investigated the functions of homophilic cell adhesion molecule, N-cadherin. The autaptic culture system is beneficial as it is possible to knockout or overexpress molecules at both pre- and postsynaptic sites with just one transfection.

To generate the autaptic microisland cultures, glial cells from a confluent monolayer (from 2.2.5) were dissociated and plated in low density on the coverslips. Glial cells were first washed with pre-warmed PBS/- to reduce the attachment of the glial cells. The cells were then incubated with 3 ml trypsin-EDTA (0.05%) for 5 min at 37°C. Trypsin reaction was neutralized by FBS containing the BME medium (5 ml). This cell suspension was transferred to 15 ml falcon tube and centrifuged for 1 min at 2000 rpm. The cell pellet was dissolved in 1 ml BME medium and to create single-cell islands, 25-30 µl of cell suspension was added drop-wise /coverslip in 2.5 ml

BME medium. They were grown for 4-5 days and at DIV 0 (days *in vitro*), 20,000 cortical neurons from 2.2.4 were seeded to each coverslip. BME medium was then replaced after 5-6 hours later with 2.5 ml NB medium + B27 supplement. From now onwards, 1 ml NB medium was exchanged on 3, 6 and 9 DIV with fresh pre-warmed NB medium.

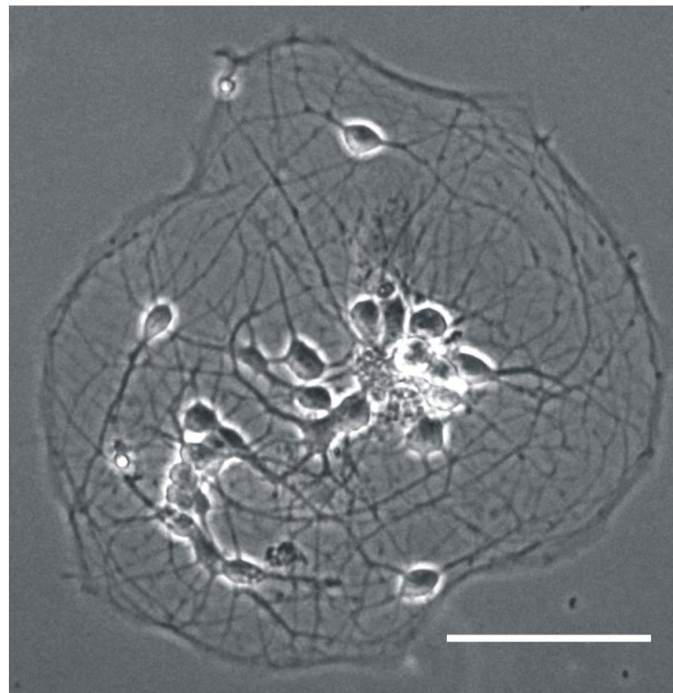
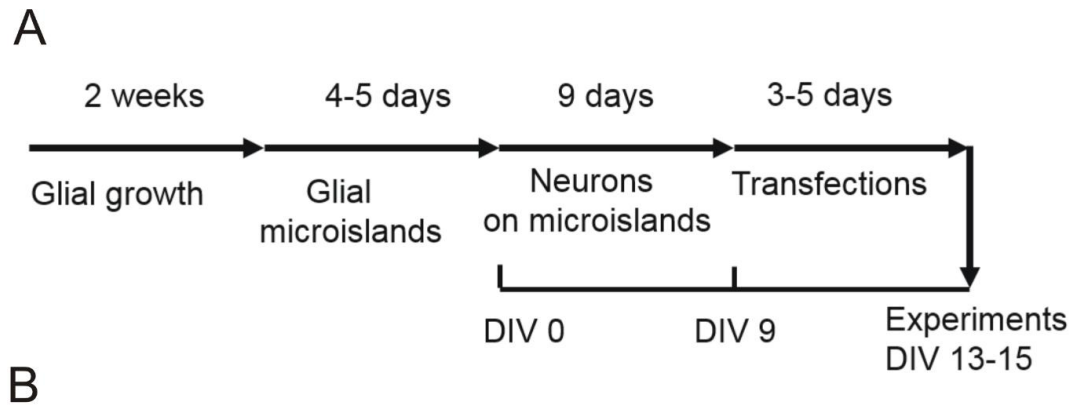


Figure 2.1 Formation of glial microisland cultures

(A-B) Schematic diagram showing the timeline of the preparation of glial microisland. (A) The glial cells were plated 4-5 days before neurons to make islands. The neurons were seeded and grown until 9 DIV before transfections. The experiments were performed at 13-15 DIV. (B) Phase contrast image of a glial microisland culture on DIV 3. Cluster of few neurons form neuronal network. The growth of

axons are confined within the limits of the glial cell which leads to the formation of synaptic contacts with the dendrite of same neuron (autaptic synapses). Scale bar 50 μm .

2.3 Transfection of primary cortical neurons

Transfections were performed to express synaptophysin-pHluorin (SypHy, a genetic probe) for studying synaptic vesicle cycling. This was combined with “a loss of function” approach to examine the functions of N-cadherin in vesicle cycling by Cre mediated conditional knockout. The cortical neurons (mass cultures) were also transfected to study the functions of proteins (LRRTM2 or Neuroligin1) using the overexpression approach. During the experiments, transfected neurons had to be visible. Therefore various plasmids for fluorescent markers (EGFP, DsRed2 or BFP) were transiently co-expressed in the neurons.

2.3.1 MagnetofectionTM for neuronal transfection

In magnetofection, individual cortical neurons were transfected by using magnetic nanoparticles (Plank et al., 2003). These magnetic particles (NeuroMag; OZ Biosciences) contain a positive charge, so they form complex with negatively charged plasmid DNA. DNA/NeuroMag-complexes, when added to the primary neurons are taken up and once inside the cell, plasmid DNA gets released from the magnetic particles and induces transient protein expression.

Plasmid DNA was mixed with Neuromag reagent (1:2 ratios) in 200 μl NB medium without B27 supplement or penicillin/streptomycin. The DNA/NeuroMag-complexes were gently mixed using a pipette and incubated for 20 minutes at room temperature (RT). The complexes were then added to the neurons drop by drop in 6 well plates. The culture plate was placed on an oscillating magnetic plate (magnefect LT; nanoTherics) in a CO₂ incubator for 30 minutes. After 30 minutes incubation, the magnetic plate was removed and fresh pre-warmed culture medium (NB medium with supplements) was added to the cells. The cultures were grown in a humidified CO₂ incubator for 2-5 days before the experiment.

2.3.2 Conditional N-cadherin knockout

One of the major focuses of this study was to investigate the functional role of N-cadherin in synaptic vesicle cycling in mature neurons. For this purpose, I decided to use N-cadherin knockout primary neurons. N-cadherin is very well known for its functions in brain tissue but it also plays an important function in the development of the embryonic heart. Therefore, mutating the N-cadherin gene leads to a lethal phenotype and the embryos die by E10 (Radice et al., 1997) since the heart tube fails to develop.

Thus it is impossible to have conventional N-cadherin knockout mice. However, Dr. Glenn Radice's laboratory (Jefferson Medical College, Philadelphia, USA) developed a conditional N-cadherin knockout mouse model (Ncadflox, Kostetskii et al., 2005). The genome of this mice was edited to introduce loxP sites flanking exon1 of the N-cadherin (Cdh2) gene. The Ncadflox homozygous mice are fertile, develop normally and are available from Jackson Labs (Kostetskii et al., 2005). For this study, dissociated primary neuronal cultures were prepared from the foetuses of Ncadflox mice (E18) identical to 2.2.4.

N-cadherin gene was deleted by transfecting individual neurons with a CreEGFP plasmid. CreEGFP protein acts on the loxP sites, thus removing the exon 1 of the N-cadherin which contains translational start sites and transcriptional regulatory sequences (Kostetskii et al., 2005). These neurons were then used to study synaptic vesicle cycling in the absence of N-cadherin to evaluate its functions.

2.4 Fluorescence microscopy

2.4.1 Imaging Setup

Except for superresolution microscopy (SIM), all experiments were performed using an inverted motorized axiovert 200M microscope (Zeiss) with a 40 x oil-immersion objective (EC Plan-Neofluor; 40x1,3 oil; Zeiss). The images were captured with a 12-bit monochrome CoolSnap ES2 Charged-Coupled-Device (CCD) camera (Photometrics) using Metavue or VisiVue software (Molecular Devices/Visitron Systems). Following filter sets were used:

- 1) Filterset 49 (DAPI) = excitation wavelength 365 nm, beam splitter 395 nm and emission is at 445/50 nm.
- 2) Filterset 17 (FITC) = excitation wavelength 485/20, beam splitter 510 nm and emission is at 515-565 nm.
- 3) Filterset 43 (CY3) = excitation wavelength 545/25, beam splitter 570 nm and emission is at 605/70 nm.

Two external shutters (Vincent associates, Uniblitz, model: VMM-D1) controlled the exposure.

2.4.1.1 Immunocytochemistry (ICC)

Immunocytochemical (ICC) staining can be used to obtain information about the proteins in cells. ICC enabled the detection of multiple proteins at the same time using different fluorophores. In this study, I stained the cortical neurons to examine the synaptogenic properties of different synaptic adhesion molecules. ICC was performed at different time points during neuronal differentiation and synaptogenic activity was measured by labeling the neurons for presynaptic vesicle clusters (VAMP2). In addition, I also examined the structural changes in the synaptic proteins associated with the strong synaptic vesicle release. In these experiments, cultures were immunostained for VGLUT1 (presynapse), N-cadherin, and PSD95 (postsynapses). The neurons were also immunocytochemically stained for Bassoon, N-cadherin, and SAP102 to study the change in N-cadherin distribution associated with synapse maturation.

The primary neuronal cultures were washed once with DPBS+/+ and then were fixed for 20 minutes using 4% paraformaldehyde (PFA). After fixations, the neurons were washed 3x10 minutes with DPBS+/+ to remove the remaining PFA. All the steps except fixation of cells were carried out at room temperature on a shaker (< 50 rpm).

Neurons were permeabilized using TritonX100 by incubating them for 30 minutes in blocking buffer I. Permeabilization of cell membrane provides sufficient access of antibodies to the intracellular proteins of interest. The neurons were then incubated in primary antibody dissolved in blocking buffer I for 1 hour at room temperature. The cells were washed again 3x10 using DPBS+/+. All the steps from now onwards were carried out in dark to prevent the photobleaching of fluorophore tagged antibodies.

The secondary antibody was applied to cultures in blocking buffer II for 1 hour at room temperature and the neurons were washed 3x10 minutes afterwards with DPBS+/. Coverslips containing stained neurons were then mounted on the glass coverslip using aqueous mounting media (FluorSave™) to prevent photobleaching and kept overnight for drying.

2.4.1.2 SypHy Fluorescence Imaging

SypHy is a pH-sensitive GFP called pHluorin (Miesenböck et al., 1998) fused to the luminal side of synaptophysin protein. It exploits the fact that synaptic vesicle lumen is acidic at rest (~5.6; Miesenböck et al., 1998), quenching the fluorescence of EGFP.

During the electrical stimulations, synaptic vesicles fuse with the presynaptic membrane exposing their luminal surface to a more alkaline pH of extracellular level (pH ~ 7.4). This leads to the unquenching of pHluorin signal and an increase in fluorescence can be observed enabling the measurement of synaptic vesicle exocytosis. SypHy fluorescence declines after some time due to the endocytosis and reacidification of the synaptic vesicles. Thus SypHy imaging depends on the dynamic changes in the pH of the vesicle lumen resulting from exo- and endocytosis of the synaptic vesicles during presynaptic activity. The net change in SypHy fluorescence observed during electrical stimulations is used as a measurement of synaptic vesicle exo- and endocytosis (Royle et al., 2008; Sankaranarayanan et al., 2000).

In this work, SypHy experiments were performed in N-cadherin knockout autaptic cultures. To examine the functions of N-cadherin in synaptic vesicle cycling, cortical neurons from floxed N-cadherin mice (Ncadfloxed; 9-10 DIV) were transfected with the SypHy-A4 plasmid (gift from Dr. L. Lagnado). DsRed2 was co-expressed to visualize the transfected neurons and used for the detection of autapses. N-cadherin was knocked out conditionally by co-expressing Cre recombinase for 5-6 days in cortical neurons. In an additional experiment, SypHy imaging was performed in autaptic cultures from wildtype mice and N-cadherin functions were inhibited by overexpressing Ncad Δ E (dominant-negative N-cadherin construct).

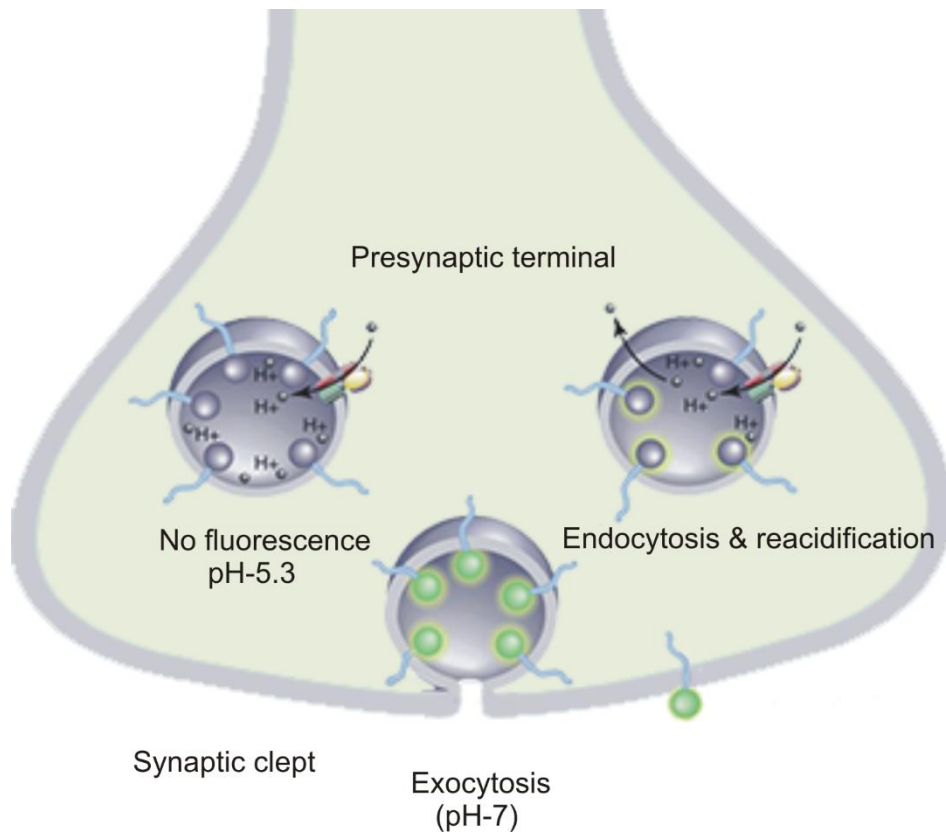


Figure 2.2 Synaptophysin-pHluorin (SypHy) as a tool to measure synaptic vesicle cycling (modified after Kavalali and Jorgensen, 2014)

Cartoon of a presynaptic terminal showing synaptic vesicle exo- and endocytosis. The pH-sensitive EGFP was fused to synaptophysin to measure the change in vesicle cycling. (Left) At rest, SypHy fluorescence is quenched because of the acidic pH (low) within the vesicles (~pH 5.3-5.5). (Middle) Electrical stimulation leads to the fusion of synaptic vesicles with the presynaptic membrane and SypHy fluorescence increases as the pH changes to more neutral (~pH 7-7.3). This increase in fluorescence can be measured as the kinetics of exocytosis. (Right) After some time, synaptic vesicles get endocytosed and reacidified via vesicular ATPase leading to disappearance of SypHy fluorescence. This decline in SypHy signal can be used as a measure of vesicle endocytosis.

To perform SypHy imaging, cortical neurons were transferred to a stimulation chamber (Live Cell Instrument) and an extracellular solution containing DL-AP5 (50 μM) and DNQX (10 μM) was added to prevent recurrent network activity. For each experiment, the change in SypHy fluorescence over time was recorded using a time-lapse sequence of 4 minutes with a time interval of 2 seconds each. This sequence included the first 10 baseline images before stimulation (-20 sec to 0 sec), then the increase in the fluorescence upon field stimulation (0-20 sec) and finally decline in

SypHy signal after stimulation (20-220 sec). Synaptic vesicle cycling was induced by stimulating the neurons with 1 ms pulses (biphasic) of 100 mA. Depending on the experiment, either 100 or 400 stimulations with a frequency of 20 Hz were applied at room (25°C) or physiological temperature (34°C). At the end of each experiment, 100 mM NH₄Cl containing extracellular solution was added to the cells to switch the pH to alkaline. This resulted in maximum SypHy fluorescence representing the total SypHy expression level and was used for the normalization of SypHy data. DsRed2 and NH₄Cl images were captured at an exposure time of 0.2s (RFP) and 0.2s (GFP) with 2 x 2 binning using 40x oil objective. Exposure time for SypHy time-lapse sequence (4 minutes) was 0.2 s (GFP).

2.4.1.3 FM1-43 and TMR-dextran Co-staining

FM1-43 and TMR-dextran co-staining was performed in dissociated cortical neurons manipulating the functions of N-cadherin. The BFP construct was expressed (9 DIV) to visualize the transfected neurons. N-cadherin was either knocked out by using Cre co-expression in cortical neurons cultured from floxed *Ncad*^{flox/flox} mice or was functionally inhibited by overexpressing *Ncad*ΔE in neuronal cultures from wildtype (C57/BL6) mice.

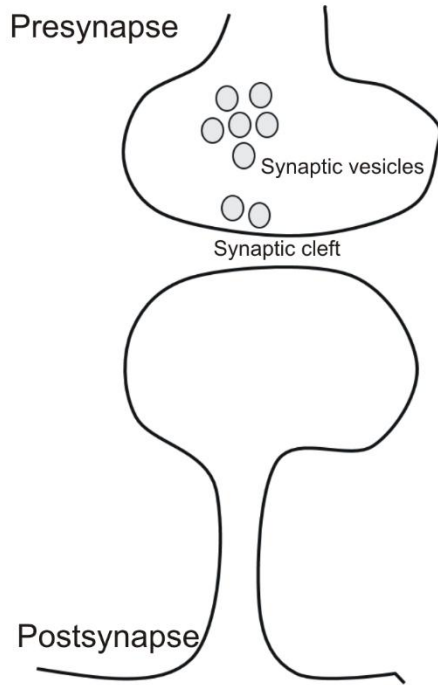
After 3 to 5 days (12-15 DIV) of transfection, active synaptic vesicles were co-stained with FM1-43 and TMR-dextran. To perform FM1-43 and TMR-dextran co-staining, coverslips containing the cortical neurons were mounted onto a stimulation chamber (Live Cell Instrument) and an extracellular solution containing DL-AP5 (50 μM) and DNQX (10 μM) was added to prevent recurrent network activity. Neurons were incubated with FM1-43 (10 μM) and TMR-dextran (50 μM) for one minute. FM is a styryl dye that binds non-selectively with the presynaptic membrane (hydrophobic) while TMR-dextran is fluid phase marker that remains in the solution. The cultures were electrically stimulated with a variety of stimulation at 20Hz (based on the experiment) to induce synaptic vesicle cycling. Electrical stimulation led to the fusion of synaptic vesicles (SVs) to the presynaptic membrane (exocytosis). FM1-43 dye present in the extracellular buffer bound to the presynaptic membrane and was taken up inside the retrieved SVs (clathrin-mediated endocytosis) or endosomes (bulk endocytosis) during the vesicle recycling. On the other hand, TMR-dextran present in the extracellular medium do not bind to the presynaptic membrane but were

accumulated inside endosomes (bulk endocytosis) non-selectively (Newton and Murthy, 2006; Clayton and Cousin, 2009). The cultures were then washed with a Ca^{2+} -free extracellular solution for 3-5 minutes to remove non-specific FM1-43 dye and TMR-dextran. This inhibited the spontaneous release.

Washing helped to reduce the background and increased the signal to noise ratio. Washing efficiency was increased by using 1 mM ADVASEP-7, a dye quencher with a higher affinity to FM1-43 than the plasma membrane. After the washing, clear FM1-43 (green) and TMR-dextran (red) puncta were visible representing the active synaptic vesicles at the synapses. The specificity of TMR-dextran uptake was made sure by always analysing its co-localisation with FM1-43 puncta. Images were captured at 0.2s (GFP) and 0.05s (RFP) rate with 2 x 2 binning using 40x oil objective.

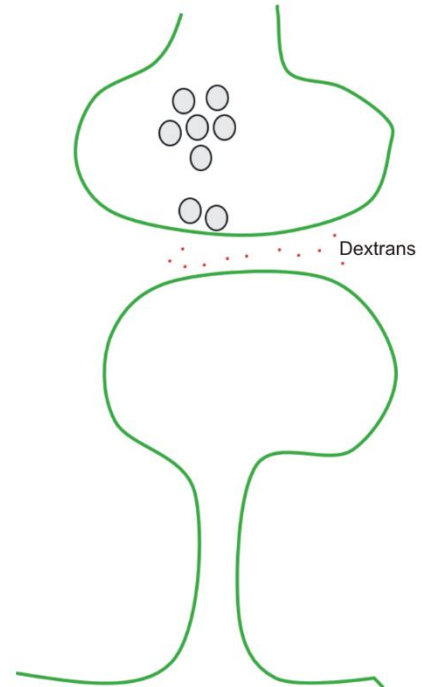
A

Incubation of cultures with normal extracellular solution



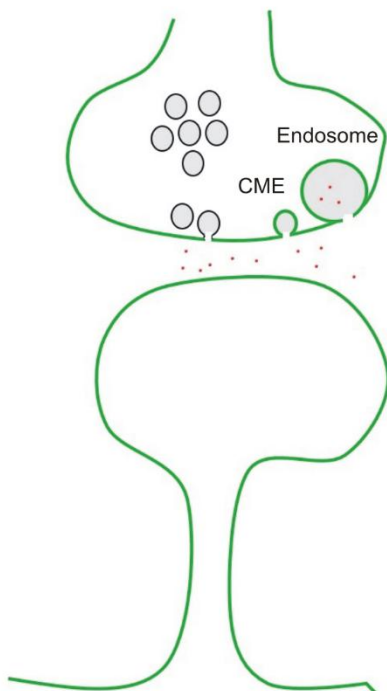
B

Addition of FM1-43+dextran
FM binds to the synaptic membrane non specifically



C

Field stimulation causes uptake of FM and dextran



D

Removal of non-specific FM and dextran by washing

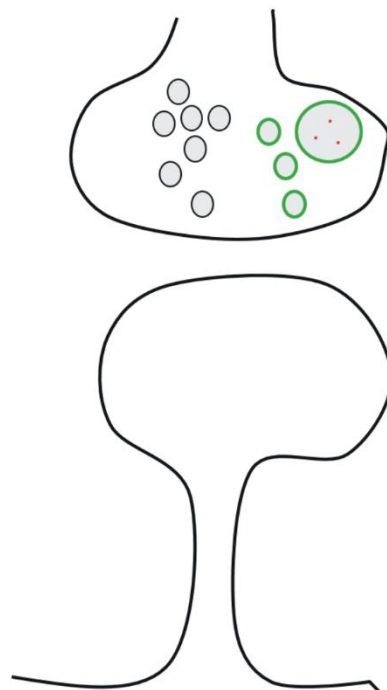


Figure 2.3 FM1-43 and TMR-dextran co-staining to label synaptic vesicle endocytosis

Illustration of FM1-43 and dextran co-staining. FM1-43 was highlighted in green and TMR-dextran in red. (A) Cartoons representing the presynaptic and postsynaptic terminals of a synapse. (B) FM1-43 dye binds to the pre-and postsynaptic membrane non-specifically and becomes fluorescent in the hydrophobic environment while TMR-dextran molecules remain in the hydrophilic extracellular solution (C) Upon stimulation, synapses undergo endocytosis via either clathrin-mediated reformation of individual vesicles or by taking up large invaginations in the form of endosomes. In both cases, FM1-43 is taken up along with the membrane. Thus FM1-43 labeled puncta represents both clathrin-mediated endocytosis and bulk endocytosis. On the other hand, TMR-dextran are taken up only in the large invaginations labeling specifically bulk endosomes. (D) Washing the cultures in Ca^{2+} free extracellular solution removes non-specific FM1-43 and TMR-dextran. At this point, active individual vesicles are visible as distinct green fluorescent puncta and endosomes appear yellowish because of co-staining of FM1-43 (green) and TMR-dextran (red).

In the initial experiments, cultures were stimulated with 200, 400 and 2000 stimulations, respectively to activate different modes of synaptic vesicle retrieval. To label clathrin-mediated endocytosis, cultures were stimulated with 200 stimulations (20Hz) at room temperature (25°C). To ensure the formation of large invaginations, cortical neurons were stimulated with 400 stimulations (20Hz) at physiological temperature (34°C).

2.4.2 SIM imaging

In a conventional wide-field microscopy, the optical resolution is limited by the diffraction limit (Abbe's equation). Several imaging techniques have been developed during the last decades to surpass the diffraction limit. One such technique is Structured Illumination Microscopy (SIM). This method was developed by John W. Sedat and colleagues (Gustafsson et al., 2008; Schermelleh et al., 2008). SIM imaging can be performed with common fluorescence dyes and does not need specialized sample preparation. SIM is relatively fast and allows multicolor imaging, making it easy to examine several molecules within one sample.

SIM imaging is based on conventional wide-field microscopy except that specialized grating patterns are kept in the path of the illuminating light. SIM imaging involves illumination of the sample using laser light with a grid-like pattern in its path. This results in a defined structured illumination of the sample. The interference produced

by frequency mixing of the excited sample structures and the grid-patterned light generates Moiré fringes. This results in down-modulation of fine sample details to lower frequencies into the regions of the detection of an optical transfer function (Jost and Heintzmann, 2013). To obtain high resolution, images were reconstructed offline using software-controlled process. SIM can typically enhance lateral resolution by twofold (Gustafsson, 2000; Schermelleh et al., 2010).

2.4.2.1 ELYRA setup

Structures illumination microscopy (SIM) imaging was done using the ELYRA PS microscope (Zeiss) at the Center for Advanced Imaging (CAI Düsseldorf). Three different laser lights (488 nm, 561 nm, and 642 nm wavelengths) were used to excite different fluorophores in triple stained cortical neurons. The laser light passes through a grating pattern before illuminating the samples. Images were captured with an alpha Plan-Apochromat 63x/1.4 oil DIC M27 objective (Zeiss) using an EM-CCD camera with 1002 x 1002 pixels for maximum resolution. SIM computationally removes out of focus light (optical sectioning) and reconstructs the superresolution images offline.

2.4.2.2 SIM imaging of N-cadherin during neuronal differentiation and upon strong synaptic activity

To examine the synaptic structures at high resolution, cortical neurons were labeled using immunocytochemical staining and SIM imaging was performed on ELYRA-PS (Zeiss). Synaptic maturity was evaluated on the basis of N-cadherin localization. Cortical neurons were immunostained at three different stages of neuronal differentiation *in vitro* (6, 12 & 28 DIV). Immature neurons (6 DIV) were labeled with Bassoon and SAP102 along with N-cadherin. For 12 and 28 DIV, synapses were labeled with VGLUT1, N-cadherin, and PSD95.

To study the changes associated with strong synaptic vesicle release, cortical neurons (12-13 DIV) were stimulated for 5 minutes in 50 mM K⁺ containing extracellular solution. The cells were immediately fixed with 4% PFA. For the control experiment, neurons were incubated in a normal extracellular solution (2.5 mM K⁺) for 5 minutes. In addition, neuronal cultures were also recovered for 30 minutes in a

normal extracellular solution (2.5 mM K⁺) after stimulation (5 minutes in 50 mM K⁺) and then fixed with 4% PFA. Next, immunocytochemical stainings were performed for VGLUT1 (pre-), PSD95 (postsynaptic), and N-cadherin. To examine the changes caused by high synaptic release, fluorescence images were acquired on ELYRA-PS (Zeiss).

2.5 Data analysis

2.5.1 SypHy signal analysis

The mean time courses of SypHy signal were analysed using offline version of Metamorph software. First, all the images were imported in the software and were calibrated.

An overlay was created using DsRed2 image and NH₄Cl induced maximal SypHy signal image. This helped in identifying autaptic puncta (synapses onto the dendrite of the transfected neuron). Only autaptic synapses were analysed for all the experiments to include the transgene expression on both pre- and postsynaptic sites. Region of Interests (ROIs) were created using a circle tool around the autapses on the overlay image. An additional ROI was drawn away from the dendrite to get the background fluorescence intensity of the image. These ROIs were then transferred to the NH₄Cl induced maximal SypHy image and average pixel intensities were measured. These ROIs were also loaded onto the time-lapse movie (121 frames) and average pixel intensities over time were calculated for all the ROIs and then exported to Microsoft Excel sheet, where I performed all the analysis. First of all, background fluorescence intensities were subtracted from all the puncta (ROIs). Next, the fluorescence intensity values of the 10th frame (baseline, 0 sec) of each ROI were subtracted from the rest of the values of the same ROI to correct for any spontaneous activity. This provided us the change in SypHy fluorescence intensities with time for each punctum. This was then normalized with the background subtracted corresponding NH₄Cl induced SypHy signals. Normalized SypHy (% NH₄Cl signal) fluorescence at the end of stimulation (20 sec, 20th frame) was measured as synaptic vesicle exocytosis.

Individual punctum that did not show an increase in the fluorescence upon stimulation were excluded from the analysis to avoid its influence on the rate of exo- and endocytosis. Time-lapse sequences with a shift in the x/y-direction were also excluded from the analysis. In the experiment with stimulation dependent evaluation of exocytosis (100 stimuli at 20 Hz), normalized SypHy (% NH₄Cl signal) fluorescence intensities of the 13th image (6 sec) were considered as exocytosis.

2.5.2 FM1-43 and TMR-dextran signal analysis

FM1-43 and TMR-dextran stainings were analysed using Metamorph software. Fluorescence images were imported to the Metamorph and were thresholded based on their intensity profiles. After thresholding, single pixels were removed using low pass filter and overlay images were generated by merging the images of BFP expressing neurons with FM1-43 and TMR-dextran stained images. Overlay images were used to find the FM1-43 or TMR-dextran puncta on the dendrites of transfected cells. Finally, regions of interest (ROIs) were created around the thresholded FM1-43 puncta that were contacting the dendrites of the transfected neurons and were evaluated for their co-localisation with TMR-dextran puncta. FM1-43 puncta density was calculated (FM puncta/ 10 μ m dendrite).

Total FM1-43 uptake gave the measurement of total endocytosis (all forms of endocytosis). FM1-43 puncta co-localising with TMR-dextran puncta were counted and measured as bulk endocytosis and finally, FM1-43 puncta that did not co-localise with TMR-dextran signal were considered as clathrin-mediated endocytosis.

2.5.3 Analysis of SIM Images

Images were captured in z-stack using Elyra PS setup (Zeiss) and maximum intensity projections were used for the analysis. First, images (individual channels) were thresholded based on the intensity profile using ImageJ Fiji. Single pixel noise was removed using median filter. An overlay was created using VGLUT1 and PSD95. The overlay was then searched for the structures where both VGLUT1 and PSD95 molecules were present together within one focal plane and an area was drawn around them. Whenever VGLUT1 and PSD95 puncta were contacting each other, this was considered as a synapse. Corresponding N-cadherin image was then

superimposed on the overlay and N-cadherin localization was determined manually in relation to the VGLUT1 or PSD95 puncta.

2.6 Statistical Analysis

All data is shown as means \pm SEM and also with individual values. Statistics for all the experiments were done using SigmaPlot 11 software. Student's t-test was used for comparing two groups and for more than two groups, one way ANOVA was used. Significance levels were: * $P < 0.05$ ** $P < 0.01$ *** $P < 0.001$. Whenever the normality test failed, ANOVA on ranks was used. All the figures were created using CoralDraw with 300dpi resolution.

03-

Results

3.1 Functional role of N-cadherin in synaptic vesicle cycling

3.1.1 Recording synaptic vesicle exo- and endocytosis using SypHy in autaptic glial microisland cultures

To study exo- and endocytosis at synapses in cultured cortical mouse neurons in a single experiment, I used Synaptophysin-pHluorin (SypHy; Granseth et al., 2006), a pH sensitive GFP (pHluorins, Miesenböck et al., 1998) construct fused with synaptophysin (a synaptic vesicle membrane protein). SypHy imaging is based on its pH sensitivity. At rest, the low pH (acidic) of the synaptic vesicle lumen quenches SypHy fluorescence. During extracellular stimulation, vesicles fuse with the presynaptic membrane exposing the pH sensitive GFP to outside pH (extracellular solution, more neutral). This change in pH results in unquenching of GFP fluorescence leading to an increase in SypHy fluorescence signal. Increased SypHy signal thus monitors vesicle exocytosis. After reaching a maximum, SypHy fluorescence starts to decline indicating that membrane is taken up again by recycling via endocytosis and newly formed vesicles undergo reacidification resulting in re-quenching of SypHy signal. The decay kinetics of the SypHy signal monitors the rate of endocytosis.

Initial experiments were done to study vesicle cycling using SypHy in autaptic glial microisland cultures. SypHy and DsRed2 were co-expressed in 9 days *in vitro* (DIV) cortical neurons and experiments were performed 5-6 days after transfection (14-15 DIV). Time lapse sequences of fluorescence images were acquired to capture the changes in SypHy fluorescence intensities over time.

At the end of each experiment, cells were exposed to 50 mM NH_4Cl containing extracellular solution thereby alkalizing all synaptic vesicles (maximum SypHy signal) (Fig. 3.1A). Quantification of SypHy signal at this point gives the total expression of SypHy and was used for normalization of SypHy fluorescence signals. For quantitative analysis, the thresholded NH_4Cl image was merged with the corresponding DsRed2 image to get an overlay (Fig. 3.1B). SypHy puncta on the dendrites of DsRed2 expressing neurons (white arrows, autapses) were analysed, and synaptic contacts made by the axon of the DsRed2 neuron with other non-transfected neurons (yellow arrows, synapses) were excluded (Fig. 3.1C). SypHy fluorescence before stimulation (0 sec) was considered as baseline level (Fig. 3.1D).

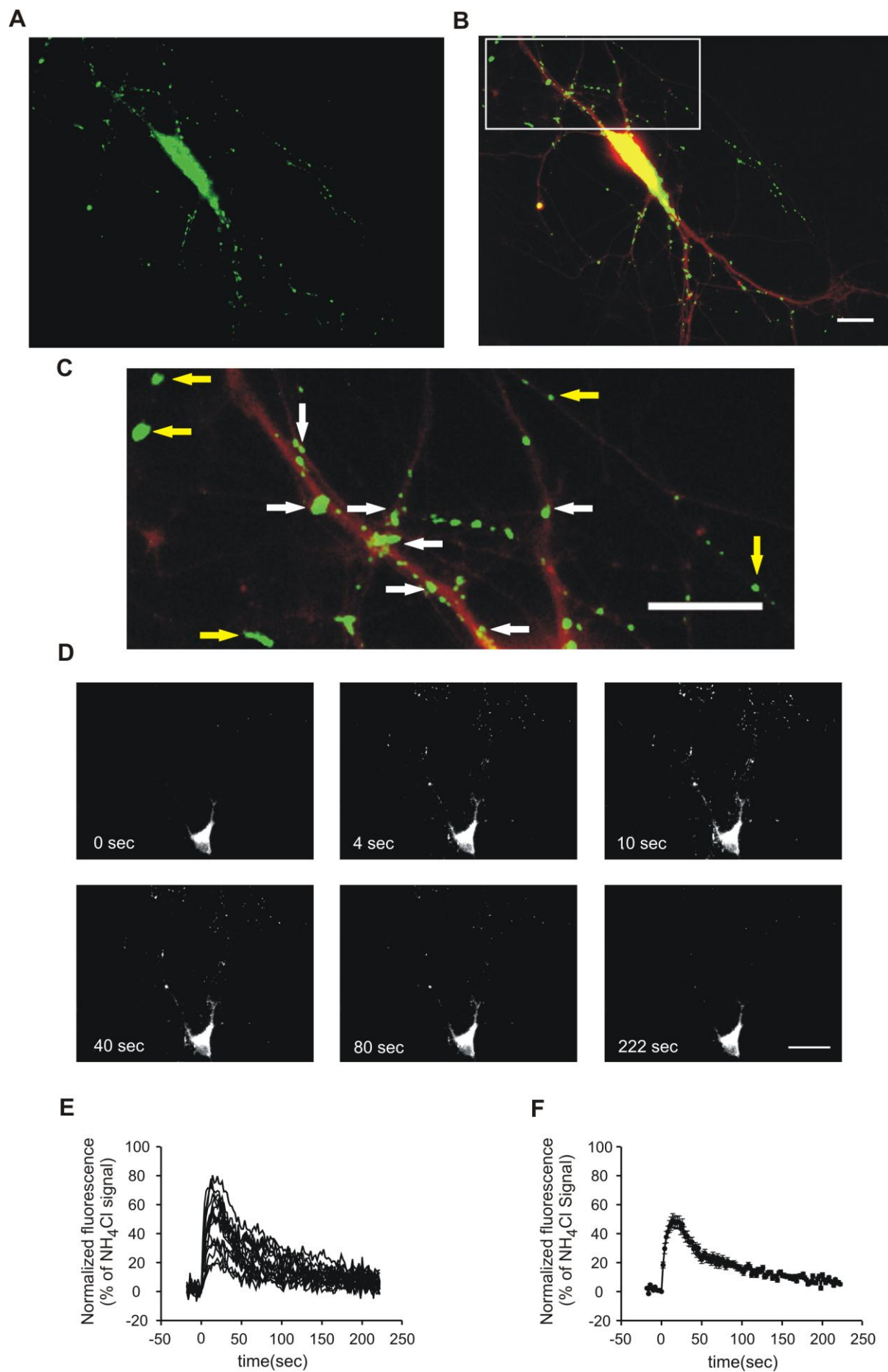


Figure 3.1 Synaptophysin-pHlourin (SypHy) imaging as a measure of synaptic vesicle exo- and endocytosis in autaptic microisland cultures

Cultured cortical neurons were co-transfected with DsRed2 and SypHy plasmid at 9 DIV and imaging was performed after 3-5 days. Vesicle cycling was induced by electrically stimulating the cultures with 400 stimuli at 20 Hz.

(A-F) Electrical stimulation leads to the fusion of synaptic vesicles to the presynaptic membrane, which results in a fast increase in SypHy fluorescence intensities (exocytosis). This is followed by endocytosis and newly formed vesicles get reacidified leading to a decline in SypHy fluorescence. DsRed2 expression was used for identification of autapses. Application of NH_4Cl at the end of the experiment gave the maximum SypHy fluorescence representing the total expression of SypHy. **(A)** Example image showing NH_4Cl -induced SypHy fluorescence. **(B)** Overlay image showing the expression of DsRed2 (red) and the corresponding NH_4Cl -induced SypHy fluorescence (green). **(C)** Magnification of indicated part of **(B)**. Autaptic contacts (white arrows) were analysed. Axonal synapses (yellow arrows) with non-transfected neurons were excluded. Scale bars: 10 μm . **(D)** Example images showing different time points from a SypHy recording of a single neuron. Scale bar: 20 μm . **(E)** Changes in SypHy fluorescence intensities over time from individual autapses from **(D)**. **(F)** Average fluorescence intensity of all SypHy puncta of the cell in **(D)** over time from **(E)**.

Upon electrical stimulation (400 stimuli, 20Hz), SypHy fluorescence intensities increased. As the stimulation ends, the fluorescence intensities of SypHy puncta declined back to the baseline level. This decay in SypHy signal was caused by synaptic vesicle endocytosis and vesicle reacidification. Traces of SypHy fluorescence intensities from each punctum were obtained by analysing the time-lapse sequences offline (Fig. 3.1E). The average of the SypHy traces of all autaptic puncta on an individual cell gave the mean curve for that cell (Fig. 3.1F).

In summary, SypHy experiments in autaptic microisland cultures enabled the quantitative measurement of synaptic vesicle cycling (exo- and endocytosis). DsRed2 co-transfection was used to visualize the transfected cell and to differentiate between autapses and synapses. Transfection in autaptic cultures lead to deletion or overexpression in both the pre- and postsynaptic sites simultaneously at autapses. This is important to study the functions of N-cadherin as it is a homophilic adhesion molecule expressed pre- and postsynaptically. Glial microisland cultures also provide the analysis of many autapses within one measurement because glial cells confine the growth of the axon within a limited space leading to the formation of a large number of autapses.

3.1.2 Effects of N-cadherin knockout on vesicle exo-and endocytosis at room temperature

To study the functional role of N-cadherin in vesicle exo- and endocytosis, SypHy imaging was performed in autaptic microisland cultures after conditional knockout of N-cadherin in individual neurons and the results were compared with control cells. Individual neurons were co-transfected (9 DIV) with DsRed2 (marker to visualize the transfected neuron) and SypHy. To knockout the N cadherin gene, neurons were additionally co-transfected with a Cre vector and SypHy imaging was done 5-6 days after transfection (14-15 DIV) at room temperature (25°C). Synaptic vesicle recycling was induced by electrically stimulating the cultures with 400 stimuli at 20Hz. At the end of the experiment, NH₄CL signal (see Fig. 3.1 for details) was measured to obtain the maximum SypHy fluorescence intensities. Only autaptic puncta were analysed to ensure N-cadherin knockout on both, pre- and postsynaptic sites and traces from all autaptic SypHy puncta (cycling vesicle cluster) from each cell were averaged.

The amplitudes of NH₄Cl-signal normalized SypHy fluorescence signals (exocytosis) at the end of stimulation were not significantly ($P=0.144$) changed in neurons after knockout of N-cadherin (35.4 ± 2.2 % of NH₄Cl signal, $n= 15$ cells) as compared to control ($40.3 \pm 2.4\%$ of NH₄Cl signal, $n= 12$ cells; Fig. 3.2A-C). Additionally, endocytosis was determined by quantifying the decline in SypHy fluorescence 90 seconds (as % of exocytosis) after the end of stimulation. N-cadherin knockout neurons showed a trend towards reduction in endocytosis ($44.7 \pm 6.8\%$ of exocytosis, $n=15$ cells) as compared to the control cells ($59.1 \pm 4.8\%$ of exocytosis, $n=12$ cells), but this decrease was not statistically significant (Fig. 3.2D). Data from individual neurons were plotted to visualize the variance in the experiment and results showed relatively high variance (Fig. 3.2E). The decay time constants (monoexponential fit) were slightly slower in N-cadherin knockout cells, 74.8 ± 13.2 s ($n= 15$ cells) as compared to 53.9 ± 6.3 s ($n= 12$ cells) in control cells. Again, this decrease in decay time constant was not significant ($P=0.199$; Fig. 3.2F, G).

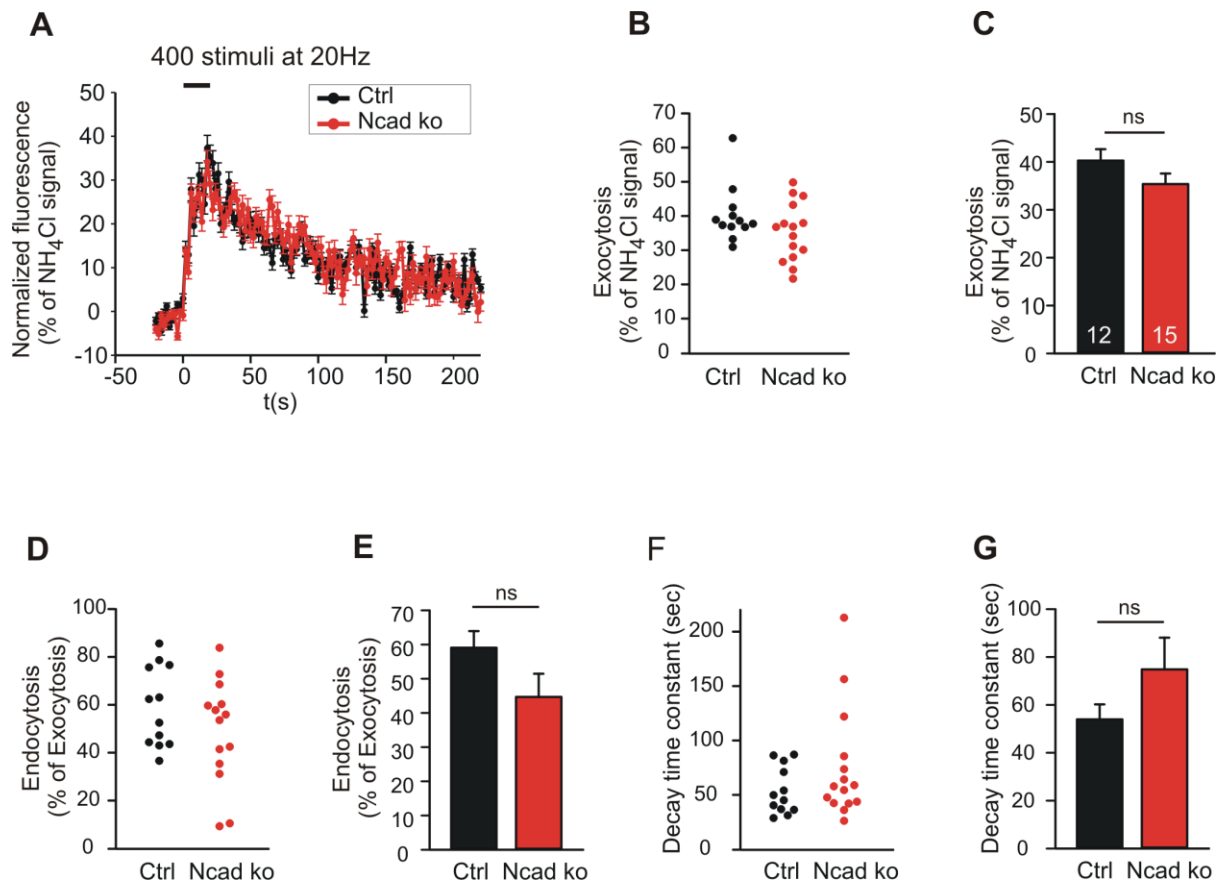


Figure 3.2 Effects of Cre mediated conditional knockout of N-cadherin on synaptic vesicle exo- and endocytosis at room temperature (25°C)

Neurons were co-transfected at 9 DIV with DsRed2 and SypHy. N-cadherin knockout was induced by co-expression of Cre for 5–6 days in individual neurons cultured from floxed N-cadherin mice. SypHy imaging was done by electrically stimulating the neurons (400 stimuli at 20 Hz) at room temperature.

(A-G) Conditional knockout of N-cadherin did not have a significant effect on synaptic vesicle exo- and endocytosis at room temperature (25°C). **(A)** Example time course traces of mean SypHy fluorescence intensities (black control cell; red N-cadherin knockout cell) after normalizing with NH₄Cl signal. **(B)** Quantification of mean SypHy amplitude (at the end of stimulation) as synaptic vesicle exocytosis in individual neurons. **(C)** Quantification of average exocytosis. **(D)** Quantitative analysis of vesicle endocytosis at 90 seconds after the end of stimulation in individual cells (SypHy signal loss as % of exocytosis signal). **(E)** Average endocytosis at 90 seconds (% of exocytosis). **(F)** Quantification of SypHy signal as decay time constant (tau of endocytosis, monoexponential fit) in individual neurons. **(G)** Average decay time constants (black control; red N-cadherin knockout; n=12/15 cells. Total SypHy puncta analysed were 267/277. Data is represented as mean \pm SEM. Student's t-test was used for statistical analysis, ns= not significant.

In summary, these findings showed a trend towards a change in vesicle endocytosis in the absence of N-cadherin. However, all changes observed were not statistically significant. Since this experiment was done at room temperature (25°C) and endocytosis is known to be highly temperature sensitive (Delvendahl et al., 2016; Chanaday and Kavalali 2018), SypHy experiments were repeated at near physiological temperature (34°C).

3.1.3 Effect of N-cadherin knockout on vesicle exo-and endocytosis at near physiological temperature (34°C)

All experimental conditions were analogous to the previous experiment except that the temperature was increased to 34°C. The amount of exocytosis at the end of stimulation remained ($P=0.214$) unaltered in N-cadherin knockout neurons (32.7 ± 2.6 % of NH_4Cl signal, $n= 14$ cells) as compared to the control cells ($28.7 \pm 1.8\%$ of NH_4Cl signal, $n= 15$ cells; Fig. 3.3A-C) at near physiological temperature. However, the decline in SypHy fluorescence 90 seconds (as % of exocytosis) after the end of stimulation showed a significant ($P<0.05$) reduction ($59.9 \pm 4.3\%$ of exocytosis, $n=14$ cells) after knockout of N-cadherin as compared to the control cells ($75.2 \pm 4.5\%$ of exocytosis, $n=15$ cells; Fig. 3.3D-E). The decay time constants (monoexponential fit) were significantly ($P<0.001$) higher in N-cadherin knockout neurons, 54.4 ± 6.7 s ($n= 14$ cells) as compared to 32.1 ± 3.1 s ($n= 15$ cells; Fig. 3.3F, G) in the control cells, indicating slower endocytosis after knockout of N-cadherin.

Interestingly, these experiments at near physiological temperature showed a role of N-cadherin in the regulation of endocytosis. However, these experiments did not reveal a change in synaptic vesicle exocytosis by N-cadherin knockout, at least in this specific experimental condition.

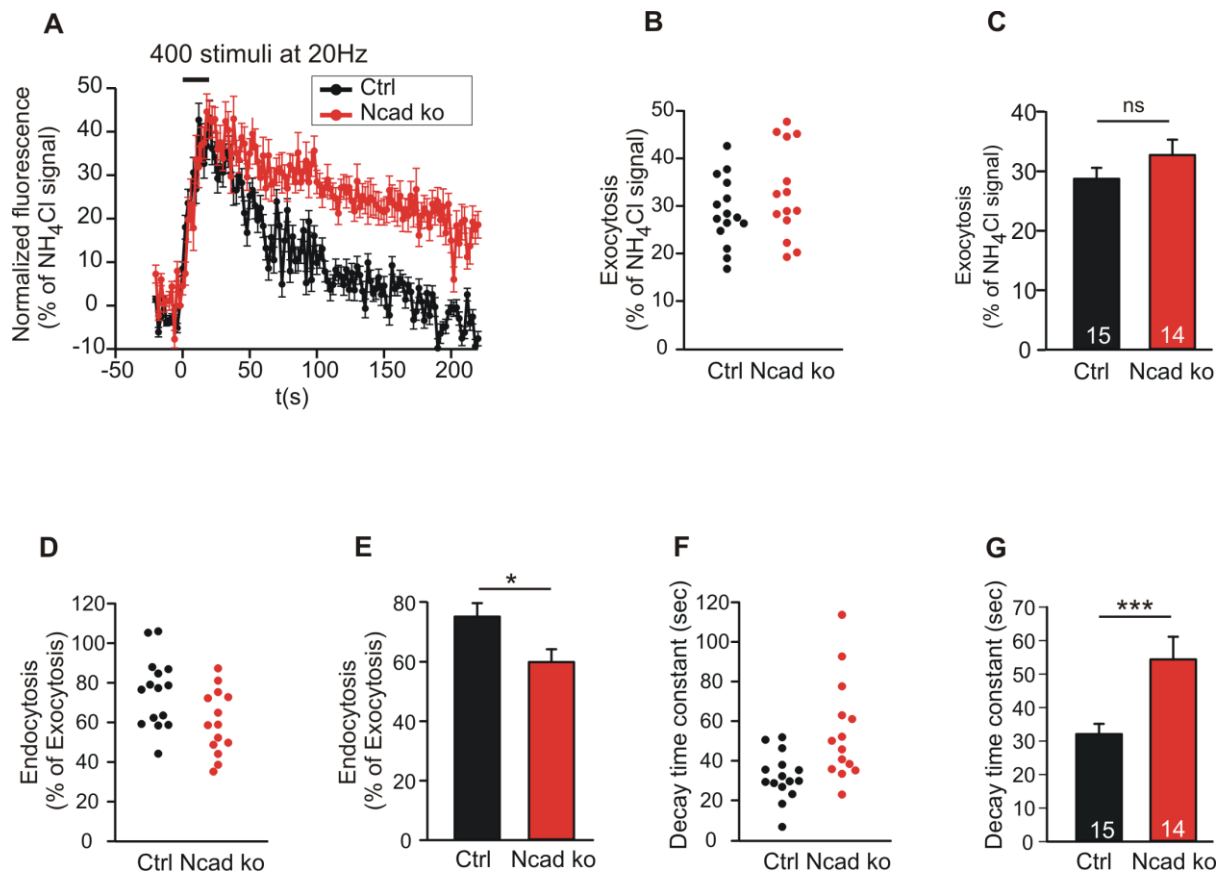


Figure 3.3 Reduced Endocytosis in N-cadherin knockout neurons at near physiological temperature (34°C)

(A-G) Conditional knockout of N-cadherin resulted in a significantly slower vesicle endocytosis without having a significant change on synaptic vesicle exocytosis at near physiological temperature (34°C). **(A)** Example time course traces of mean SypHy fluorescence intensities (black control cell; red N-cadherin knockout cell) after normalizing with NH₄Cl signal. **(B)** Quantification of mean SypHy fluorescence intensities (at the end of stimulation) as synaptic vesicle exocytosis in individual neurons. **(C)** Average exocytosis. There was no significant change in synaptic vesicle exocytosis upon N-cadherin knockout. **(D)** Quantitative analysis of vesicle endocytosis at 90 seconds after the end of stimulation (SypHy signal loss as % of exocytosis signal) in individual neurons. **(E)** Quantification of average endocytosis at 90 seconds (% of exocytosis). N-cadherin knockout resulted in reduced synaptic vesicle endocytosis. **(F)** Quantification of SypHy signal as decay time constants (tau of vesicle endocytosis, monoexponential fit) in individual neurons. **(G)** Average decay time constants (black control; red N-cadherin knockout; n=15/14 neurons). Synaptic vesicle endocytosis was slower in N-cadherin knockout neurons indicating a defect in endocytosis. Total SypHy puncta analysed were 203/268. Data is represented as mean \pm SEM. * P<0.05 ** P<0.01 (Student's t-test).

To directly confirm the effects of temperature on vesicle cycling, I additionally compared the control results from room temperature and near physiological temperature experiments. SypHy signal related to exocytosis appeared to be decreased in control neurons at near physiological temperature ($28.7 \pm 1.8\%$ of NH_4Cl signal, $n=15$ cells) as compared to room temperature ($40.3 \pm 2.4\%$ of NH_4Cl signal, $n=12$ cells; Fig. 3.4A-C). As expected, the decay in SypHy fluorescence was stronger ($P<0.05$) at 34°C ($75.2 \pm 4.5\%$ of exocytosis, $n=15$ cells) than at 25°C ($59.1 \pm 4.8\%$ of exocytosis, $n=12$ cells; Fig. 3.4D-E) in control cells. Furthermore, increasing the temperature to 34°C resulted in significantly ($P<0.01$) faster decay kinetics in control cells (32.1 ± 3.1 s; $n=15$ cells) as compared to 25°C data (53.9 ± 6.3 s; $n=12$ cells; Fig. 3.4F-G).

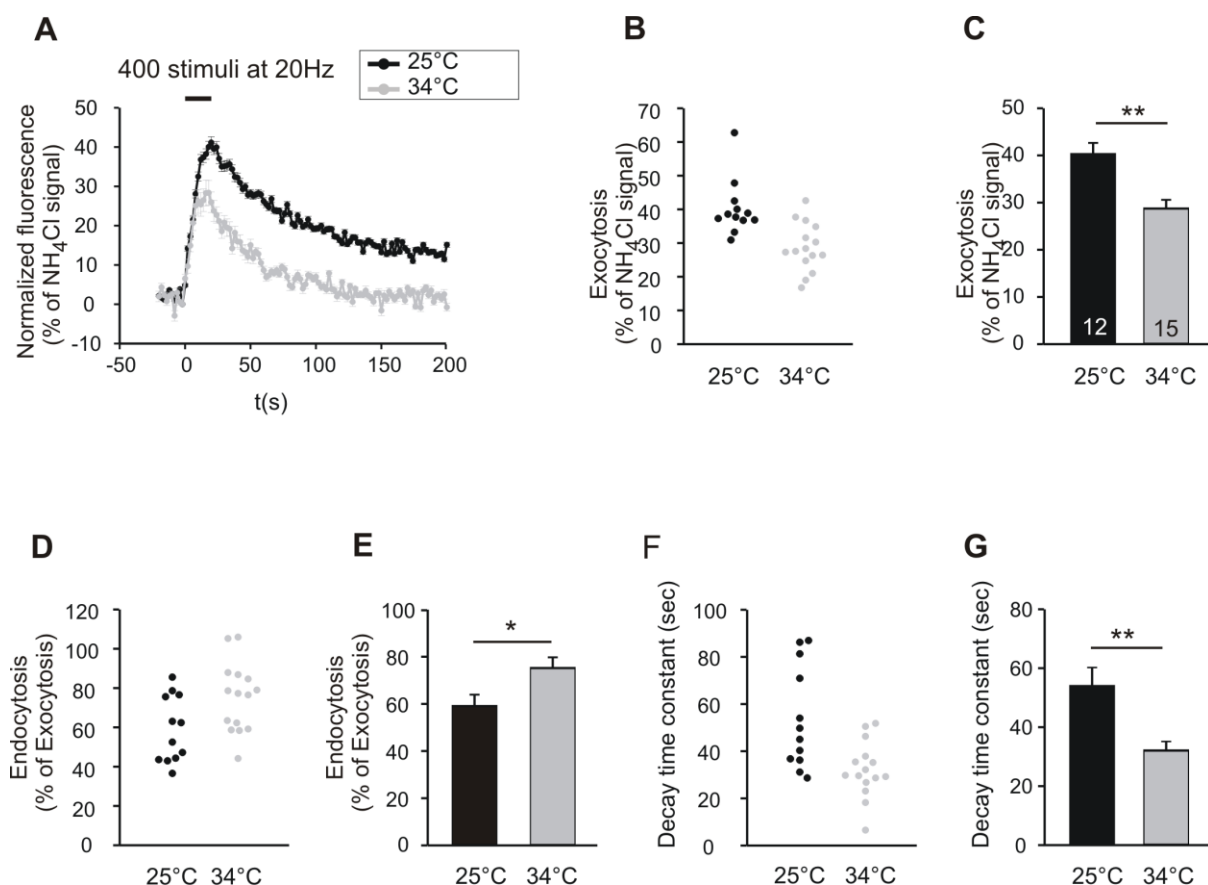


Figure 3.4 Effects of temperature on synaptic vesicle exo- and endocytosis

(A-G) Increasing the temperature from room (25°C) to near physiological (34°C) temperature had an enhancing effect on synaptic vesicle endocytosis. **(A)** Example traces of mean SypHy fluorescence intensities (black 25°C ; gray 34°C). **(B)** Quantification of mean SypHy amplitude (at the end of

stimulation) as synaptic vesicle exocytosis in individual neurons. **(C)** Average exocytosis. Increasing the temperature from 25°C to 34°C resulted in reduced exocytosis related SypHy signal. **(D)** Quantification of vesicle endocytosis at 90 seconds after the end of stimulation (SypHy signal loss as % of exocytosis) in individual neurons. **(E)** Quantification of average endocytosis at 90 seconds (% of exocytosis). Synaptic vesicles are endocytosed faster at near physiological temperature than at room temperature. **(F)** Quantification of SypHy signal as decay time constants (tau of endocytosis, monoexponential fit) in individual neurons. **(G)** Average decay time constants at room and near physiological temperature (black 25°C; gray 34°C; n=12/15 neurons). Synaptic vesicle endocytosis was significantly slower at room temperature. Total SypHy puncta analysed were 267/203. * P<0.05 ** P<0.01 (Student's t-test). Whenever normality test failed, Mann-Whitney's test on ranks was performed, *** P<0.001. The data in this figure are the same as control data in Fig 3.2 and Fig 3.3.

In summary, these results showed that increasing the temperature to 34°C resulted in faster endocytosis confirming its strong sensitivity towards temperature. On the other hand, the exocytosis related SypHy signal seemed to be reduced at near physiological temperature. This somewhat unexpected result is most likely a consequence of the faster endocytosis thus limiting the number of vesicles accumulating in the presynaptic membrane and thereby reducing the amplitude of the exocytosis related SypHy signal.

3.1.4 Effects of NcadΔE mediated inhibition of N-cadherin functions on vesicle cycling at near physiological temperature

Next, I used an alternative approach to confirm the N-cadherin knockout results. N-cadherin functions were inhibited by overexpressing a dominant-negative N-terminal truncated N-cadherin construct lacking the extracellular domains (NcadΔE). NcadΔE inhibits the functions of endogenous N-cadherin by binding with various catenin's and thus interfering with actin signaling (Togashi et al., 2002; Stan et al., 2010; Andreyeva et al., 2012). Cortical neurons from control (C57/BL6) mice were cultured in an autaptic microisland system and co-transfected with DsRed2 and SypHy at 9 DIV. To inhibit the functions of endogenous N-cadherin, NcadΔE was co-transfected additionally. Vesicle cycling was induced by electrical stimulation (400 stimuli at 20Hz) and SypHy imaging was performed (12-13 DIV) at near physiological temperature (34°C).

The normalized SypHy fluorescence intensities (exocytosis) at the end of stimulation were not altered after inhibiting N-cadherin functions (29.6 ± 2.4 % of NH_4Cl signal, $n=11$ neurons) as compared to controls (29.6 ± 2.4 % of NH_4Cl signal, $n=16$ neurons; Fig. 3.5A-C). The amount of SypHy fluorescence lost by vesicle endocytosis 90 seconds after the end of stimulation (as % of exocytosis) was significantly ($P<0.01$) reduced in Ncad ΔE overexpressing neurons (60.1 ± 4.4 % of exocytosis, $n=11$ cells) as compared to the control cells (76.5 ± 3.5 % of exocytosis, $n=16$ cells; Fig. 3.5D, E). The mean decay time constant showed a significant ($P<0.001$) increase (48.3 ± 5.05 s; $n=11$ cells) in neurons with inhibited N-cadherin functions as compared to the control cells (29.4 ± 3.7 s; $n=16$ cells Fig. 3.5F, G) indicating slower SypHy signal decay kinetics after inhibition of N-cadherin functions.

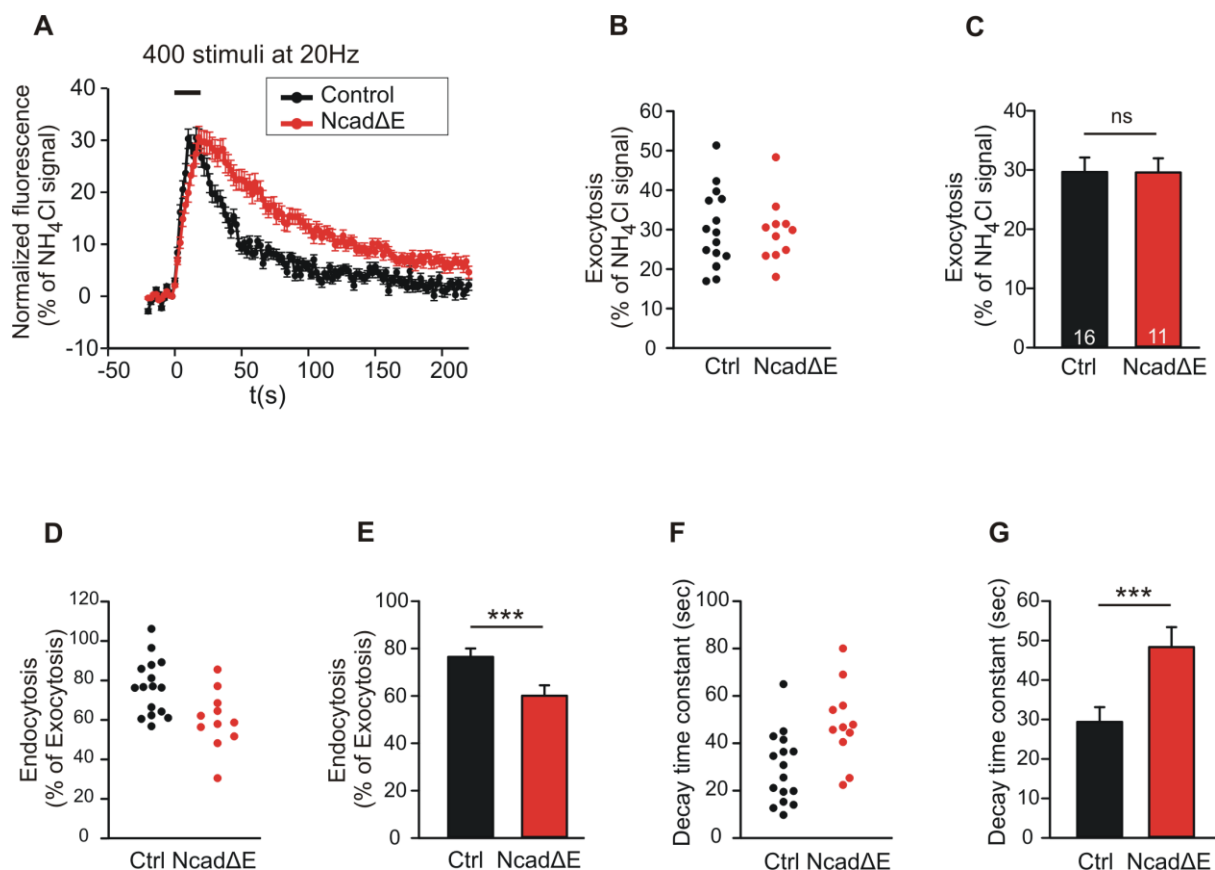


Figure 3.5 Effects of inhibiting the functions of N-cadherin by Ncad ΔE overexpression on vesicle exo- and endocytosis

Neurons were co-transfected with DsRed2 and SypHy at 9 DIV. N-cadherin functions were inhibited by co-expressing a dominant negative (Ncad Δ E) construct of N-cadherin lacking extracellular domains for 3-4 days in individual cortical neurons cultured from wildtype (C57/BL6) mice and SypHy imaging was done on 12-13 DIV by electrically stimulating the cultures (400 stimuli, 20 Hz) at near physiological temperature (34°C).

(A-G) Synaptic vesicle endocytosis was significantly slower upon blocking the functions of N-cadherin at near physiological temperature (34°C). **(A)** Example time course traces of mean SypHy puncta fluorescence intensities after normalizing with NH₄Cl signal (black control; red Ncad Δ E expression). **(B)** Quantification of mean SypHy amplitude (at the end of stimulation) as synaptic vesicle exocytosis in individual neurons. **(C)** Average exocytosis. **(D)** Quantitative analysis of SypHy signal lost by vesicle endocytosis at 90 seconds after stimulation (normalized to the % of exocytosis signal) in individual neurons. **(E)** Average endocytosis at 90 seconds (% of exocytosis). Vesicle endocytosis was reduced after disrupting the functions of N-cadherin. **(F)** Quantification of the rate of endocytosis as decay time constant of the SypHy signal (tau of endocytosis, monoexponential fit) in individual neurons. **(G)** Average decay time constants (black control; red Ncad Δ E; n=16/11 neurons). Vesicle endocytosis was significantly slower after inhibiting the N-cadherin functions. Total number of SypHy puncta analysed was 463/187. * P<0.05 ** P<0.01 (Student's t-test).

These findings strongly confirmed our previous observations that N-cadherin plays an important regulatory role in synaptic vesicle endocytosis. Exocytosis seemed not to be affected by inhibition of N-cadherin functions.

3.1.5 Effects of N-cadherin knockout on vesicle exocytosis in weak stimulation condition

Next experiment was designed to address the functional effects of N-cadherin knockout on vesicle exocytosis.

A previous paper from our lab (Jüngling et al., 2006) had reported impairment in the replenishment of the readily releasable vesicle pool indicating a defect in vesicle exocytosis in the absence of N-cadherin. But I did not observe any change in synaptic vesicle exocytosis in the above experiments. However, I used electrical field stimulation of 400 stimuli at 20 Hz to induce the vesicle cycling in all the previous experiments. This stimulation condition resulted in a strong synaptic vesicle release which was required to quantify the decay time kinetics (vesicle endocytosis). But this strong (long-lasting) vesicle release might have led to the depletion of readily releasable vesicle pool and thereby forcing the synapses to recruit synaptic vesicles

from the other vesicle pools available at the synapses thus obscuring the defect in vesicle exocytosis. Therefore, despite the defect in vesicle exocytosis in the absence of N-cadherin, we observed no change simply because of the experimental conditions.

To test this hypothesis, cortical neurons were co-transfected at 9 DIV with DsRed2 and SypHy. N-cadherin knockout was induced by co-expressing Cre for 5-6 days. Synaptic vesicle cycling was induced with 100 stimuli at 20 Hz and SypHy imaging was performed at near physiological temperature. 100 stimuli led to a relatively weak synaptic vesicle release in the control neurons as indicated by a strong reduction in the amplitude of the SypHy signal (exocytosis) as compared to the control cells in Fig. 3.3. The results were compared with SypHy amplitude obtained from N-cadherin knockout neurons. The mean amplitude of normalized SypHy fluorescence signals (exocytosis) at the end of stimulation was significantly ($P < 0.05$) lower in N-cadherin knockout neurons (19.3 ± 1.9 % of NH_4Cl signal, $n = 20$ cells) as compared to the control cells (24.9 ± 1.9 % of NH_4Cl signal, $n = 20$ cells; Fig. 3.6A-C). I also analysed the exocytosis related SypHy signals at single puncta level. Direct comparison of the SypHy fluorescence signals obtained from individual puncta also revealed a significant ($P < 0.001$) reduction in synaptic vesicle exocytosis in N-cadherin knockout neurons (21.3 ± 0.77 % of NH_4Cl signal, $n = 366$ SypHy puncta) as compared to the control cells (27.4 ± 0.81 % of NH_4Cl signal; $n = 333$ SypHy puncta; Fig. 3.6F). The decay kinetics of SypHy signal could not be reliably determined because of the strong noise in SypHy traces. So, to avoid the fitting of these noisy SypHy traces, loss of SypHy fluorescence signal (% of exocytosis) 44 seconds after the end of the stimulation was quantified and measured as vesicle endocytosis. N-cadherin knockout neurons showed a significantly ($P < 0.05$) reduced endocytosis-related SypHy signal loss (47.4 ± 7.3 % of exocytosis, $n = 20$ cells) as compared to the control cells (66.3 ± 5.0 % of exocytosis, $n = 20$ cells; Fig. 3.6D, E).

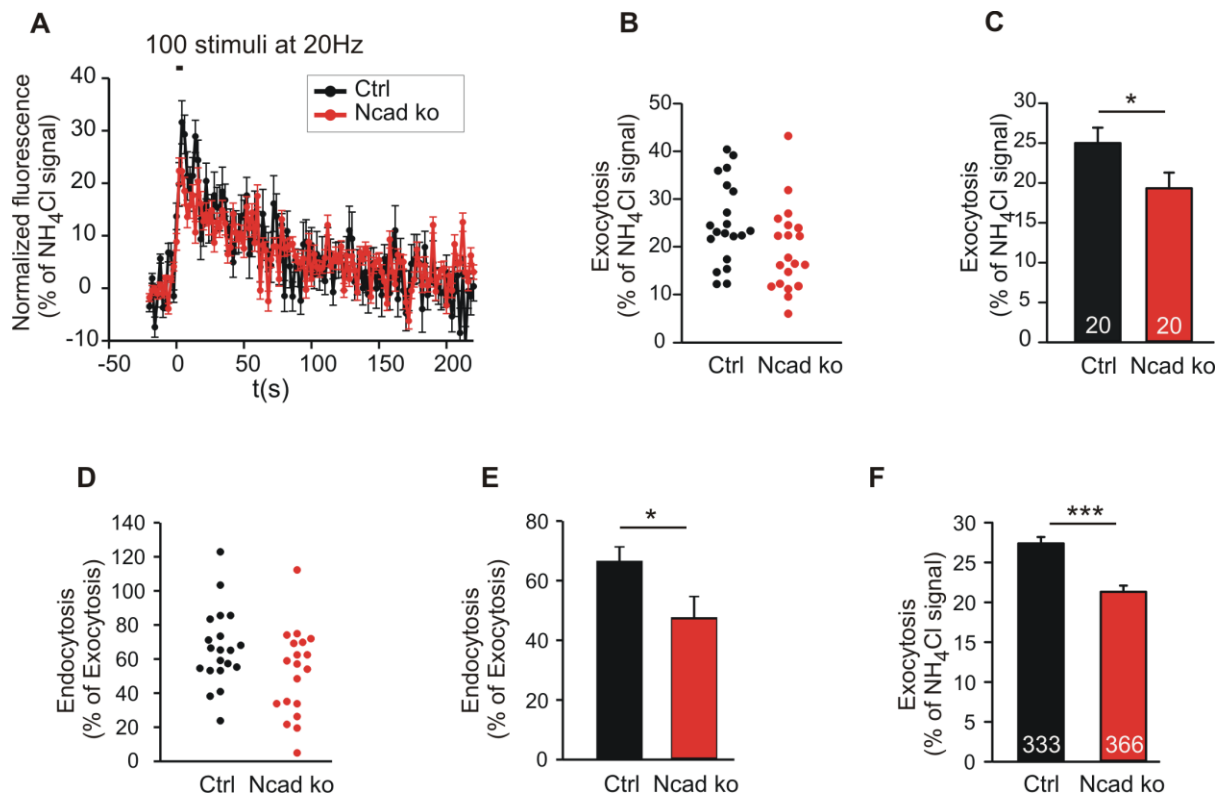


Figure 3.6 Release dependent effects of N-cadherin knockout on synaptic vesicle exocytosis

Cortical neurons were co-transfected with DsRed2 and SypHy at 9 DIV. Cre was co-expressed for 5-6 days to remove N-cadherin gene in individual cortical neurons and SypHy imaging was performed at 14-15 DIV at near physiological temperature (34°C). Vesicle cycling was induced with 100 stimuli (20 Hz) to evoke weak release.

(A-E) N-cadherin knockout resulted in a reduced synaptic vesicle exo- and endocytosis during slow release conditions at near physiological temperature (34°C). **(A)** Average normalized SypHy traces in response to 100 stimuli at 20Hz (black control cell; red N-cadherin knockout cell). **(B)** Quantification of mean SypHy amplitude (SypHy signal normalized with NH₄Cl signal) as a vesicle exocytosis at the end of stimulation in individual neurons. **(C)** Average Exocytosis. Note the reduction in normalized SypHy signal (vesicle exocytosis) at the end of stimulation in N-cadherin knockout neurons. **(D)** Quantification of vesicle endocytosis at 44 seconds after the end of stimulation (SypHy signal loss as % of exocytosis) in individual neurons. **(E)** Average endocytosis at 44 seconds (% of exocytosis; n=20/20 neurons) after the end of stimulation. Synaptic vesicle endocytosis was significantly reduced in N-cadherin knockout neurons during weak stimulations. **(F)** Quantification of average SypHy amplitude (SypHy signal normalized with NH₄Cl signal) as a vesicle exocytosis at puncta level. Total SypHy puncta analysed were 333/366. * P<0.05 (Student's t-test). Whenever normality test failed, Mann-Whitney's test on ranks was done, *** P<0.001.

With this experiment, I showed that N-cadherin also affects the synaptic vesicle exocytosis but only during weak stimulation conditions (weak vesicle release). These data together with previously published results (Jüngling et al., 2006; Vitreira et al., 2011; van Stegen et al., 2017) confirmed that N-cadherin plays an important regulatory role in both vesicle exo- and endocytosis.

SypHy imaging depends on the intravesicular pH change of the synaptic vesicles and don't differentiate between the single synaptic vesicle retrieval (clathrin-mediated endocytosis) and endosomes (bulk endocytosis). Therefore, SypHy imaging can't be used to examine different modes of vesicle retrieval.

Next experiments were performed to differentially label clathrin-mediated endocytosis and bulk endocytosis using fluorescent molecules.

3.2 Monitoring the functional role of N-cadherin in synaptic vesicle endocytosis using FM1-43 and tetramethylrhodamine (TMR)-dextran uptake

As a next step, I explored the functional role of N-cadherin in regulation of different modes of vesicle endocytosis in detail. At central synapses, presynaptically fused vesicular membranes are required to be recycled to restore the presynaptic terminal's original surface area, and to prevent depletion of vesicle pools. This recycling can be achieved by various modes of vesicle endocytosis like clathrin-mediated endocytosis and activity-dependent bulk endocytosis (bulk endocytosis). Clathrin-mediated endocytosis (CME) is relatively slow and retrieves single synaptic vesicles from the presynaptic plasma membrane by forming coats of clathrin protein. On the other hand, bulk endocytosis is triggered during intense vesicle release and is characterized by large invaginations of plasma membrane to form endosome-like structures. Various fluorescent probes are available to differentially label clathrin-mediated endocytosis and bulk endocytosis. One such fluorescent marker is FM1-43, an activity-dependent hydrophobic dye known to specifically label actively cycling vesicles (Cousin and Robinson, 1999; Harata et al., 20001). FM1-43 binds non-specifically to the presynaptic membrane. Upon synaptic stimulation, FM1-43 is taken up inside the invaginations irrespective of the size of the endocytic pits, thus

reporting all forms of endocytosis. Bulk endocytosis can be visualized by monitoring the uptake of tetramethylrhodamine-dextran (TMR-dextran, 40 kDa). TMR-dextran is a high molecular weight fluid phase marker conjugated to a fluorescent molecule and labels specifically endosomes (bulk endocytosis) (Clayton and Cousin, 2009).

3.2.1 Stimulation and temperature dependent characteristics of FM1-43 and TMR-dextran uptake

First experiments were done to test whether FM1-43 and TMR-dextran can distinguish between clathrin-mediated endocytosis and bulk endocytosis.

To address this, dissociated cortical neurons (from C57/BL mice) were stimulated with three different electrical field stimulations (200, 400, and 2000 stimuli at 20Hz) to obtain variation in synaptic vesicle release (weak to strong release) at room temperature (RT, 25°C) and at 34°C in the presence of FM1-43 and TMR-dextran. After washing, a punctate staining was observed for both FM1-43 and TMR-dextran (Fig 3.7).

FM1-43 puncta correspond to the active synaptic vesicle clusters. The FM1-43 fluorescence image was merged with the TMR-dextran image to get an overlay. These images were first compared for their subcellular distribution of FM 1-43 dye and TMR-dextran. Overlay images showed co-localisation of FM1-43 with TMR-dextran puncta confirming the specific uptake of the majority of TMR-dextran puncta at synaptic terminals. The fraction (%) of FM1-43 puncta co-localising with TMR-dextran per field of view were counted and plotted as a measure of bulk endocytosis.

When the cortical neurons were stimulated with 200 stimuli at 20Hz at room temperature (25°C), the majority of synaptic terminals were labeled with FM1-43 (Fig. 3.7A, left). Only a few FM1-43 labeled puncta (15.11 ± 3.39 %; Fig. 3.7D) showed a co-localisation with TMR-dextran puncta, indicating little TMR-dextran uptake (bulk endocytosis) at this experimental condition. This indicated that clathrin-mediated endocytosis is the main mode of vesicle retrieval at this condition. Increasing the temperature to 34°C resulted in a increased co-localisation of FM1-43 (33.78 ± 3.45 %, Fig. 3.7D) labeled puncta with TMR-dextran stained puncta showing increased bulk endocytosis at 34°C (Fig. 3.7A, right).

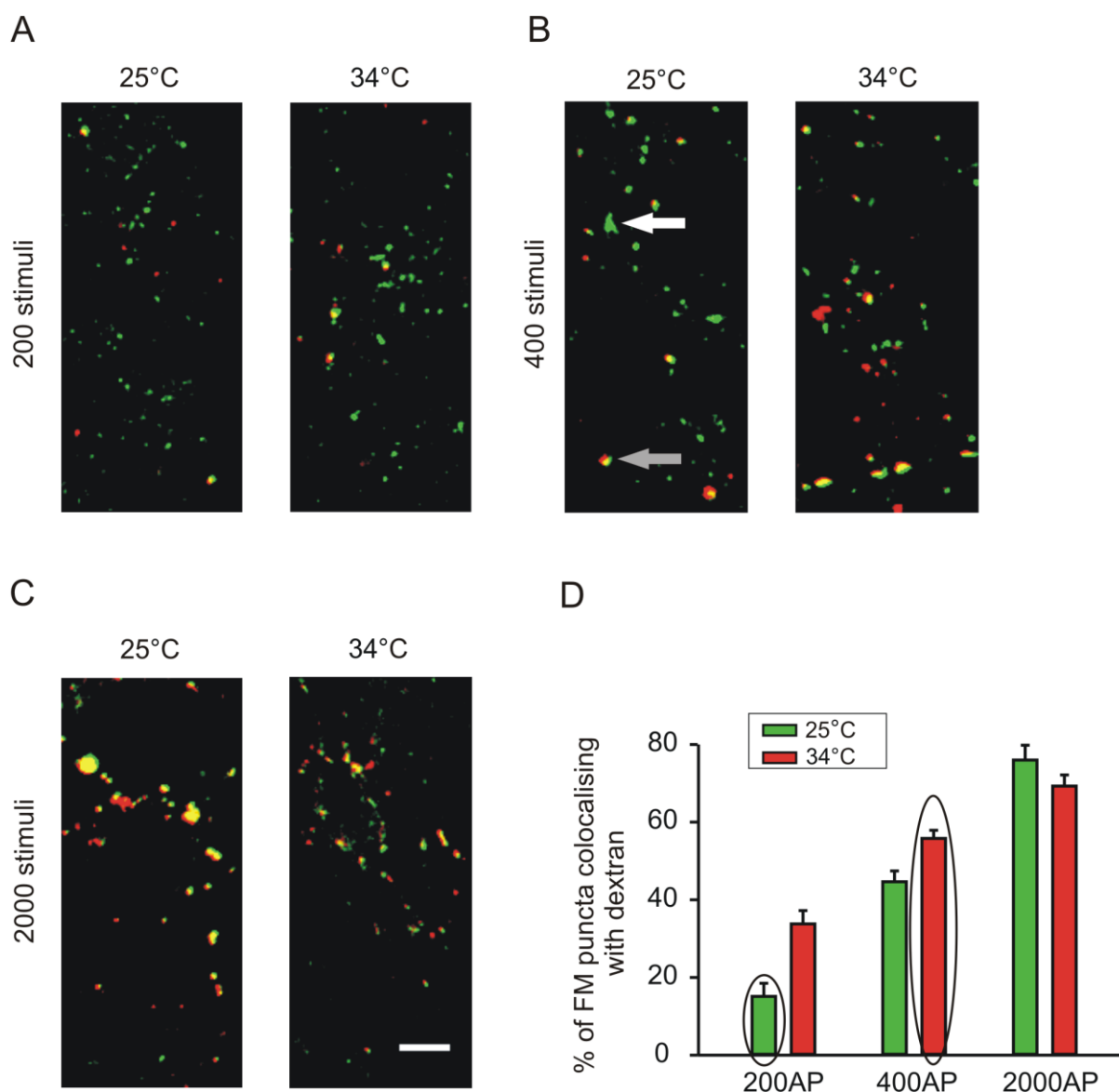


Figure 3.7 Differential labeling of clathrin-mediated endocytosis and bulk endocytosis using FM1-43 and tetramethylrhodamine-dextran (TMR-dextran) uptake

Cortical neurons were co-stained with FM1-43 and dextran using different stimulation paradigm at room (25°C) and near physiological temperature (34°C) to distinguish clathrin-mediated endocytosis from bulk endocytosis. FM puncta without TMR-dextran uptake (green) represented clathrin-mediated endocytosis, while FM1-43 + TMR-dextran (yellow) represented bulk endocytosis.

(A) Representative overlay images of FM1-43 (green) and TMR-dextran (red) loading induced by 200 stimuli at either 25°C or 34°C. At this stimulation (25°C), the majority of the vesicular membrane is endocytosed via clathrin-mediated endocytosis (green puncta). With increase in temperature, there was a slight increase in the TMR-dextran uptake (yellow puncta). **(B)** Example overlay images of FM1-43 (green puncta) and TMR-dextran (red puncta) uptake induced by 400 stimuli at either 25°C or 34°C. An electrical field stimulation of 400 stimuli at 34°C resulted in an increase in both FM1-43 and TMR-dextran uptake. **(C)** Example overlay images of FM1-43 and TMR-dextran loading induced by

2000 stimuli at either 25°C or 34°C. Most of the puncta were co-stained with FM1-43 and TMR-dextran (yellow). No effect of temperature change was observed. **(D)** Quantification of the percentage of FM 1-43 positive puncta co-localising with TMR-dextran. Scale bar 5 μ m. n=8/11/6/9/9/9, n represents fields of view.

With the increase in stimulation (400 stimuli at 20Hz, 25°C), there was an overall increase in the percentage of FM1-43 labeled puncta co-localising with TMR-dextran stained puncta (44.65 ± 2.76 %). Increased temperature (400 stimuli, 34°C) also resulted in a higher TMR-dextran uptake (55.80 ± 2.09 % of synapses had both FM1-43 and dextran staining) confirming that strong vesicle release and near physiological temperature, both have an enhancing effect on TMR-dextran staining (uptake) (Fig. 3.7B). Synapses undergo bulk endocytosis along with slower clathrin-mediated endocytosis at this experimental condition.

In another experiment, intense synaptic vesicle exocytosis was induced by stimulating the cortical neurons with 2000 stimuli at 25°C (Fig. 3.7C, left). 75.99 ± 3.81 % of the synapses (Fig. 3.7D) were labeled with both FM1-43 and TMR-dextran, indicating that the majority of synaptic vesicles was recycled via bulk endocytosis during strong synaptic release. When the temperature was increased to 34°C while keeping the stimulation at 2000 stimuli, 69.29 ± 2.85 % of FM1-43 puncta co-localised with TMR-dextran, showing no effect of temperature at this stimulation condition (Fig. 3.7C, right, D).

In summary, these results confirmed that synapses undergo clathrin-mediated endocytosis during weak stimulation. In contrast, long lasting synaptic vesicle release demands faster synaptic vesicle retrieval and synapses meet this demand by retrieving large pieces of presynaptic membrane in the form of bulk endosomes (bulk endocytosis).

The data from this experiment helped to select two stimulation conditions to differentially induce clathrin-mediated endocytosis and bulk endocytosis. For further experiments, clathrin mediated endocytosis (CME) was studied using an electrical stimulation with 200 stimuli at 25°C, and bulk endocytosis was studied with 400 stimuli stimulation at 34°C.

3.2.2 Functional role of N-cadherin in regulating clathrin-mediated endocytosis and bulk endocytosis

To investigate the functional role of N-cadherin in clathrin-mediated endocytosis and in bulk endocytosis, Cre mediated conditional knockout and Ncad Δ E induced inhibition of N-cadherin function approaches were used.

3.2.2.1 Effects of N-cadherin knockout on clathrin-mediated endocytosis (CME)

To investigate the effects of N-cadherin on clathrin-mediated endocytosis, cortical neurons were cultured from homozygous floxed mice (Ncad^{flox/flox}) on PO coated coverslips. At 9 DIV, neurons were co-transfected with Cre and BFP to knockout the postsynaptic N-cadherin. BFP was used to visualize the individual transfected neurons. At 14-15 DIV, FM1-43 and TMR-dextran staining was done by electrically stimulating the neurons with 200 stimuli at 20Hz at room temperature (25°C). Most of the synaptic contacts were loaded up with FM1-43 dye confirming that clathrin-mediated endocytosis is the main mode of vesicle recycling at this experimental condition (as shown in Fig. 3.8). There was also a slight TMR-dextran staining probably representing baseline uptake. To quantify the effects of N-cadherin knockout on clathrin-mediated endocytosis, FM1-43 puncta on dendrites were counted and the puncta density (/10 μ m of dendrite length) was calculated.

Although TMR-dextran staining was relatively weak at this experimental condition, FM1-43 puncta co-localising with TMR-dextran were still quantified to examine the change in bulk endocytosis. Overlay images showed reduced FM1-43 uptake in N-cadherin knockout neurons at 14-15 DIV (Fig. 3.8A). Cre-mediated conditional knockout of N-cadherin significantly ($P < 0.05$) decreased the total FM1-43 puncta density (1.24 ± 0.16 puncta/10 μ m dendrite, $n = 13$ cells) as compared to control cells (BFP, 1.80 ± 0.20 puncta/10 μ m dendrite, $n = 16$ cells; Fig. 3.8B, C). However, the number of FM1-43 puncta co-localising with TMR-dextran puncta were not altered significantly after N-cadherin knockout (BFP: 0.69 ± 0.08 puncta/10 μ m dendrite, $n = 16$ cells; N-cadherin knockout + BFP: 0.58 ± 0.12 puncta/10 μ m dendrite, $n = 13$ cells; Fig 3.8D, E). In contrast, FM1-43 puncta without any TMR-dextran staining (representing pure CME) were significantly ($P < 0.01$) reduced (0.66 ± 0.12 puncta/10 μ m dendrite, $n = 13$ cells) in N-cadherin knockout neurons as compared to control cells (1.11 ± 0.13 puncta/10 μ m dendrite, $n = 16$ cells; Fig 3.8F, G).

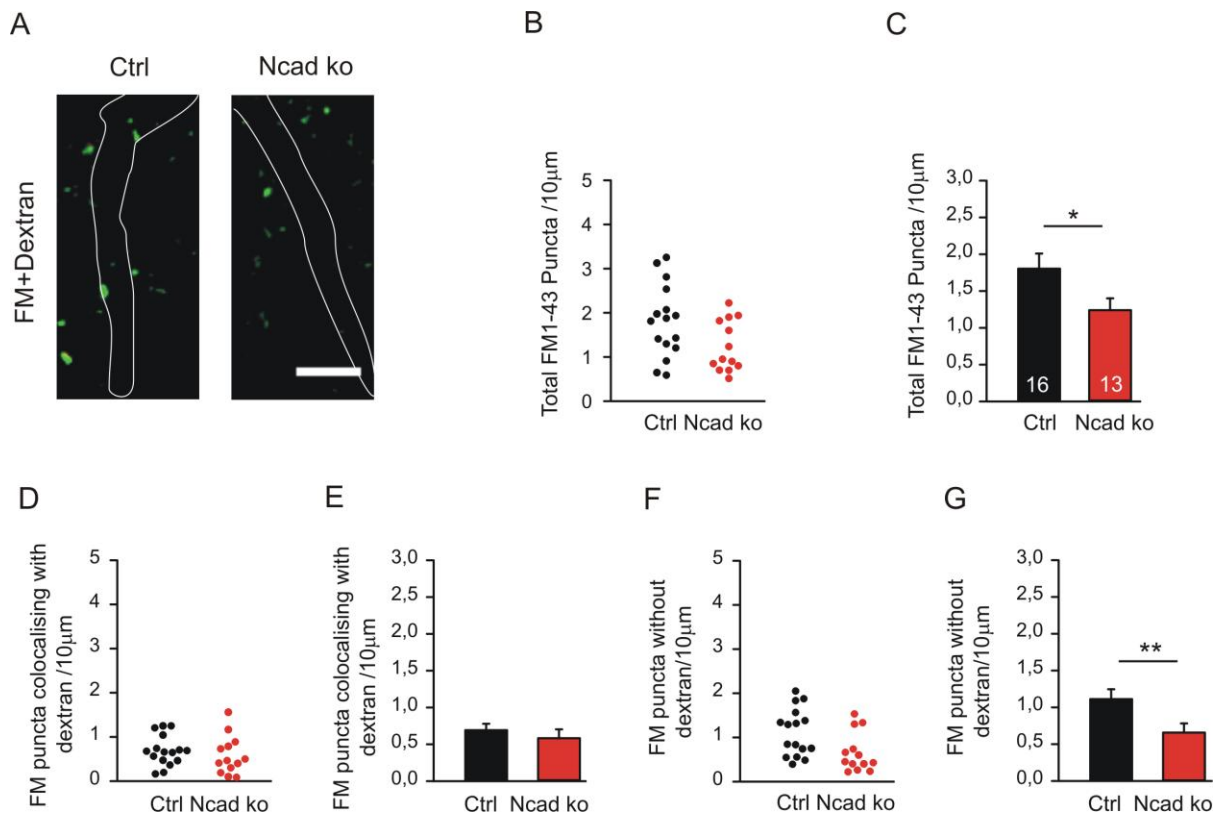


Figure 3.8 Reduction in clathrin-mediated endocytosis in N-cadherin knockout neurons

Knockout of N-cadherin was induced by postsynaptic expression of Cre (for 5-6 days) in individual cortical neurons. FM1-43 and TMR-dextran uptake was induced by electrical stimulation (200 stimuli, 20Hz at 25°C).

(A-G) Cre mediated conditional knockout of N-cadherin (postsynaptic) resulted in a reduced clathrin-mediated endocytosis (CME) at 14-15 DIV cortical neurons. **(A)** Example overlay images of FM1-43 labeled vesicle clusters (green) and TMR-dextran labeled endosomes (red (Ctrl left; +cre right). Dendrites are shown by white outlines. **(B)** Quantification of dendritic density of total FM1-43 labeled puncta in individual neurons in the presence and after knockout of N-cadherin. **(C)** Quantification of the average density of total FM1-43 puncta on the dendrites of the transfected neurons (black control cells; red +cre cells). There is a clear reduction in total FM1-43 uptake (CME only) in N-cadherin knockout cells. **(D)** Quantification of the dendritic density of FM1-43 puncta co-localised with TMR-dextran in individual neurons. **(E)** Quantification of the average density of FM1-43 puncta co-localised with TMR-dextran. Dextran uptake is very weak at given experimental conditions (probably baseline uptake). **(F)** Quantification of the dendritic density of FM1-43 puncta (no co-localisation with TMR-dextran) in individual neurons. **(G)** Quantification of the average dendritic density of FM1-43 (n=16/13 cells). There was a strong reduction in the number of puncta with only FM uptake indicating a defect in clathrin-mediated endocytosis after N-cadherin knockout. BFP: n=16; CreEGFP + BFP= 13 (n represents number of cells). Scale bar 5 µm. * P<0.05 (Student's t-test). Whenever the normality test failed, Mann-Whitney's test on ranks was used, ** P<0.01.

In summary, knockout of N-cadherin from mature cortical neurons (14-15 DIV) resulted in a reduction in total FM1-43 puncta indicating a defect in endocytosis (mainly clathrin-mediated endocytosis). There were a few FM1-43 puncta which showed co-localisation with TMR-dextran puncta indicating weak bulk endocytosis. This indicated that neurons probably have some basal uptake of TMR-dextran at weak stimulation condition and that this uptake is not affected by N-cadherin knockout. FM1-43 puncta without any TMR-dextran represented pure clathrin-mediated endocytosis and pure FM1-43 puncta number was significantly reduced in N-cadherin knockout neurons confirming altered clathrin-mediated endocytosis.

3.2.2.2 Effect of N-cadherin knockout on bulk endocytosis

All experimental conditions were analogous to the previous experiment except that vesicle cycling was induced with 400 stimuli at 20Hz in the presence of FM1-43 and TMR-dextran at near physiological temperature (34°C). To study activity-dependent bulk endocytosis, neuronal cultures were transfected with BFP and stimulated. Overlay images showed a striking co-localisation of FM1-43 signal and TMR-dextran puncta (Fig. 3.9A) confirming that during strong stimulations, synapses undergo vesicle recycling via bulk endocytosis. There was an increase in total FM1-43 uptake also.

To evaluate the N-cadherin knockout effect on bulk endocytosis, total FM1-43 puncta density /10 μm of dendrite length (bulk endocytosis + CME) as well as FM1-43 puncta density co-localising with TMR-dextran puncta (bulk endocytosis) were calculated. Total FM1-43 puncta density was significantly ($P < 0.001$) decreased after knockout of N-cadherin (1.32 ± 0.12 puncta/10 μm dendrite; $n = 28$ cells) as compared to control cells expressing only BFP (2.29 ± 0.21 puncta/10 μm dendrite, $n = 23$ cells; Fig. 3.9B-C). Importantly, the dendritic density of FM1-43 puncta co-localising with TMR-dextran puncta (bulk endocytosis) was also significantly ($P < 0.05$) reduced after N-cadherin knockout (Cre + BFP: 0.84 ± 0.08 puncta/10 μm dendrite; $n = 28$ cells) as compared to control cells (BFP: 1.37 ± 0.18 puncta/10 μm dendrite; $n = 23$ cells; Fig. 3.9D-E) indicating a defect in bulk endocytosis. Furthermore, pure clathrin-mediated endocytosis (CME) was calculated by counting the FM1-43 puncta without any TMR-dextran signal.

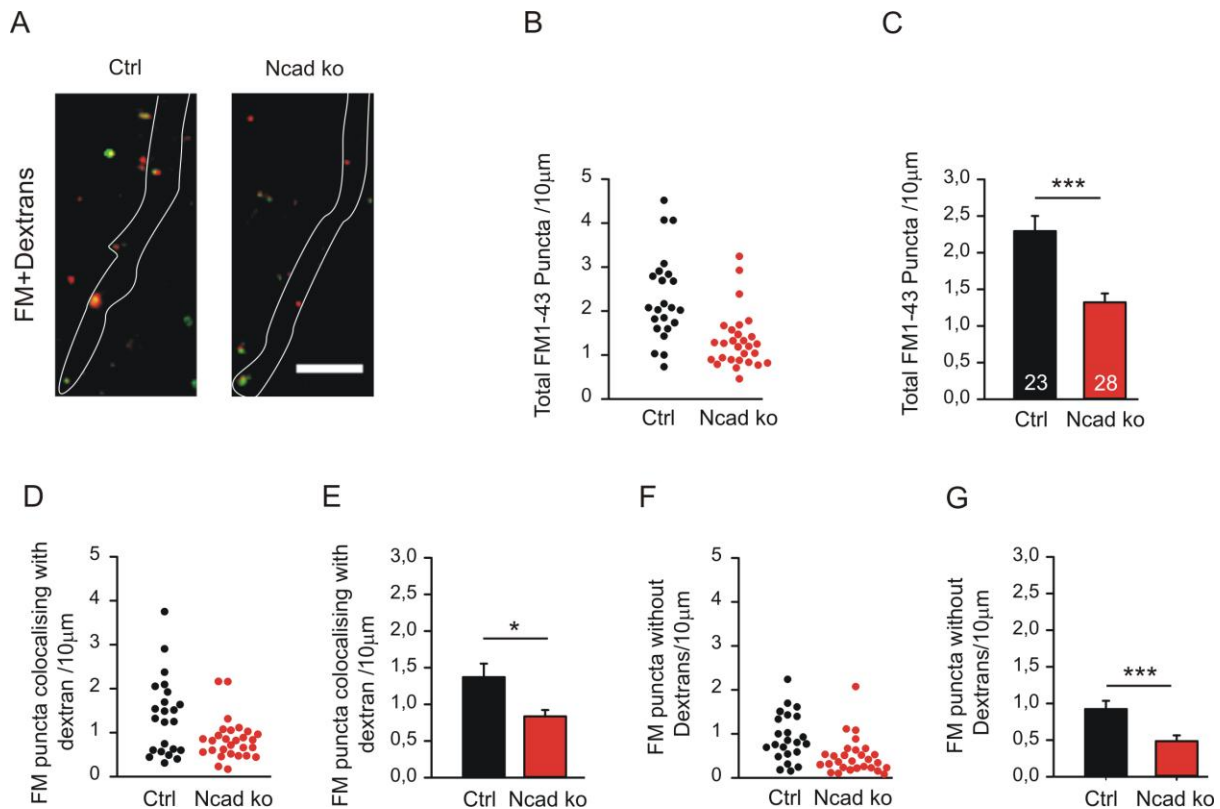


Figure 3.9 N-cadherin regulates both clathrin-mediated endocytosis and bulk endocytosis

Cortical neurons were co-transfected at 9 DIV and FM1-43 + TMR-dextran co-staining was done at 14-15 DIV. Vesicle cycling was induced by electrical stimulation (400 stimuli, 20Hz) at near physiological temperature (34°C).

(A-G) Postsynaptic knockout of N-cadherin by Cre expression resulted in a significant reduction in both clathrin-mediated endocytosis (CME) and bulk endocytosis. **(A)** Representative overlay images of cortical neurons double labeled with FM1-43 (green) and TMR-dextran (red) in control (left) and N-cadherin knockout neurons (+cre right). Dendrites are shown as white outlines. **(B)** Quantification of the dendritic density of total FM1-43 puncta (CME + bulk endocytosis) in individual neurons. **(C)** Quantification of the average density of total FM1-43 puncta. Total FM puncta number was significantly reduced after the knockout of N-cadherin indicating a strong reduction in total endocytosis (CEM + bulk endocytosis). **(D)** Quantification of the dendritic density of FM1-43 puncta co-localised with TMR-dextran in individual neurons. **(E)** Quantification of the average density of FM1-43 puncta co-localised with TMR-dextran. Interestingly, there was a strong reduction in TMR-dextran uptake in N-cadherin knockout neurons indicating reduced bulk endocytosis. **(F)** Quantification of the dendritic density of FM1-43 puncta (no co-localisation with TMR-dextran) in individual neurons and the average density of FM1-43 puncta **(G)**. BFP: n = 23 cells; CreEGFP + BFP = 28 (n represents number of neurons) Scale bar 5 µm. * P<0.05; ** P<0.01; *** P<0.001 (Mann-Whitney's test on ranks).

The results showed that FM1-43 puncta (representing pure CME) were also significantly ($P=0.001$) reduced (0.48 ± 0.07 puncta/ $10 \mu\text{m}$ dendrite; $n=28$ cells) in N-cadherin knockout neurons as compared to control cells (0.92 ± 0.11 puncta/ $10 \mu\text{m}$ dendrite; $n=23$ cells; Fig. 3.9F-G).

These results demonstrated that the expression of N-cadherin in mature neurons is important for both clathrin-mediated endocytosis as well as bulk endocytosis, confirming its role in vesicle recycling.

3.2.2.3 Effect of Ncad Δ E overexpression on clathrin-mediated endocytosis

Next, experiments were done to confirm the above described N-cadherin knockout findings using an alternative experimental approach. N-cadherin functions were inhibited by overexpressing a dominant-negative N-terminal truncated construct of N-cadherin lacking extracellular domains.

Dissociated cortical neurons were cultured from C57/BL mice on PO coated coverslips. At 9 DIV, individual neurons were co-transfected with BFP and Ncad Δ E to inhibit the functions of postsynaptic N-cadherin. Expression of BFP only was used as control. Transfected neurons were co-stained (12-13 DIV) with FM1-43 and TMR-dextran by stimulating with 200 stimuli (20Hz) at room temperature. This experimental condition was used to ensure that vesicle recycling occurs mainly via clathrin-mediated endocytosis (from Fig. 3.7A, left & Fig. 3.8). FM1-43 labeled vesicle clusters were counted and compared with control to quantify the effects of N-cadherin on vesicle endocytosis. Overlay images indicated that the majority of synaptic terminals were loaded up only with FM1-43 dye (Fig. 3.10A). The dendritic density of total FM1-43 puncta did not show any significant change after inhibiting the functions of N-cadherin (1.60 ± 0.18 puncta/ $10 \mu\text{m}$ dendrite; $n=18$ cells; Fig. 3.10B-C) as compared to control cells (1.76 ± 0.20 puncta/ $10 \mu\text{m}$ dendrite; $n=16$ cells; Fig. 3.10B-C). TMR-dextran labeling was relatively rare (basal uptake) at this experimental condition, but TMR-dextran uptake was still counted to observe the change in the basal uptake of TMR-dextran in Ncad Δ E overexpressing neurons.

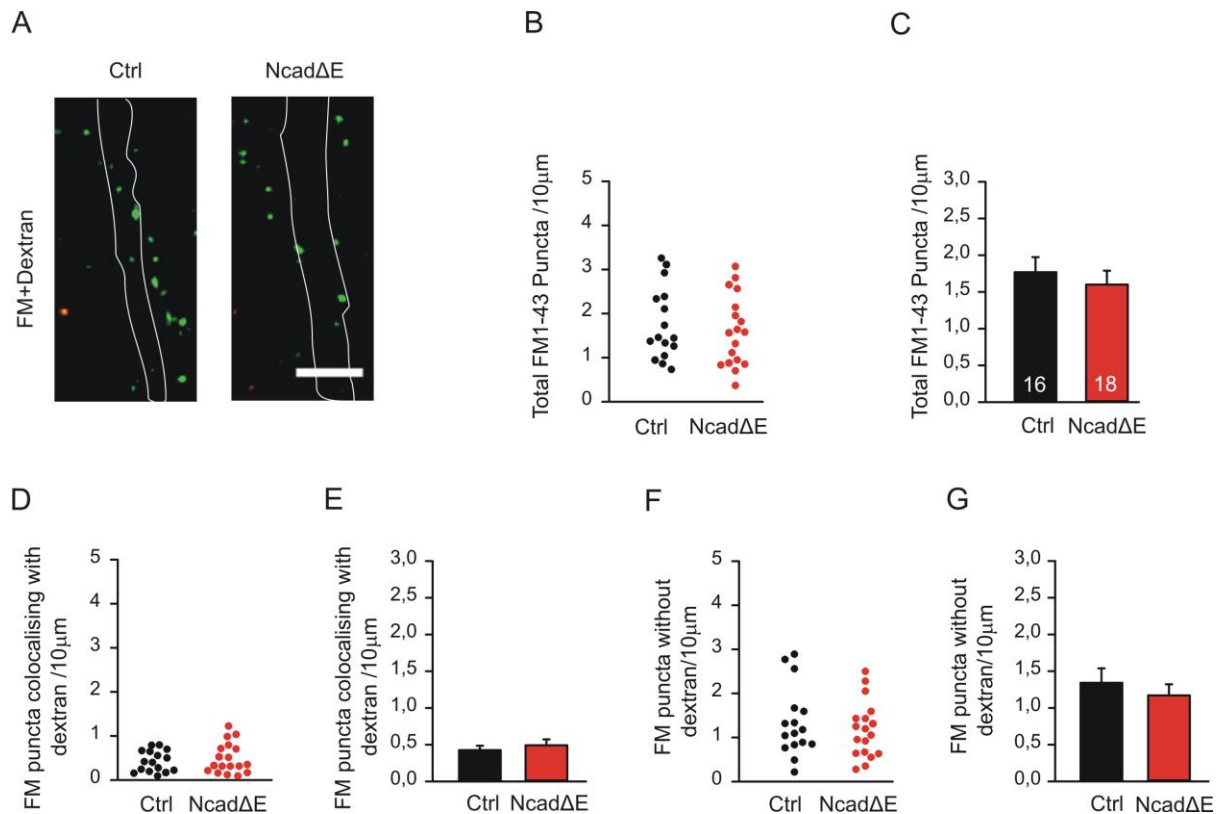


Figure 3.10 Effects of Ncad Δ E-mediated inhibition of N-cadherin functions on clathrin-mediated endocytosis

N-cadherin functions were inhibited by co-expressing a dominant-negative (Ncad Δ E) N-terminally truncated construct of N-cadherin lacking extracellular domains at 9 DIV in individual cortical neurons. FM1-43 and TMR-dextran staining was done at 12-13 DIV (after 3-4 days) by electrically stimulating the cells (200 stimuli, 20 Hz) at room temperature (25°C).

(A-G) Ncad Δ E mediated functional block of N-cadherin (postsynaptic) did not show any significant change in clathrin-mediated endocytosis (CME) in mature cortical neurons. **(A)** Example overlay images of FM1-43 (green) and TMR-dextran (red) co-staining in control neurons (left) and after inhibiting the functions of N-cadherin (Ncad Δ E, right). Dendrites are shown as white outlines. **(B)** Quantification of the dendritic density of total FM1-43 puncta in individual neurons. **(C)** Quantification of the average density of total FM1-43 puncta. Total FM1-43 puncta numbers were not affected after the inhibition of N-cadherin functions. **(D)** Quantification of the dendritic density of FM1-43 puncta co-localised with TMR-dextran puncta in individual neurons. **(E)** Quantification of the average density of FM1-43 puncta co-localised with TMR-dextran signal. TMR-dextran uptake is very low at given experimental conditions (probably baseline uptake). **(F)** Quantification of the dendritic density of FM1-43 puncta (not co-localising with TMR-dextran) in individual neurons and the mean density of FM1-43 **(G)**. FM puncta without any TMR-dextran signal were quantified as pure clathrin-mediated

endocytosis. CME was also not affected after inhibiting the functions of N-cadherin. $n=16/18$ neurons. Scale bar 5 μm . For statistics, Mann-Whitney's test on ranks was used.

FM1-43 puncta co-localising with dextran in control cells were low in number (BFP: 0.43 ± 0.06 puncta/10 μm dendrite; $n= 16$ cells; Fig. 3.10D-E) and their dendritic density was not altered significantly after overexpression of Ncad Δ E (Ncad Δ E + BFP: 0.49 ± 0.08 puncta/10 μm dendrite; $n= 18$ cells; Fig. 3.10D-E). Furthermore, the density of FM1-43 puncta (not co-localising with TMR-dextran, pure CME) also did not show any significant change (1.17 ± 0.15 puncta/10 μm dendrite; $n= 16$ cells) in Ncad Δ E overexpressing neurons as compared to control cells (1.34 ± 0.19 puncta/10 μm dendrite; $n= 18$ cells; Fig. 3.10F-G).

In summary, these results indicated that inhibiting the functions of N-cadherin by overexpressing Ncad Δ E did not have a significant effect on clathrin-mediated endocytosis in mature neurons (DIV 14-15). These results are different from that of N-cadherin knockout suggesting a weaker inhibition than obtained by gene knockout.

3.2.2.4 Effect of Ncad Δ E overexpression on bulk endocytosis

All experimental conditions were analogous to 3.2.2.3 except that the vesicle cycling was induced with 400 stimuli at 20Hz in the presence of FM1-43 and TMR-dextran at near physiological temperature (34°C). FM1-43 and TMR-dextran images were merged to make an overlay and the dendritic density of FM1-43 was calculated. Overlay images showed that stronger stimulation resulted in an increased co-localisation of FM1-43 and TMR-dextran puncta (Fig. 3.11A) in control cells, thereby confirming the activity-dependent uptake of both FM1-43 and TMR-dextran. With increased synaptic activity, bulk endocytosis also increased.

Total dendritic density of FM1-43 puncta was significantly ($P < 0.001$) decreased in neurons expressing Ncad Δ E (Ncad Δ E + BFP: 1.19 ± 0.09 puncta/10 μm dendrite; $n= 28$ cells) as compared to control cells. (BFP: 1.95 ± 0.17 puncta/10 μm dendrite; $n= 21$ cells; Fig. 3.11B-C). Interestingly, the dendritic density of FM1-43 puncta co-localising with TMR-dextran puncta (bulk endocytosis) was also significantly ($P < 0.001$) reduced after inhibiting the functions of N-cadherin (Ncad Δ E + BFP: 0.43 ± 0.04 puncta/10 μm dendrite; $n= 28$ cells) as compared to control cells (BFP: $1.07 \pm$

0.15 puncta/10 μm dendrite; $n = 21$ cells; Fig. 3.11D-E) indicating a defect in bulk endocytosis. However, the density of FM1-43 puncta not co-localising with TMR-dextran (pure CME) was not changed significantly ($P < 0.001$) (Ncad ΔE + BFP: 0.76 ± 0.09 puncta/10 μm dendrite, $n = 28$ cells; control cells, BFP: 0.87 ± 0.10 puncta/10 μm dendrite; $n = 21$ cells; Fig. 3.11F-G).

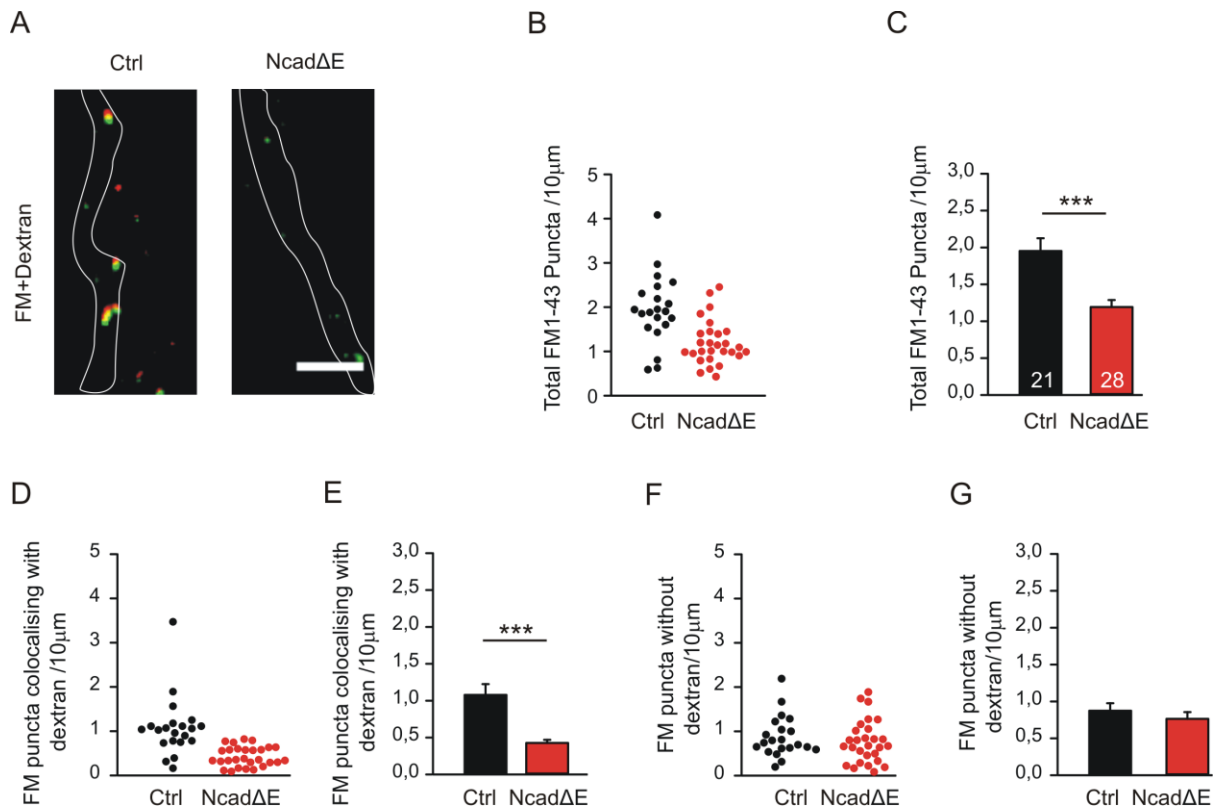


Figure 3.11 Effects of Ncad ΔE -mediated inhibition of N-cadherin functions on bulk endocytosis

Cortical neurons were co-transfected with BFP and Ncad ΔE at 9 DIV and FM + TMR-dextran co-staining was done at 12-13 DIV by electrical field stimulation (400 stimuli, 20 Hz) at near physiological temperature (34°C). Ncad ΔE overexpression led to the inhibition of N-cadherin functions.

(A-G) Postsynaptic inhibition of N-cadherin functions by Ncad ΔE overexpression resulted in a significant loss in bulk endocytosis. **(A)** Example overlay images of FM1-43 (green) and TMR-dextran (red) in control (left) and Ncad ΔE overexpressing neurons (right). Dendrites are shown as white outline. **(B)** Quantification of total FM1-43 puncta /10 μm dendrites in individual neurons. **(C)** Average dendritic density of total FM1-43 puncta. Total FM1-43 puncta numbers were strongly reduced after the inhibition of N-cadherin functions. **(D)** Quantification of the dendritic density of FM1-43 puncta co-localised with TMR-dextran puncta in individual neurons. **(E)** Quantification of the average dendritic

density of FM1-43 puncta co-localised with TMR-dextran signal. There was a strong reduction in dextran uptake after inhibiting the functions of N-cadherin indicating reduced bulk endocytosis. **(F)** Quantification of the dendritic density of FM1-43 puncta (not co-localising with TMR-dextran) in individual neurons and the average puncta density of FM1-43 that did not co-localise with TMR-dextran signal **(G)**. FM puncta without TMR-dextran co-localisation represented pure clathrin-mediated endocytosis. CME was not reduced significantly after inhibiting the functions of N-cadherin. n= 21/28 cells. Scale bar 5 μ m. *** P<0.001 (Mann-Whitney's test on ranks).

These results confirmed that similar to N-cadherin knockout, Ncad Δ E overexpression also inhibited bulk endocytosis. However, clathrin-mediated endocytosis was not affected by overexpression of Ncad Δ E suggesting a weaker inhibition than obtained with gene knockout. Ncad Δ E overexpression might be too weak to block all the interactions of endogenous N-cadherin. Clathrin-mediated endocytosis seemed not to be so sensitive, therefore it didn't show any alteration after the inhibition of N-cadherin functions in the above experiments (200 stimuli, 25°C and 400 stimuli, 34°C). In contrast, bulk endocytosis seemed very sensitive to any change in N-cadherin interactions; therefore, it showed reduction after the inhibition of N-cadherin functions.

To summarize, these results demonstrated that FM1-43 and TMR-dextran co-staining labeled clathrin-mediated endocytosis and bulk endocytosis differentially. N-cadherin knockout and Ncad Δ E mediated block of N-cadherin functions resulted in a reduction in bulk endocytosis. In addition, N-cadherin knockout also resulted in a decrease in clathrin-mediated endocytosis. On contrary, clathrin-mediated endocytosis remained largely unaffected by Ncad Δ E mediated inhibition of N-cadherin functions.

3.3 Mechanisms of the regulation of synaptic vesicle endocytosis by N-cadherin

In this study, I showed the functional role of N-cadherin in regulating both clathrin-mediated endocytosis and bulk endocytosis. But the mechanisms involved in the regulation of vesicle endocytosis by N-cadherin are not clear. Therefore, I next

examined the mechanisms involved in the regulation of clathrin-mediated endocytosis and bulk endocytosis by N-cadherin. First, I explored the roles of F-actin in synaptic vesicle endocytosis using a selective pharmacological actin polymerizing drug, jasplakinolide.

3.3.1 N-cadherin regulates synaptic vesicle endocytosis via actin

Individual neurons were co-transfected with DsRed2 and SypHy at 9 DIV. In addition, Cre was co-expressed for 5-6 days to knockout N-cadherin and SypHy imaging was performed at 14-15 DIV by electrically stimulating the cortical neuronal cultures with 400 stimuli (20 Hz) at near physiological temperature (34°C). The cells were treated with 5 μ M jasplakinolide for 5 minutes before imaging.

The mean amplitude of the normalized SypHy signal (vesicle exocytosis) at the end of stimulation was not significantly changed in N-cadherin knockout neurons (41.7 ± 3.15 % of NH_4Cl signal, $n= 16$ cells) as compared to control cells ($39.9 \pm 4.47\%$ of NH_4Cl signal, $n= 15$ cells; Fig. 3.12A1, B-C) at near physiological temperature. Addition of jasplakinolide (5 μ M, + Jaspla) to control cells did not affect the SypHy fluorescence signals significantly (Control + Jaspla; 44.98 ± 5.29 % of NH_4Cl signal, $n= 13$ cells; Fig. 3.12A2, B-C) as compared to untreated control cells (control; $39.9 \pm 4.47\%$ of NH_4Cl signal, $n= 15$ cells; Fig. 3.12A2, B-C). Moreover, the average SypHy amplitude (vesicle exocytosis) remained unchanged in N-cadherin knockout neurons after drug treatment (N-cadherin knockout +Jaspla; 45.87 ± 5.17 % of NH_4Cl signal, $n= 13$ cells; N-cadherin knockout: 41.7 ± 3.15 % of NH_4Cl signal, $n= 16$ cells; Fig. 3.12A3, B-C).

As expected, N-cadherin knockout resulted in a significant decrease in SypHy signal (% of exocytosis, at 90 seconds) related to vesicle endocytosis (red, 61.94 ± 4.42 % of exocytosis; $n= 16$ cells) as compared to control cells (black, 81.49 ± 4.39 % of exocytosis; $n= 15$ cells; Fig. 3.12D-E). However, jasplakinolide treated control cells did not show a significant change in the decay of the SypHy signal (control + Jaspla green; 79.77 ± 2.41 % of exocytosis; $n= 13$ cells; Fig. 3.12D-E) as compared to the untreated control cells (control black; 81.49 ± 4.39 % of exocytosis; $n= 15$ cells).

Interestingly, the F-actin stabilizing drug jasplakinolide significantly accelerated the decay kinetics of the SypHy signal in N-cadherin knockout neurons showing a

prominent role of F-actin in synaptic vesicle endocytosis. N-cadherin knockout neurons treated with jasplakinolide (blue N-cadherin knockout + Jaspla; 72.96 ± 5.57 % of exocytosis; $n= 13$ cells; Fig. 3.12D-E) showed stronger decay in SypHy fluorescence (90 seconds after the end of stimulation) than that of untreated knockout cells (N-cadherin knockout red; 61.94 ± 4.42 % of exocytosis; $n= 16$ cells; Fig. 3.12D-E), indicating a positive effect of the actin polymerizing drug on vesicle retrieval. Treatment of control cells with jasplakinolide resulted in a trend towards faster decay kinetics (green control + Jaspla; 24.55 ± 1.98 s; $n=13$ cells) but this was not significant, indicating an efficient vesicle retrieval in control cells (black control; 33.66 ± 1.77 s; $n= 15$ cells).

The SypHy signal decay kinetics were significantly slower in N-cadherin knockout neurons as compared to control neurons as shown by a higher decay time constant (red N-cadherin knockout; 47.68 ± 3.73 s; $n= 16$ cells; black control; 33.66 ± 1.77 s; $n= 15$ cells; Fig. 3.12F, G), indicating slower endocytosis. Most interestingly, addition of jasplakinolide to the N-cadherin knockout neurons resulted in a faster decay time constant of 31.20 ± 3.02 s (blue N-cadherin knockout + Jaspla; $n=13$ cells; Fig. 3.12F, G) as compared to 47.68 ± 3.73 s in N-cadherin knockout neurons (red N-cadherin knockout; $n= 16$ cells; Fig. 3.12F, G) confirming the rescue effect of jasplakinolide.

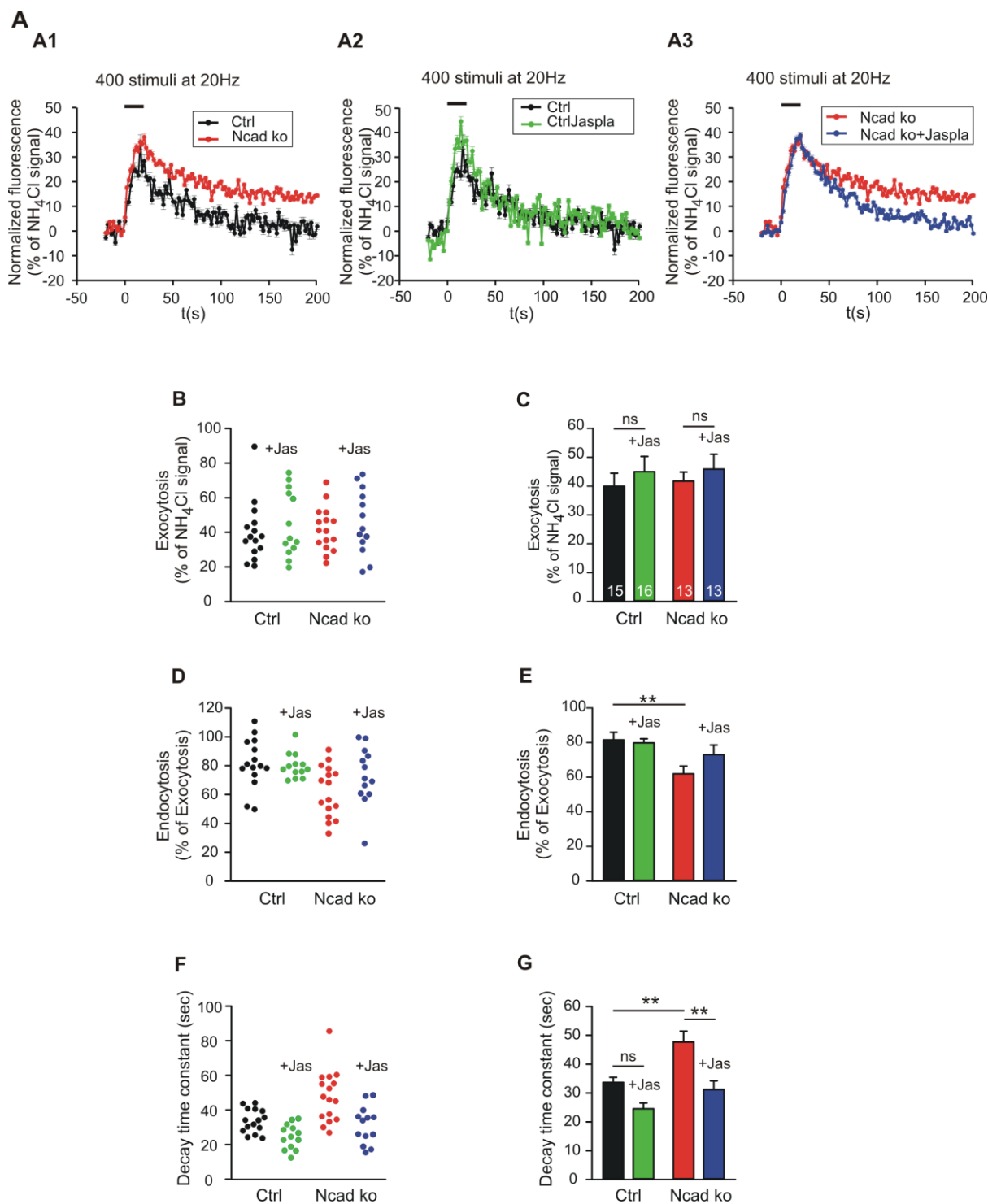


Figure 3.12 The F-actin polymerizing drug Jasplakinolide (Jaspla) reverses the endocytosis defect caused by conditional knockout of N-cadherin

Cortical neurons were co-transfected at 9 DIV with DsRed2 and SypHy. N-cadherin knockout was induced by Cre co-expression for 5-6 days (14-15 DIV) in individual neurons cultured from floxed N-cadherin mice. Cells were treated with 5 μM jasplakinolide before imaging. Vesicle cycling was

induced by electrical stimulation (400 stimuli at 20Hz) and SypHy imaging was performed at near physiological temperature (34°C).

(A-G) Jasplakinolide, an actin polymerizing drug, was able to reverse the reduced vesicle endocytosis in N-cadherin knockout neurons. Treatment of control cells with this drug had a small non-significant effect on vesicle endocytosis. **(A1-A3)** Representative time course traces of average (all puncta of one cell) normalized SypHy fluorescence intensities. **(A1)** Example time course traces of mean SypHy fluorescence intensities (black control cell; red N-cadherin knockout cell). **(A2)** Example time course traces of mean SypHy fluorescence signal (black control; green control + jasplakinolide). **(A3)** Example time course traces of mean SypHy fluorescence signal (red N-cadherin knockout; blue N-cadherin knockout + jasplakinolide). **(B)** Quantification of the mean normalized SypHy fluorescence signal at the end of stimulation (vesicle exocytosis) in individual neurons. **(C)** Average exocytosis. As expected, the SypHy signal related to vesicle exocytosis was not affected after knockout of N-cadherin. Treatment of N-cadherin knockout neurons with jasplakinolide also did not change the mean SypHy amplitude (exocytosis). **(D)** Quantitative analysis of SypHy signal lost by vesicle endocytosis at 90 seconds after stimulation (normalized to the % of exocytosis signal) in individual neurons. **(E)** Average endocytosis at 90 seconds (% of exocytosis). Vesicle endocytosis was reduced after disrupting the functions of N-cadherin. Vesicle endocytosis was reduced in N-cadherin knockout neurons confirming the change in endocytosis in the absence of N-cadherin and addition of jasplakinolide to N-cadherin knockout neurons was able to reverse this effect. **(F)** Quantification of SypHy signal decay time constants (τ of endocytosis, monoexponential fit) in individual neurons. **(G)** Average decay time constants (black control; green control + Jaspla; red N-cadherin knockout; blue N-cadherin knockout + Jaspla, $n=15/13/16/13$ cells). There was an endocytosis defect in N-cadherin knockout neurons. Interestingly, addition of the actin polymerizing drug was able to rescue the knockout effect of N-cadherin. Total SypHy puncta analysed were 341/430/316/378. ** $P < 0.01$, *** $P < 0.001$, ns not significant (one-way ANOVA followed by Holm-Sidak's test).

In summary, these results showed that the F-actin polymerizing drug jasplakinolide rescued the reduced vesicle endocytosis in N-cadherin knockout neurons. These findings suggest that N-cadherin regulates synaptic vesicle endocytosis via actin polymerization. Therefore, polymerization of actin in the absence of N-cadherin had a positive effect on synaptic vesicle endocytosis.

3.3.2 Mechanisms of regulation of bulk endocytosis by N-cadherin

N-cadherin has been described to dimerize and become protease resistant in response to strong synaptic activity (Tanaka et al., 2000). N-cadherin has also been shown to re-localise during strong synaptic release (Yam et al., 2013). Because strong synaptic vesicle release results in bulk endocytosis, I used a similar

experimental approach to understand the mechanisms involved in regulation of bulk endocytosis. Dissociated cortical neurons were stimulated using a high K^+ concentration to induce strong vesicle release, and N-cadherin clusters were immunostained immediately thereafter. Structured illumination microscopy (SIM) imaging was performed to study the changes in N-cadherin clusters after strong vesicle release.

3.3.2.1 Structured illumination microscopy (SIM) of N-cadherin and pre- and postsynaptic markers

An optical microscope has a fundamental diffraction limit. The resolution of a conventional wide-field fluorescence microscope is limited to 200 nm. This made them not suitable to examine individual synaptic structures. However, modern super-resolution methods have been developed, which made it possible to surpass the resolution limit. I used one such method known as structured illumination microscopy (SIM). With high resolution SIM imaging, it was possible to enhance the lateral spatial resolution by twofold.

3.3.2.2 Comparison of wide field imaging with SIM imaging

Initial experiments were done to compare the resolution of wide field epifluorescence images with SIM images. Cortical cultured neurons were immunostained at 12-13 DIV with VGLUT1, PSD95, and N-cadherin. First, images were captured using a conventional microscope with 63x objective. Neurons from the same preparation were also imaged using SIM with 63x objective. Images were analysed with ImageJ Fiji using their intensity profiles.

All the three channels were merged to generate an overlay. Overlay of wide field images showed partial to almost complete co-localisation of VGLUT1, PSD95, and N-cadherin (Fig. 3.13A, A1-A2). In contrast, SIM images showed a clearly separate distribution of VGLUT1, PSD95, and N-cadherin (red) confirming higher resolution (Fig. 3.13B, B1-B2). Sometimes, they did show co-localisation but mostly clusters of VGLUT1 and PSD95 were present in close contact with each other (synapses; Fig. 3.13B1-B2).

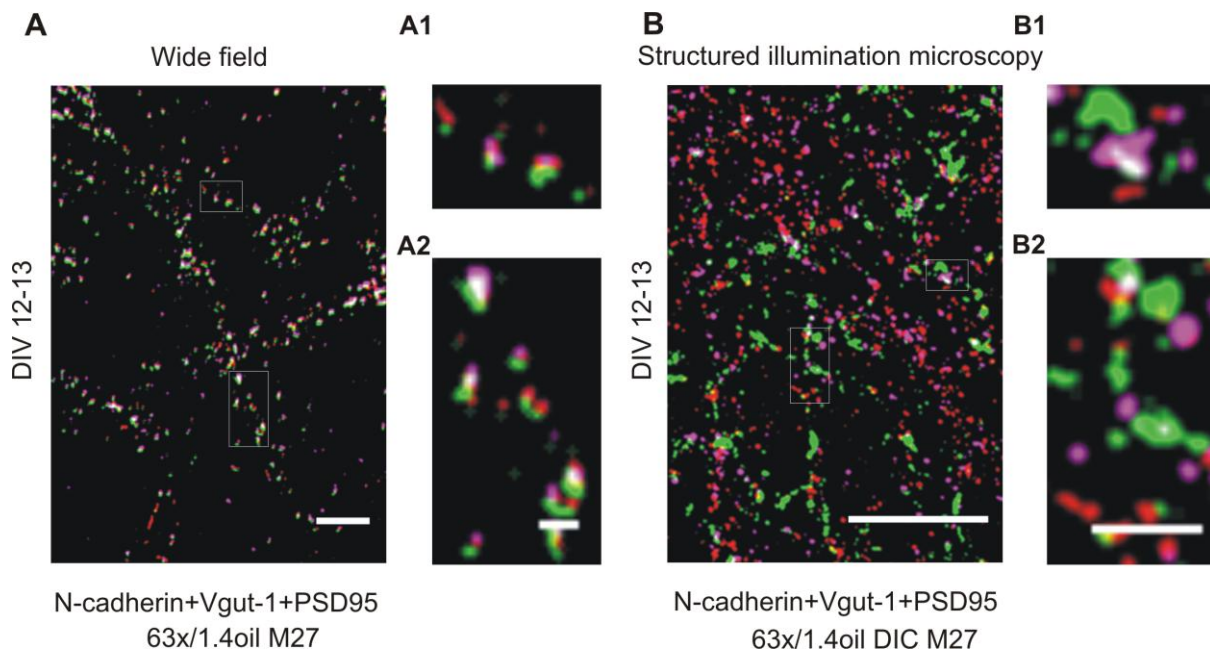


Figure 3.13 Comparison of wide field imaging with structured illumination microscopy (SIM) imaging

(A-B) Cortical neurons were triple stained for VGLUT1, N-cadherin, and PSD95 at 12-13 DIV. **(A)** Overlay of representative images showing triple staining for VGLUT1 (green), PSD95 (magenta) and N-cadherin (red). Images were captured using Axiovert 200M with 63x/1.4 oil objective. **(A1 & A2)** Magnification of the boxed regions shown in image A indicates the partial overlap of both pre- and postsynaptic molecules along with N-cadherin. **(B)** Overlay example images showing VGLUT1, PSD95, and N-cadherin staining with SIM imaging. Images were captured using Elyra PS with 63x/1.4 oil objective. **(B1 & B2)** Higher magnification view of the boxed regions shown in B to indicate spatially resolved pre- and postsynaptic (high resolution) molecules along with N-cadherin. Scale bar 5 μm **(A & B)** and 1 μm **(A1, A2 & B1, B2)**.

3.3.2.3 Spatial correlation of N-cadherin expression to pre- and postsynaptic molecules

Cortical neurons at 12-13 DIV were fixed with PFA and immunostained for N-cadherin, VGLUT1 (presynapse), and PSD95 (postsynapse). Images were acquired using Elyra PS setup (Zeiss) and were analysed with ImageJ Fiji. An overlay was created using VGLUT1 and PSD95 images. This overlay was then searched for synaptic structures where both pre- (VGLUT1) and postsynaptic (PSD95) puncta

were present together within one focal plan. Whenever VGLUT1 and PSD95 were in close contact, it was considered as a synapse. Next, the corresponding N-cadherin image was superimposed on the overlay and N-cadherin localization was determined in relation to the above identified synapse. N-cadherin has been well known to be present at the peri-active zone (Fannon and Colman, 1996; Uchida et al 1996; Benson and Tanaka, 1998) and I found that the majority of the synapses had N-cadherin located in the vicinity of the active zone (between VGLUT1 and PSD95) often flanking one side of the active zone (peri-active zone), thus confirming the previous results.

Compared to the conventional fluorescence microscopy, SIM enabled more precise examination of the spatial alignment of N-cadherin in relation to the pre- and postsynaptic molecules. Triple-staining of cortical neurons showed various alignments of the synaptic molecules. N-cadherin was found to be located at the peri-synaptic (active) zone in association with VGLUT1 and PSD95. At some synapses, N-cadherin was located within the synaptic cleft (active zone) between VGLUT1 and PSD95 clusters, although only rarely present in this alignment.

On the basis of N-cadherin localization, I divided synapses into four different types:-

- 1) Synapses with cleft associated N-cadherin: - majority of the synapses had N-cadherin puncta (clusters) located in close contact with cleft (a part of N-cadherin was located in between VGLUT1 and PSD95 at the active zone, and another part was flanking the synaptic cleft i.e. at the peri-active zone) (Fig. 3.14A-A1).
- 2) Synapses without cleft associated N-cadherin: - these synapses had sometimes N-cadherin puncta on either VGLUT1 side or PSD95 side but without any contact with the cleft. This category of synapses had either mis-localized N-cadherin or they might be in the process of acquiring N-cadherin (Fig. 3.14B-B1).
- 3) Synapses with only synaptic N-cadherin: - N-cadherin puncta were present only at the active zone (in between VGLUT1 and PSD95). These synapses were very rare (Fig. 3.14C-C1).
- 4) Synapses without N-cadherin: - there were quite a lot of synapses without any N-cadherin cluster associated (Fig. 3.14D-D1).

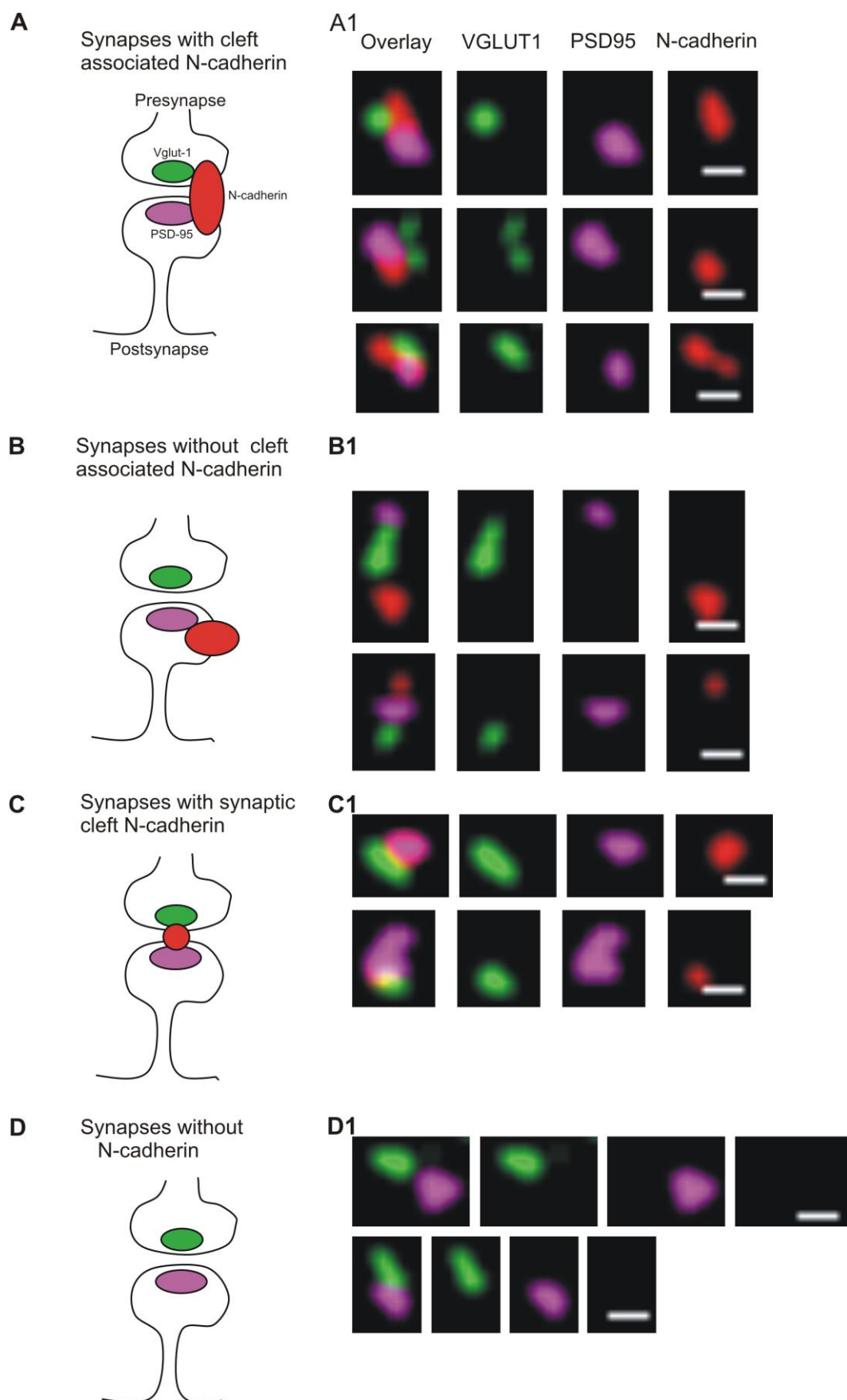


Figure 3.14 Classification of synapses based on N-cadherin localization using SIM imaging

(A-D) Schematic diagrams of a synapse showing the organisation of pre- and postsynaptic proteins and the spatial alignment of N-cadherin in relation to VGLUT1 (presynaptic) and PSD95 (postsynaptic). **(A)** Synapses with cleft associated N-cadherin: - a schematic diagram of a synapse showing the localization of N-cadherin in close contact with active and peri-active zone. **(A1)** Example SIM images showing overlay, presynapse (VGLUT1; green), postsynapse (PSD95, magenta) and N-cadherin (red) to show cleft associated N-cadherin. The majority of the synapses had N-cadherin associated with synaptic cleft thus representing mature synapses. **(B)** Synapses without cleft associated N-cadherin: - a schematic diagram of a synapse indicating the localization of N-cadherin away from the active zone. These synapses seemed to have mis-localized N-cadherin. **(B1)** Example SIM images showing overlay, presynapse (VGLUT1; green), postsynapse (PSD95, magenta), and N-cadherin (red). N-cadherin was not in contact with the active or peri-active zone. These synapses had N-cadherin in contact with either VGLUT1 or PSD95, but away from the synaptic cleft. **(C)** Synapses with synaptic cleft N-cadherin: - a schematic diagram showing the localization of N-cadherin inside the synaptic cleft. **(C1)** Example SIM images showing overlay, presynapse (VGLUT1; green), postsynapse (PSD95, magenta), and N-cadherin (red). N-cadherin was present only in between VGLUT1 and PSD95 (inside the active zone). Only few synapses had only synaptic N-cadherin. **(D)** Synapses without N-cadherin: - a schematic diagram of a synapse with only presynapse (green) and post synapse (magenta). **(D1)** Example SIM images showing overlay, presynapse (VGLUT1; green) and postsynapse (PSD95, magenta). These synapses were not associated with N-cadherin. Scale bars 250 nm.

For further experiments, the proportions of these four different classes of synapses were quantified to examine changes in N-cadherin distribution.

3.3.2.4 Developmental changes in synaptic localization of N-cadherin

As a first step to examine the N-cadherin clusters at synapses, cultured cortical neurons at different stages of maturation (*in vitro*) were immunostained for VGLUT1, PSD95, and N-cadherin to label pre- and postsynaptic parts of the synapse. Three different time points (6 DIV, 12 DIV and 28 DIV) were selected to compare N-cadherin distribution at synapses during neuronal differentiation. To label immature synapses at 6 DIV, Bassoon (presynaptic) and SAP102 (postsynaptic) was used, while neurons at 12 DIV and 28 DIV were immunostained for VGLUT1 and PSD95. SIM images were compared across time in culture to find differences in the distribution of N-cadherin during neuronal maturation.

Synapses were divided into four different categories based on N-cadherin localization. 1) Synapses with cleft associated (active + peri-active zone) N-cadherin, 2) synapses without cleft associated N-cadherin, 3) synapses with synaptic (cleft) N-cadherin, and 4) synapses without any N-cadherin (see Fig. 3.14). These four types of synapses were quantified and results showed that at 6 DIV (relatively immature neurons), $45.83 \pm 3.05\%$ (Fig. 3.15A, D; $n=15$ dendrites) of the synapses had cleft associated N-cadherin and this fraction increased during neuronal differentiation. There was a significant increase in the fraction of synapses with cleft associated N-cadherin at 28 DIV (mature neurons; 71.66 ± 2.72 ; Fig. 3.15C, D; $n=12$ dendrites) as compared to 6 DIV ($45.83 \pm 3.05\%$; $n=15$ dendrites) and 12 DIV (52.51 ± 2.25 ; Fig. 3.15B, D; $n=15$ dendrites). Quantification of the percentage of synapses without N-cadherin showed that at 6 DIV, $28.76 \pm 2.65\%$ ($n=15$ dendrites; Fig. 3.15D) of the synapses didn't have any N-cadherin cluster associated and this fraction of synapses was significantly ($P<0.05$) decreased to $11.05 \pm 2.47\%$ ($n=12$ dendrites; Fig. 3.15 D) at 28 DIV suggesting that synapses acquire N-cadherin during in vitro maturation. There was no significant change in the number of synapses without N-cadherin (24.44 ± 2.12 ; $n= 15$ dendrites; Fig. 3.15D) at 12 DIV as compared to 6 DIV ($28.76 \pm 2.65\%$) indicating that these neurons were still differentiating.

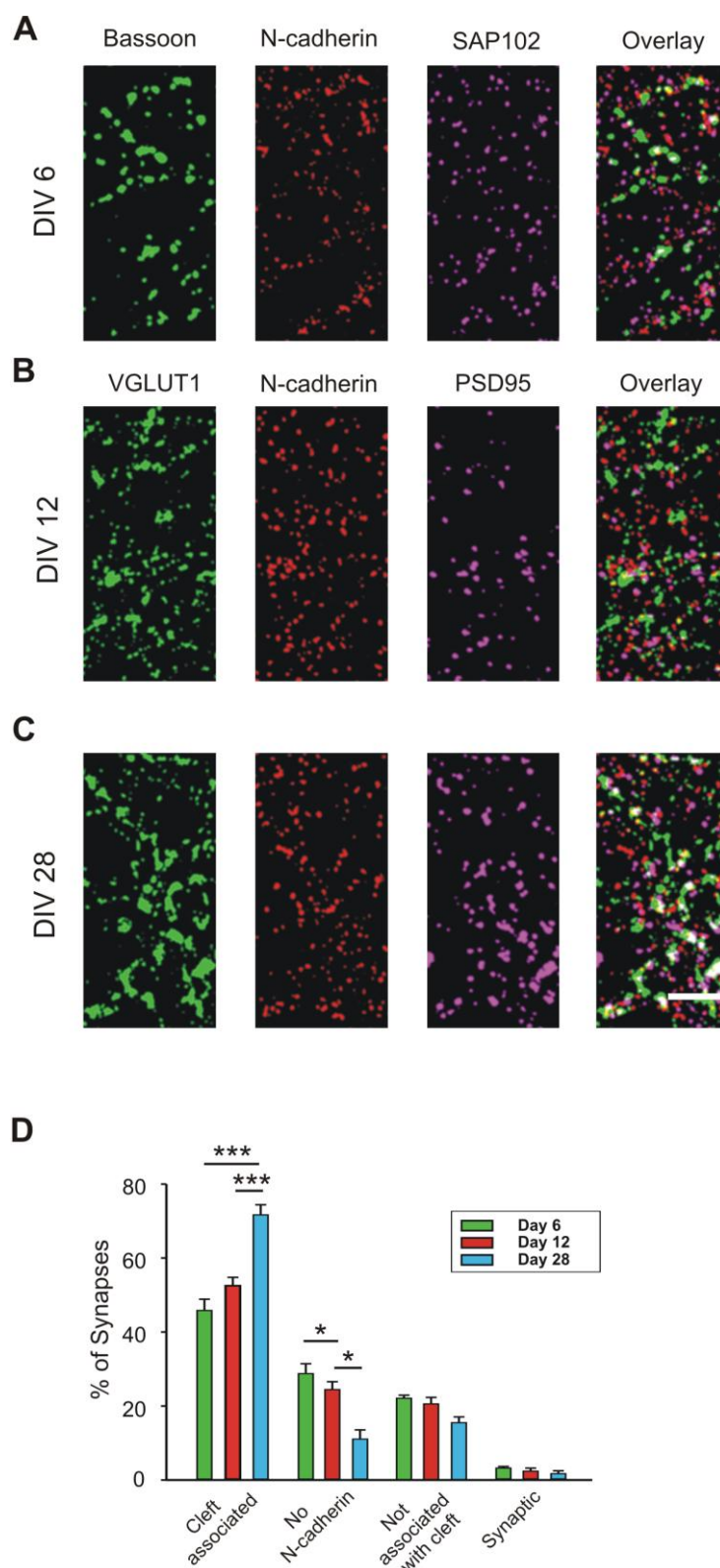


Figure 3.15 Recruitment of N-cadherin to synapses during neuronal differentiation as revealed by SIM imaging

Cortical neuronal cultures at different stages during *in vitro* maturation (6, 12 and 28 DIV) were immunostained for pre- and post synaptic proteins along with N-cadherin. To label the pre- and post synapse at 12-13 DIV and 28 DIV, VGLUT1 and PSD95 were used. Bassoon and SAP102 was used

to label pre- and postsynapses at 6 DIV. **(A-D)** Differentiation of neurons *in vitro* led to the recruitment of N-cadherin to synapses. **(A)** Example SIM images showing Bassoon (green, presynapse), N-cadherin (red), SAP102 (magenta, postsynapse), and overlay at 6 DIV (immature) neurons. **(B)** Example SIM images of VGLUT1 (green), N-cadherin (red), PSD95 (magenta), and overlay at 12-13 DIV. **(C)** Example SIM images of VGLUT1 (green), N-cadherin (red), PSD95 (magenta), and overlay at 28 DIV. **(D)** Quantification of the fractions of synapses based on N-cadherin localization during neuronal differentiation. Mature neurons (28 DIV) had significantly more synapses with cleft associated N-cadherin indicating more mature synapses. The synapse fraction without any N-cadherin was reduced significantly during neuronal differentiation (from 6 DIV to 28 DIV) again indicating maturation of synapses. n=12/15/15 dendrites. Scale bar 2 μm . Data is represented as mean \pm SEM. Statistics was done using one-way ANOVA with Holm-Sidak posthoc test, *** $P < 0.001$. Kruskal-Wallis one-way ANOVA on ranks with Dunn's method was used whenever the normality test failed, *** $P < 0.001$.

To summarize, SIM imaging demonstrated that nascent synapses recruit N-cadherin during neuronal differentiation. These results also showed that N-cadherin was present in close association with the active and the peri-active zone (cleft associated) at mature synapses and there was a continuous increase in the number of synapses with cleft associated N-cadherin during neuronal differentiation. This initial data confirmed the importance of SIM imaging in analysing changes at the synapse level.

3.3.2.5 Effects of strong synaptic stimulation on N-cadherin synaptic localization

Bulk endocytosis is the main mode of synaptic vesicle endocytosis during intense synaptic activity because synapses need to restore the original surface area of the presynaptic terminal to maintain its normal functions. Treatment of neuronal cultures with high K^+ is known to induce strong synaptic release and at this condition, synapses require a fast mechanism to retrieve vesicles (bulk endocytosis). Strong vesicle release was induced by stimulating cortical neurons (12-13 DIV) for 5 min with 50 mM K^+ containing extracellular solution and the cells were immediately fixed with 4% PFA. As a control, neurons were placed in the normal extracellular solution containing 5 mM K^+ for 5 minutes. To check for reversibility, stimulated cells were allowed to recover by keeping them in a normal extracellular solution (5 mM K^+) for

30 minutes. Finally, neurons were immunostained for VGLUT1, PSD95, and N-cadherin. To observe the effects of strong stimulation on the distribution of N-cadherin, I evaluated the synaptic localization of N-cadherin at neuronal dendrites. Furthermore, PSD95 distribution was also evaluated to examine any changes.

3.3.2.6 Redistribution of N-cadherin induced by strong release (K^+ stimulation)

High $[K^+]$ stimulation resulted in a strong release of synaptic vesicles inducing the redistribution of synaptic molecules. First, I examined N-cadherin puncta after K^+ stimulation and compared them with the non-stimulated control cells. K^+ stimulation led to the enlargement of N-cadherin puncta (Fig. 3.16B, upper). They appeared to be more elliptical (elongated) after K^+ stimulation as compared to round N-cadherin puncta in control cells (Fig. 3.16A, upper). K^+ stimulation seemed to induce the fusion of N-cadherin puncta. In recovery, the majority of the N-cadherin puncta returned to their round shape but some remained elliptical (Fig. 3.16C upper). In contrast, postsynaptic PSD95 didn't show any significant qualitative change upon stimulation (Fig. 3.16A-C, lower images).

Next, I quantified the changes in N-cadherin puncta area and found that mean N-cadherin puncta area was significantly ($P < 0.05$) increased from $0.024 \pm 0.001 \mu\text{m}^2$ ($n = 22$ dendrites) in control neurons to $0.032 \pm 0.002 \mu\text{m}^2$ ($n = 16$ dendrites; Fig. 3.16D) in K^+ stimulated neurons. When the stimulated neurons were kept in the normal extracellular solution ($5 \text{ mM } K^+$) to recover for 30 min after K^+ stimulation, the N-cadherin puncta size recovered to $0.027 \pm 0.001 \mu\text{m}^2$ ($n = 14$ dendrites; Fig. 3.16D). K^+ stimulation did not result in a significant change in the PSD95 puncta size (control: $0.032 \pm 0.001 \mu\text{m}^2$, $n = 22$ dendrites; K^+ stimulated: $0.033 \pm 0.002 \mu\text{m}^2$, $n = 16$ dendrites; Recovery: $0.034 \pm 0.002 \mu\text{m}^2$, $n = 14$ dendrites; Fig. 3.16E).

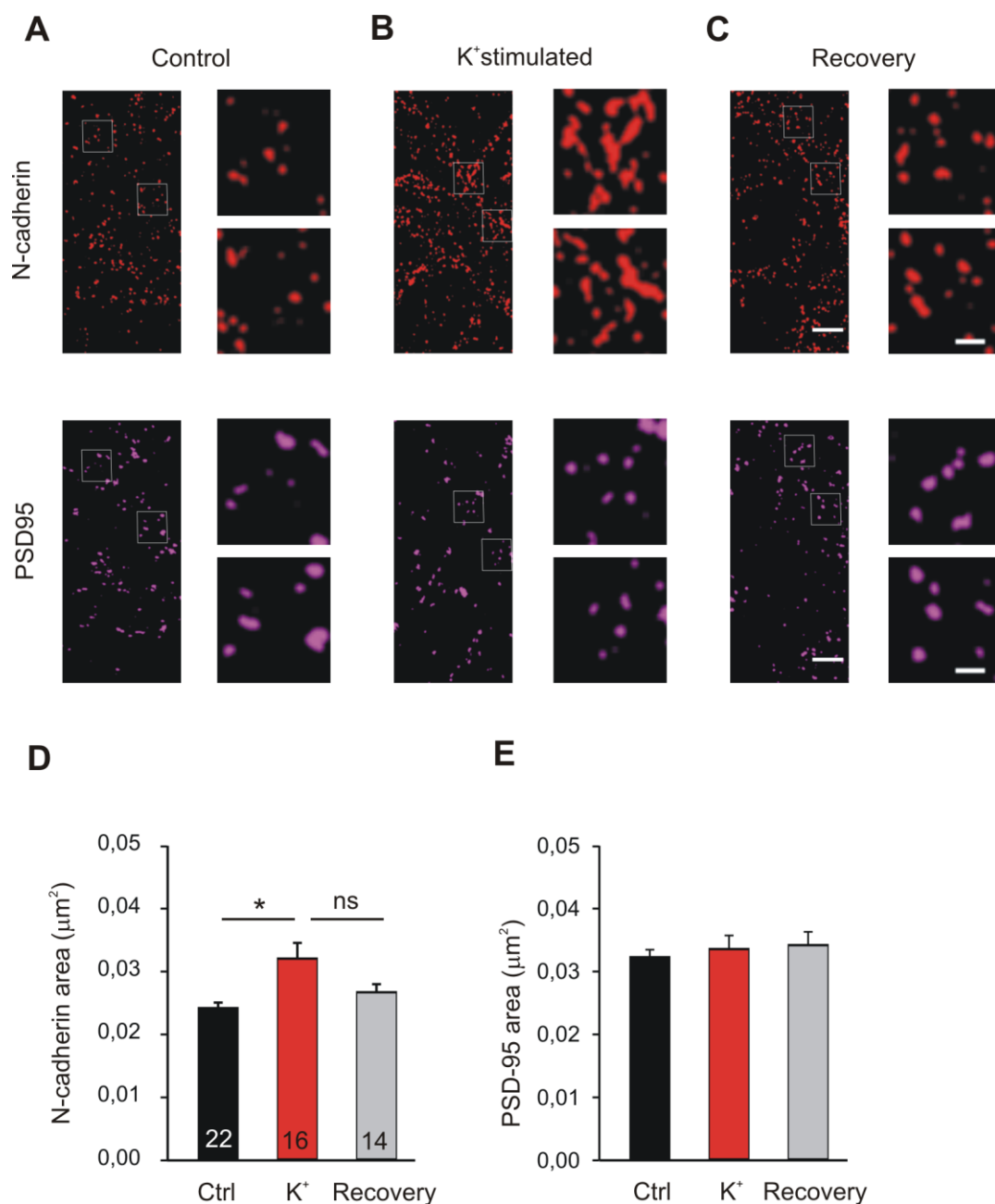


Figure 3.16 Changes in the distribution of N-cadherin induced by high $[\text{K}^+]$ stimulation

Cultured cortical neurons were stimulated with high $[\text{K}^+]$ to induce strong release of synaptic vesicles and were immunostained for pre- (VGLUT1) and postsynaptic (PSD95) proteins along with N-cadherin at 12-13 DIV. The change in N-cadherin puncta was evaluated using SIM imaging and compared with non-stimulated control and after recovery of 30 minutes.

(A-D) Strong synaptic vesicle release led to a significant increase in N-cadherin puncta area. **(A)** Example images showing N-cadherin (upper) and PSD95 (lower) immunostaining in non-stimulated control cells. Higher magnification view of the boxed regions indicated in A showing a few individual N-cadherin puncta (upper right) and PSD95 puncta (lower right). In control neurons, N-cadherin

puncta were roundish. **(B)** Example images showing N-cadherin (upper) and PSD95 immunostaining (lower) after 50 mM K^+ stimulation. Higher magnification views of the boxed regions in B showing a few individual N-cadherin (upper right) and PSD95 puncta (lower right). High K^+ stimulation induced strong synaptic release led to the fusion of N-cadherin puncta. **(C)** Example images showing N-cadherin (upper) and PSD95 (lower) immunostaining of the recovered neurons (upper). Higher magnification views of the boxed regions in C showing roundish N-cadherin puncta (upper right) and PSD95 puncta (lower right). When the neurons were allowed to recover after K^+ stimulation, some of the N-cadherin puncta returned to their round shape. Scale bar 2 μ m and 500 nm. **(D)** Quantification of the mean N-cadherin puncta area. High K^+ stimulation resulted in a significant increase in N-cadherin area. **(E)** Quantification of the mean PSD95 puncta area. High K^+ stimulation did not induce a significant change in the PSD95 puncta area (black control; red K^+ stimulated; gray after recovery; $n=22/16/14$ dendrites). Data is represented as mean \pm SEM from four independent experiments. Statistics were done by Kruskal-Wallis one-way ANOVA on Ranks with Dunn's method, * $P < 0.05$.

In summary, high K^+ (50 mM) stimulation led to an increase in N-cadherin puncta area, indicating the need for more N-cadherin at the synapses during strong vesicle release. Qualitatively, N-cadherin puncta appeared to be fused. In contrast, the PSD95 distribution showed no significant change after high K^+ stimulation.

3.3.2.7 Spatial distribution of N-cadherin at synapses after strong K^+ stimulation

To further examine the changes associated with N-cadherin puncta in strong stimulation condition (50 mM K^+), I analysed the spatial distribution of N-cadherin at synapses after high K^+ stimulation (5 minutes). Imaging and analysis were done analogous to Fig. 3.14 and Fig. 3.15. There were four different types of synapses based on N-cadherin localization similar to Fig. 3.15.

These four different categories of synapses were counted in control, K^+ stimulation and recovery conditions. Fractions (%) of synapses were calculated and plotted. The results showed that $55.64 \pm 1.77\%$ (Fig. 3.17A, D; $n=12$ dendrites) of the synapses had cleft associated N-cadherin in control cells suggesting that this category represents mature synapses.

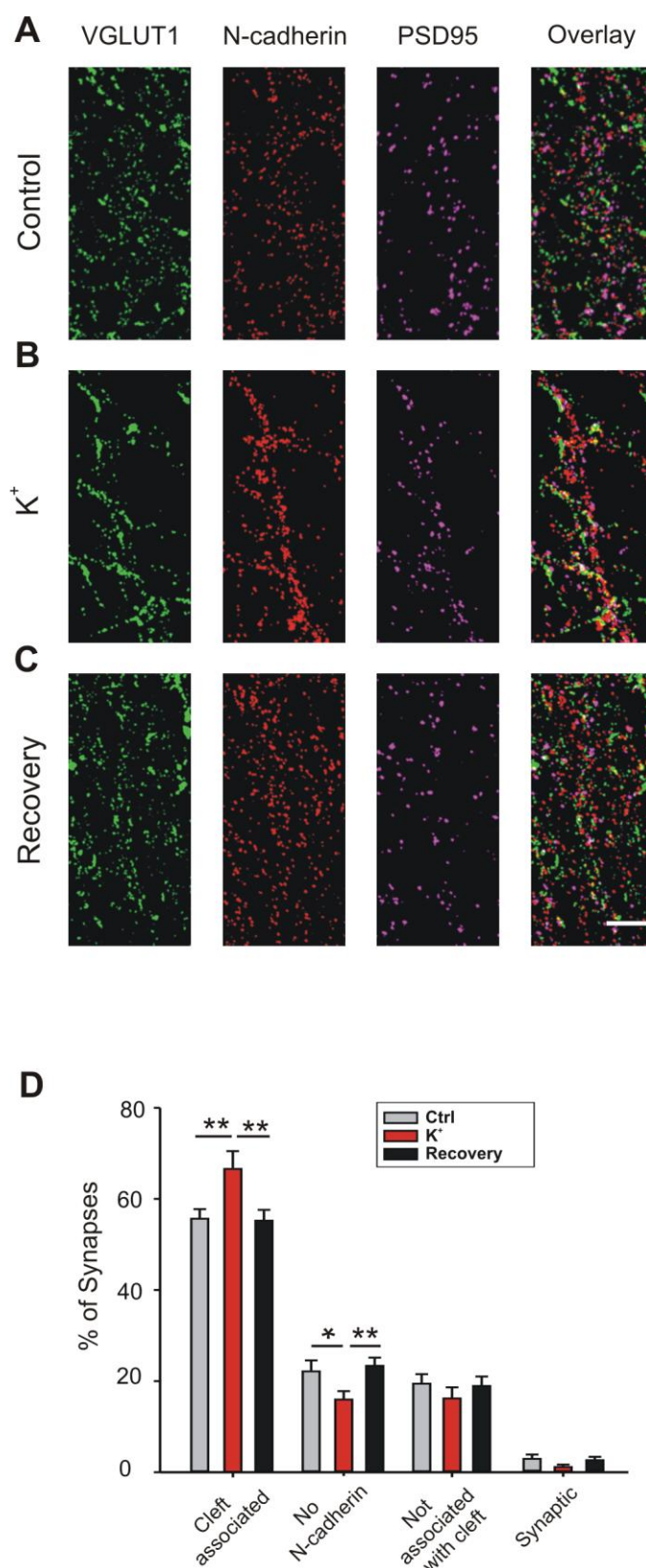


Figure 3.17 Recruitment of N-cadherin to synapses upon strong synaptic release (High [K⁺] stimulation)

Cortical neurons were stimulated with high [K⁺] to induce strong release of synaptic vesicles and were immediately fixed with PFA followed by immunostaining for pre- (VGLUT1) and postsynaptic (PSD95)

proteins along with N-cadherin at 12-13 DIV. Synapses were identified by apposed or overlapping VGLUT1 and PSD95 stained clusters and were classified based on N-cadherin localization analogous to figure 3.14.

(A-D) Strong synaptic vesicle release induced by high K^+ resulted in the recruitment of N-cadherin to the synapses. **(A)** Example SIM images of VGLUT1 (green), N-cadherin (red), PSD95 (magenta), and overlay in control neurons **(A)**, K^+ stimulated neurons **(B)** and after recovery **(C)**. **(D)** Quantification of the fraction of synapses after K^+ stimulation. Strong release of synaptic vesicles led to a significant increase in the fraction of synapses with cleft associated N-cadherin ($n=12$ dendrites, 4 independent experiments). Scale bar 2 μm . * $P < 0.05$; ** $P < 0.01$ (one-way ANOVA with Holm-Sidak posthoc test).

After 5 minutes of K^+ stimulation, there was a significant ($P < 0.01$) increase in the fraction of synapses with cleft associated N-cadherin ($66.70 \pm 3.57\%$; Fig. 3.17B, D $n=12$ dendrites), indicating activity-induced recruitment of N-cadherin to synapses. When the cells were allowed to recover for 30 minutes after K^+ stimulation, the fraction of synapses with cleft associated N-cadherin decreased to $55.21 \pm 2.04\%$ (Fig. 3.17C, D; $n=12$), indicating a reversibility of the redistribution process.

Next, I compared the fraction of synapses which did not have any N-cadherin. The fraction of synapses with no N-cadherin also showed a significant reduction ($15.96 \pm 1.54\%$; Fig. 3.17B, D; $n=12$ dendrites) in K^+ stimulated neurons as compared to control cells ($22.15 \pm 2.09\%$; Fig. 3.17 A, D; $n=12$ dendrites), and this fraction again showed an increase ($23.35 \pm 1.48\%$; Fig. 3.17C, D; $n=12$), when the cultures were recovered for 30 minutes after K^+ stimulation.

These findings confirmed the recruitment of N-cadherin to synapses that were previously devoid of it in an activity-dependent manner, and this recruitment process was found to be reversible. These results suggested that during strong synaptic vesicle release, synapses recruit N-cadherin to enhance synaptic vesicle retrieval by taking up invaginations in the form of bulk endosomes.

3.4 Comparative analysis of the synaptogenic activities of Neuroligin1 and LRRTM2 in cortical neurons

Previous studies have demonstrated a role for postsynaptic N-cadherin in the regulation of the presynaptic vesicle clustering activity of NLG1. N-cadherin postsynaptically recruited Neuroligin1 via S-SCAM (synaptic scaffolding molecule),

and Neuroligin1 in turn, enhanced vesicle clustering (Stan et al., 2010; Aiga et al., 2011; van Stegen et al., 2017). LRRTM2 is another recently identified synaptogenic cell adhesion molecule (Linhoff et al., 2009). Both Neuroligin1 and LRRTM2 are expressed at postsynaptic sites, interact presynaptically with Neurexins and are thought to play an important role in synapse formation. Similar to Neuroligin1, LRRTM2 is also known to induce vesicle clustering in the contacting axon (de Wit et al., 2009; Ko et al., 2009). But it's not known if N-cadherin regulates the synaptogenic activity of LRRTM2. Therefore, next, I studied the dependency of LRRTM2's synaptogenic activity on N-cadherin.

3.4.1 Synptogenic activities of Neuroligin1 and LRRTM2

As a first step, the synptogenic activities of Neuroligin1 (NLG1) and LRRTM2 were compared in both immature and mature cortical neurons by examining their presynaptic vesicle cluster inducing effects. Dissociated cortical neurons (mass cultures) were cultured from wild type (C57/BL6) mice on poly-L-ornithine (PO) coated glass coverslips. The neurons were co-transfected with NLG1-EGFP or LRRTM2 + EGFP expression vectors, respectively. EGFP expression was used as a control.

3.4.1.1 Synptogenic activities of Neuroligin1 and LRRTM2 in immature neurons

Cortical neurons were transfected at 4 DIV with NLG1-EGFP or LRRTM2 + EGFP and were fixed 2-3 days after transfection (6-7 DIV) with 4% paraformaldehyde (PFA). To investigate the roles of NLG1 and LRRTM2 in the induction of presynaptic vesicle clusters, transfected cortical neurons were immunocytochemically stained for the synaptic vesicle protein synaptobrevin-2 (VAMP2).

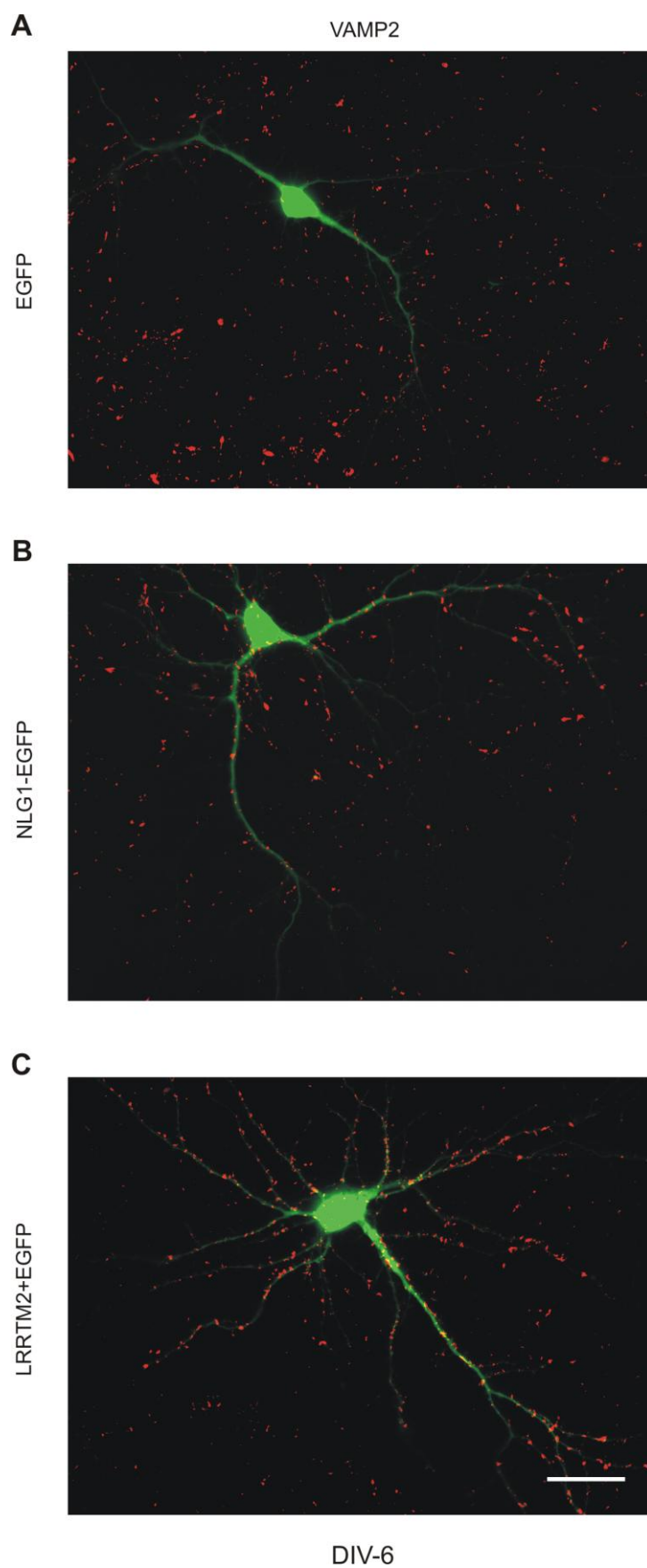


Figure 3.18 Overexpression of the synaptic adhesion molecules Neuroligin1 (NLG1) and LRRTM2, respectively in immature neurons (6 DIV)

Cultured cortical neurons were co-transfected with Neuroligin1-EGFP fusion protein and LRRTM2 + EGFP (co-expression), respectively at 4 days *in vitro* and their synaptogenic effects were studied by immunostaining for the synaptic vesicle protein VAMP2 at 6-7 days *in vitro* (DIV). **(A)** Enhanced green fluorescent protein (EGFP) expression was used as a control and helped to visualize transfected neurons by EGFP fluorescence. VAMP2 staining showed a punctate distribution. Only a few VAMP2 puncta were in contact with the dendrites of the transfected neurons. **(B)** Example overlay image of a Neuroligin1 expressing neuron (green EGFP; red VAMP2) indicating strong accumulation of VAMP2 positive puncta in contact with the dendrites of the transfected neuron. **(C)** Example overlay image of a LRRTM2 overexpressing neuron (green EGFP; red VAMP2) showing a strong accumulation of vesicle clusters (VAMP2 puncta) on the dendrites of the transfected neuron (green). Scale bar 30 μm .

EGFP (transfection marker images were overlaid with the corresponding VAMP2 stainings to identify VAMP2-immunopositive puncta on the dendrites of transfected neurons. VAMP2 puncta density was then calculated as the number of puncta/10 μm of the dendrite length.

At 6-7 DIV, postsynaptic overexpression of both NLG1 and LRRTM2 resulted in a strong accumulation of presynaptic vesicle clusters (VAMP2 positive clusters) onto the dendrites of the transfected neurons as compared to control cells (Fig. 3.18A-C). The overexpression of NLG1-EGFP led to a significant increase in ($P < 0.01$) VAMP2 puncta density (3.54 ± 0.27 puncta/10 μm dendrite; $n=10$ cells; Fig. 3.19A-C) as compared to control cells (EGFP; 2.22 ± 0.21 puncta/10 μm dendrite, $n=11$ cells). LRRTM2 overexpression also resulted in a statistically significant ($P < 0.001$) increase in VAMP2 puncta density (4.42 ± 0.24 puncta/10 μm dendrite, $n=12$ cells; Fig. 3.19A-C) indicating a strong vesicle clustering effect. These data showed that postsynaptic overexpression of both NLG1 and LRRTM2 resulted in an increased presynaptic vesicle clustering in immature neurons and thus, both adhesion molecules promote the formation of new synapses.

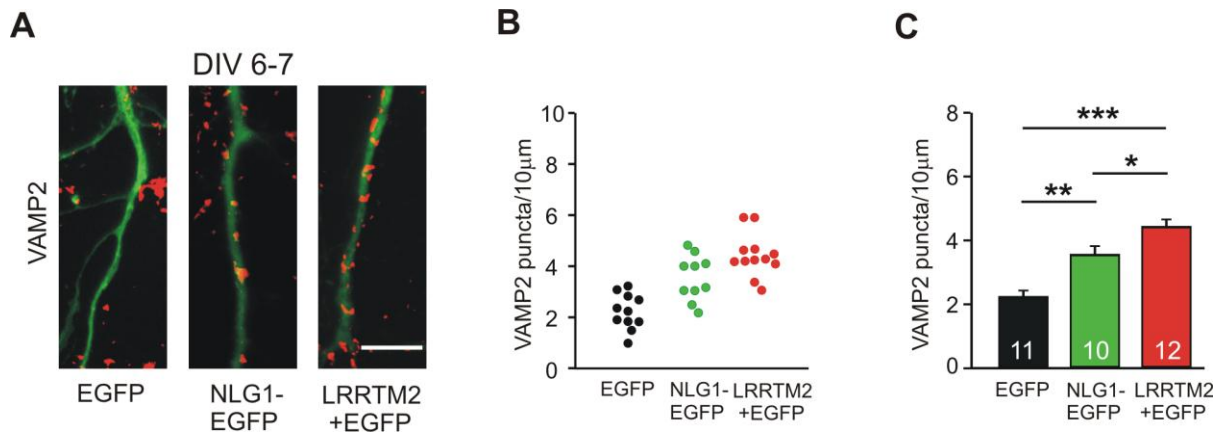


Figure 3.19 Synaptogenic activities of NLG1 and LRRTM2 in immature cortical neurons (6-7 DIV)

(A-C) Postsynaptic expression of NLG1-EGFP and LRRTM2+EGFP, respectively increased the dendritic density of immunocytochemically stained VAMP2 puncta in immature neurons (6-7 DIV). **(A)** Representative overlay images showing parts of dendrites (green) and VAMP2 (red) staining of neurons expressing EGFP (left), NLG1-EGFP (middle) and LRRTM2+EGFP (right), respectively. Scale bar 10 μm. **(B)** Quantification of VAMP2 puncta density / 10 μm dendrite length in individual neurons. **(C)** Quantification of mean VAMP2 puncta / 10 μm dendrite length (n=11/10/12, n represents the number of neurons). Data are represented as mean ± SEM. * P < 0.05; ** P < 0.01; *** P < 0.001 (One-way ANOVA with Holm-Sidak posthoc test).

3.4.1.2 Synaptogenic activities of Neuroligin1 and LRRTM2 in mature neurons (12-13 DIV)

To investigate the synapse formation activity of NLG1 and LRRTM2 in mature neurons, primary dissociated cortical mouse neurons were co-transfected at 9 DIV with NLG1-EGFP and LRRTM2 + EGFP, respectively. Presynaptic vesicle clusters were labeled 3-4 days after transfection using VAMP2 immunostaining (12-13 DIV) and VAMP2 puncta density was calculated.

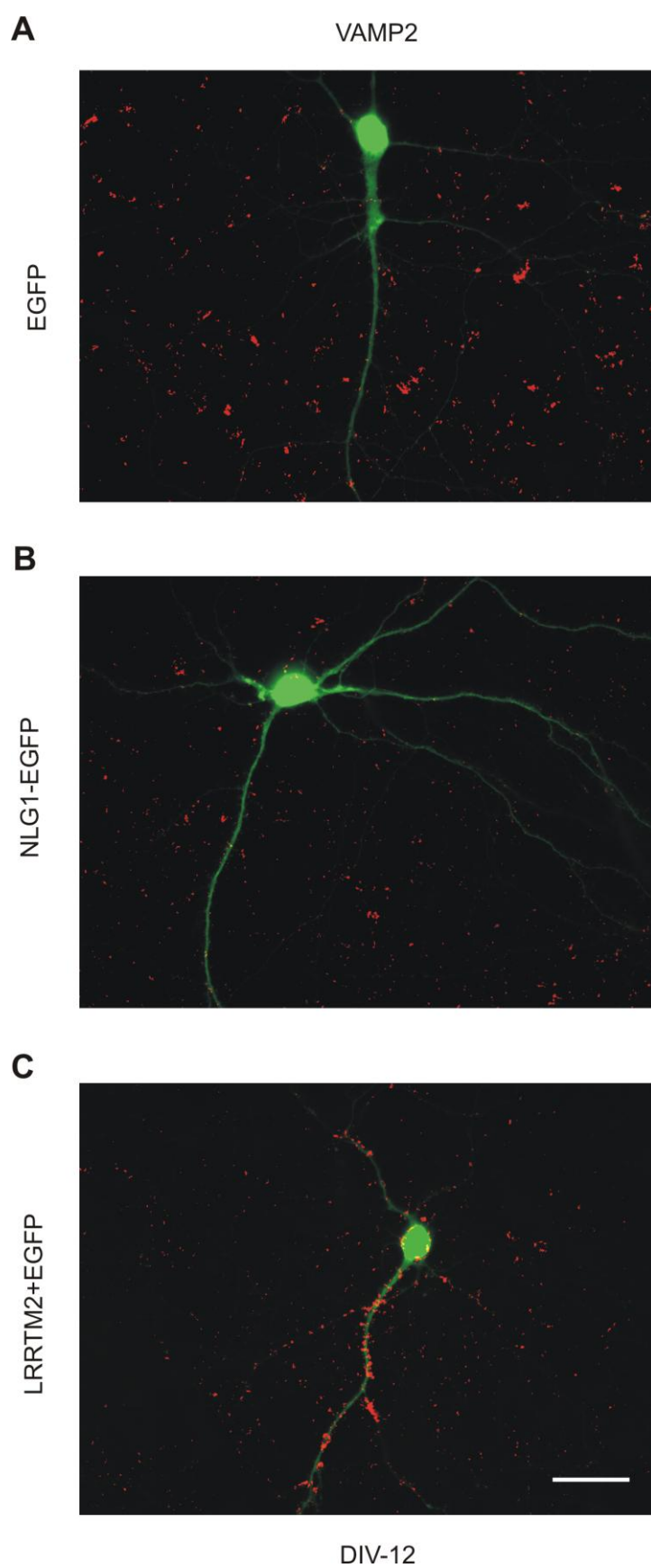


Figure 3.20 Overexpression of the synaptic adhesion molecules Neuroligin1 (NLG1) and LRRTM2, respectively in relatively mature neurons (12-13 DIV)

Postsynaptic overexpression of LRRTM2 induces additional presynaptic vesicle clustering in mature cortical neurons (12-13 DIV). **(A)** Example fluorescence image of VAMP2 immunostained puncta (red) onto the dendrites of EGFP (green) overexpressing neurons. EGFP expressing neurons showed a few VAMP2 puncta (EGFP green; VAMP2 red) contacting the dendrite of the transfected neurons. **(B)** Example overlay image of a Neuroligin1 expressing neuron (green EGFP; red VAMP2) with only a few VAMP2-positive puncta (similar to control levels) contacting the dendrites of the transfected neurons. **(C)** Example overlay image of a LRRTM2 overexpressing neuron (green EGFP; red VAMP2) showing strong accumulation of vesicle clusters (VAMP2 puncta) onto the dendrites of the transfected neuron (green). Scale bar 30 μm .

At 12-13 DIV, overexpression of NLG1 did not induce a significant change in VAMP2 puncta density as compared to control cells (Fig. 3.20A-B). In contrast, postsynaptic overexpression of LRRTM2 resulted in a strong accumulation of VAMP2 clusters onto the dendrites of transfected neurons (Fig. 3.20C) indicating a strong synaptogenic effect.

Cortical neurons expressing only EGFP showed an overall increase (2.97 ± 0.22 puncta/ $10 \mu\text{m}$ dendrite, $n=12$ cells; Fig. 3.21) in dendritic VAMP2 puncta density as compared to control cells in immature neurons (EGFP; 2.22 ± 0.21 puncta/ $10 \mu\text{m}$ dendrite, $n=11$ cells; Fig. 3.19) indicating an increase in synapse number during neuronal differentiation. There was no significant change in VAMP2 puncta density (4.14 ± 0.47 puncta/ $10 \mu\text{m}$ dendrite, $n=10$ cells) in NLG1-EGFP overexpressing cells as compared to control cells (2.97 ± 0.22 puncta/ $10 \mu\text{m}$ dendrite, $n=12$ cells; Fig. 3.21A-C) indicating that NLG1 did not induce presynaptic vesicle clustering in mature neurons.

Postsynaptic overexpression of LRRTM2 resulted in a strong increase ($P<0.001$) in VAMP2 immunopositive puncta density (6.89 ± 0.57 puncta/ $10 \mu\text{m}$ dendrite, $n=10$ cells) as compared to control cells (EGFP, 2.97 ± 0.22 puncta/ $10 \mu\text{m}$ dendrite, $n=12$ cells; Fig. 3.21A-C). This increase in VAMP2 puncta density was even stronger than that induced by LRRTM2 overexpression in immature neurons. These results showed that LRRTM2 was synaptogenic in mature neurons while NLG1 lost the synaptogenic activity in mature neurons.

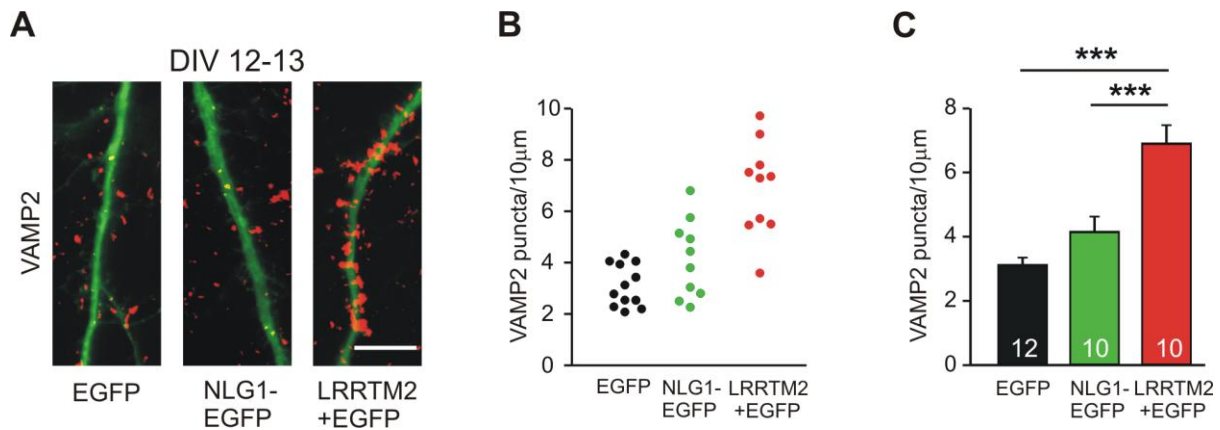


Figure 3.21 Synaptogenic activities of LRRTM2 and NLG-1 in mature cortical neurons (12-13 DIV)

(A-C) Postsynaptic expression of NLG1-EGFP did not have any effect on presynaptic vesicle clusters (VAMP2 puncta), while LRRTM2 (+EGFP) overexpression significantly increased the VAMP2 puncta density in mature neurons (12-13 DIV). **(A)** Representative overlay images showing parts of dendrites (green, EGFP fluorescence) and VAMP2 (red) staining in EGFP (left), NLG1-EGFP (middle) and LRRTM2 + EGFP (right) expressing neurons, respectively. Scale bar 10 µm. **(B)** Quantification of the dendritic density of VAMP2 puncta in individual neurons. **(C)** Quantification of average dendritic density of VAMP2 puncta (n=12/10/10, n represents the number of neurons). NLG-1 synaptogenic properties were lost during neuronal differentiation. In contrast, LRRTM2 showed a strong synaptogenic effect even in mature neurons. Data are represented as mean ± SEM. *** P < 0.001 (one way ANOVA with Holm-Sidak posthoc test).

In summary, Neuroligin1 and LRRTM2 exhibited strong synaptogenic effects in immature neurons indicating a role in presynaptic vesicle clustering early in development. However, only LRRTM2 showed a synaptogenic effect in mature neurons, while Neuroligin1's synaptogenic effect was lost during neuronal differentiation. These results demonstrated that the synaptogenic activities of Neuroligin1 and LRRTM2 were differentially regulated during development.

3.4.2 Regulation of the synaptogenic properties of NLG1 and LRRTM2 by N-cadherin

Next, experiments were done to determine the dependency of LRRTM2 synaptogenic activity on N-cadherin expression. To test this, effect of LRRTM2 overexpression was studied in N-cadherin knockout neurons (both immature and mature). N-cadherin is known to regulate synaptogenic activity of Neuroligin1. Therefore, Neuroligin1 was used as a positive control.

3.4.2.1 Effect of N-cadherin knockout on the synaptogenic activities of Neuroligin1 and LRRTM2 in immature neurons (9 DIV)

To investigate the role of N-cadherin in regulating the synaptogenic activities of Neuroligin1 and LRRTM2, primary cortical neurons were cultured from homozygous floxed N-cadherin mice ($Ncad^{flox/flox}$; Kostetskii et al., 2005). Control Cells were transfected at 4 DIV with NLG1-EGFP and LRRTM2 + EGFP, respectively and N-cadherin knockout was induced by co-transfecting the neuronal cultures with a Cre expression vector. Synaptogenic activities were studied by immunocytochemically staining the neuronal cultures for VAMP2 clusters at 9 DIV. VAMP2 puncta density/10 μm dendrite length was calculated (Fig. 3.22).

Results showed that VAMP2 puncta density was significantly reduced ($P < 0.05$) after knockout of N-cadherin (1.48 ± 0.163 puncta/10 μm dendrite, $n=11$ cells) from immature neurons as compared to control cells (2.18 ± 0.24 puncta/10 μm dendrite, $n=11$ cells; Fig. 3.22A-C). As expected, NLG1-EGFP overexpression resulted in a significant increase ($P < 0.001$) in VAMP2 puncta density (3.80 ± 0.31 puncta/10 μm dendrite, $n=12$ cells; Fig. 3.22D). However, Cre mediated conditional knockout of N-cadherin led to a reduction in VAMP2 puncta density (2.19 ± 0.29 puncta/10 μm dendrite, $n=15$ cells; Fig. 3.22D-F) to control levels, thereby inhibiting the vesicle cluster accumulating activity of NLG1. Overexpression of LRRTM2 also led to a strong increase in VAMP2 puncta density to 6.43 ± 0.50 puncta/10 μm of dendrite ($n=13$ cells; Fig. 3.22G). Interestingly, this increase in VAMP2 puncta density didn't show any significant change even after the knockout of postsynaptic N-cadherin in LRRTM2 overexpressing cells (6.366 ± 0.42 puncta/10 μm dendrite, $n=16$ cells; Fig. 3.22G-I), indicating no effect of N-cadherin knockout on the synaptogenic activity of LRRTM2.

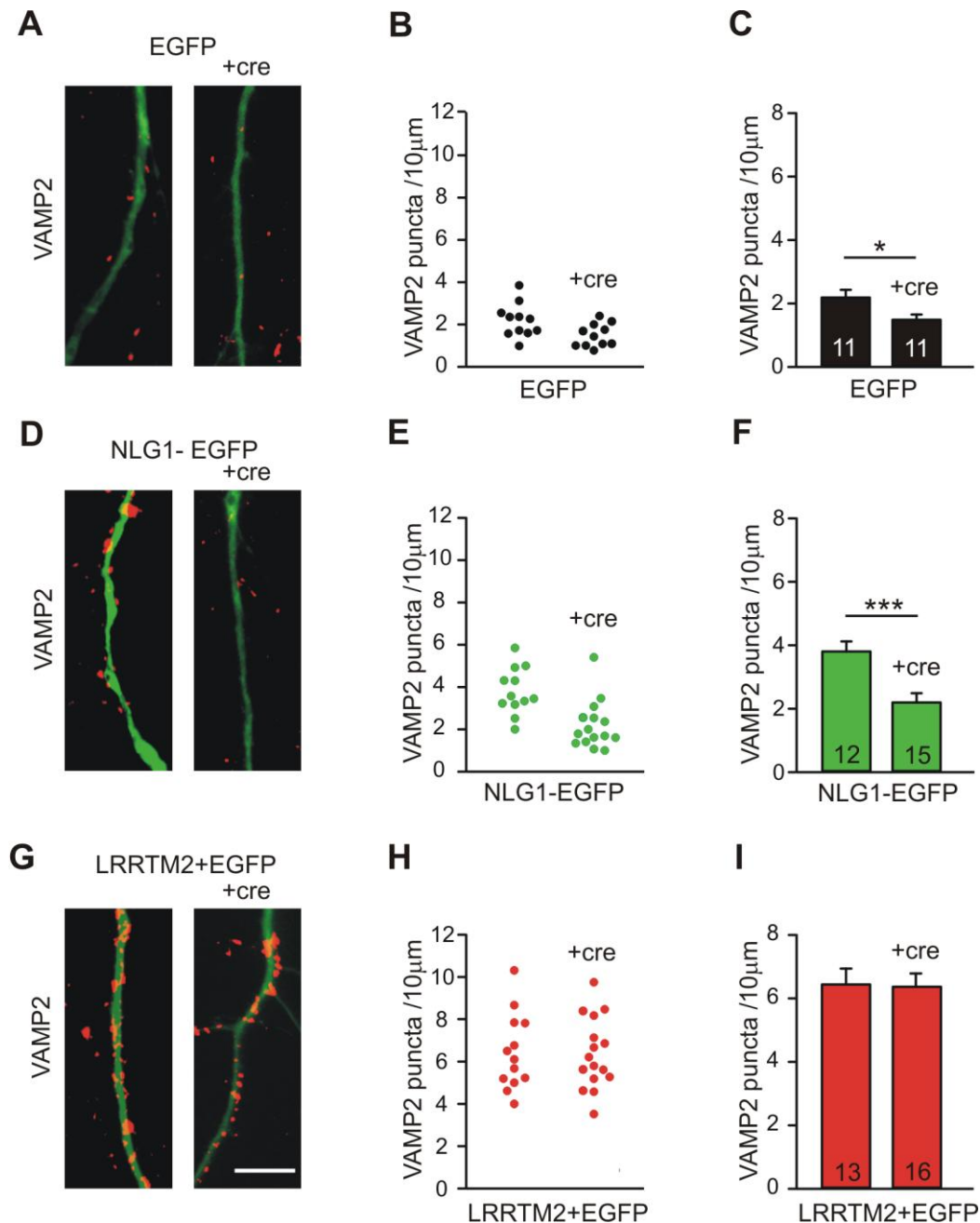


Figure 3.22 Differential dependence of synaptogenic properties of NLG1 and LRRTM2 on N-cadherin expression in immature neurons (9 DIV)

(A-C) Conditional knockout of N-cadherin by Cre expression resulted in a slight reduction in the VAMP2 puncta density in immature neurons (9 DIV). **(A)** Fluorescence overlay images of VAMP2 immunostained puncta (red) on the dendrites of EGFP expressing cortical neurons. +cre: co-expression of Cre to induce knockout of N-cadherin (right). **(B)** Quantification of the dendritic density of VAMP2 puncta in individual neurons. **(C)** Quantification of average VAMP2 puncta density ($n=11/11$ neurons). **(D-F)** The increased VAMP2 puncta density upon NLG1 overexpression was significantly reduced after knockout of N-cadherin. **(D)** Example overlay images of VAMP2 staining on the dendrites of NLG1-EGFP expressing neurons (left). +cre: co-expression of Cre to induce knockout

of N-cadherin (right). **(E)** Quantification of the dendritic density of VAMP2 puncta in individual neurons in the presence and upon knockout of N-cadherin (+cre) in NLG1-EGFP overexpressing neurons. **(F)** Quantification of the average dendritic density of VAMP2 puncta (n=12/15 neurons). **(G-I)** The increased density of dendritic VAMP2 puncta upon overexpression of LRRTM2 was not altered significantly after knockout of N-cadherin. **(G)** Example overlay images of VAMP2 immunostained puncta (red) on dendrites from LRRTM2 + EGFP co-transfected cells (left). +cre: co-expression of Cre to induce knockout of N-cadherin (right). **(H)** Quantification of the dendritic density of VAMP2 puncta in individual neurons. **(I)** Quantification of average VAMP2 puncta density (n=13/16, n represents the number of neurons). Scale bar 10 μ m. *P<0.05, **P<0.01 (Student's t-test).

In summary, knockout of N-cadherin from NLG1 overexpressing cells resulted in a strong reduction of VAMP2 puncta, while not affecting VAMP2 puncta density in LRRTM2 overexpressing cells. These findings indicated that N-cadherin controls the synaptogenic activity of NLG1 in immature neurons, while the synaptogenic properties of LRRTM2 were not dependent on N-cadherin expression.

3.4.2.2 Effect of Ncad Δ E mediated inhibition of N-cadherin function on the synptogenic activities of NLG1 and LRRTM2 in immature neurons (6-7 DIV)

To confirm the N-cadherin knockout results, next, I used a dominant-negative truncated version of N-cadherin protein to inhibit the functions of N-cadherin. This protein was lacking the extracellular domains (Ncad Δ E) of full length N-cadherin. Dissociated cortical neurons were cultured from wildtype mice (C57/BL6) and transfected at 4 DIV analogous to the previous experiment except that Ncad Δ E was used instead of Cre for co-transfection. These cells were immunostained for VAMP2 clusters at 6-7 DIV and analyzed further for VAMP2 puncta density (Fig. 3.23).

Overexpression of Ncad Δ E alone did not result in a significant change in VAMP2 puncta density (1.93 ± 0.17 puncta/10 μ m dendrite, n=21 cells) as compared to control cells (2.21 ± 0.15 puncta/10 μ m dendrite n=20 cells, Fig. 3.23A-C). Postsynaptic overexpression of NLG1-EGFP resulted in a significant (P<0,001) increase in VAMP2 density (3.40 ± 0.23 puncta/10 μ m dendrite, n=21 cells) and this increase in VAMP2 clusters disappeared (2.30 ± 0.24 puncta/10 μ m dendrite, n=23 cells, Fig. 3.23D-F) after co-expressing Ncad Δ E in NLG1 expressing neurons, confirming that functional N-cadherin was required for Neuroligin1 synaptogenic activity.

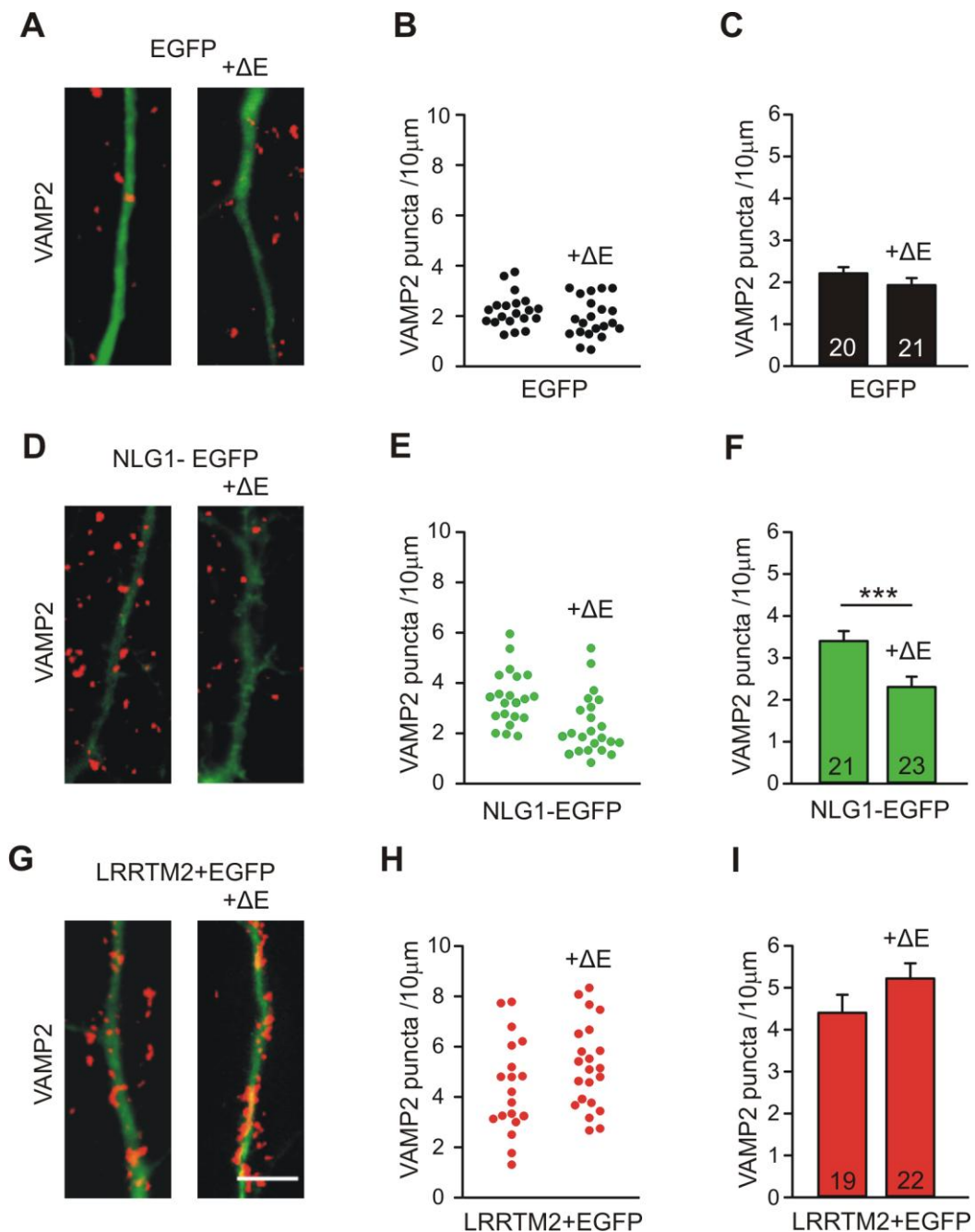


Figure 3.23 Differential dependence of synaptogenic properties of NLG1 and LRRTM2 on N-cadherin function in immature neurons (7 DIV)

(A-C) There was a slight reduction in VAMP2 puncta density on the dendrites of the transfected neurons upon inhibiting the function of N-cadherin by overexpressing NcadΔE (+ΔE), a dominant-negative mutant of N-cadherin lacking the extracellular domains. **(A)** Fluorescence overlay images of VAMP2 immunostained puncta (red) on the dendrites of EGFP expressing neurons (left). +ΔE: co-expression of NcadΔE to inhibit the functions of endogenous N-cadherin (right). **(B)** Quantification of VAMP2 puncta density on dendrites in individual neurons. **(C)** Quantification of average VAMP2 puncta density (n=20/21 neurons). **(D-F)** Increased VAMP2 puncta density induced by the overexpression of NLG1 was significantly reduced upon blocking N-cadherin function. **(D)**

Fluorescence overlay images of VAMP2 puncta (red) on the dendrites of NLG1-EGFP overexpressing neurons (left). + Δ E: co-expression of Ncad Δ E to inhibit the functions of N-cadherin in NLG1-EGFP expressing neurons (right). **(E)** Quantification of the dendritic density of VAMP2 puncta in individual neurons. **(F)** Quantification of the average VAMP2 density in NLG1-EGFP overexpressing neurons in the presence of N-cadherin and after Ncad Δ E expression (n=21/23). **(G-I)** Increased VAMP2 puncta density induced by the overexpression of LRRTM2 was not altered significantly after inhibiting the function of N-cadherin. **(G)** Fluorescence overlay images of VAMP2 puncta (red) on the dendrites of LRRTM2 overexpressing neurons (Left). Δ E: co-expression of Ncad Δ E to inhibit N-cadherin function in LRRTM2 overexpressing neurons (right). **(H)** Quantification of VAMP2 puncta density on the dendrites of individual neurons. **(I)** Quantification of the average VAMP2 density (n=19/22, n represents number of neurons). Scale bar 5 μ m. Statistics was done using student's t-test. *P<0.01.

Next, the LRRTM2 mediated vesicle clustering effect was analysed and as expected, LRRTM2 expressing neurons showed a strong increase in VAMP2 puncta density (4.40 ± 0.42 puncta/10 μ m dendrite, n=19 cells) as compared to EGFP expressing neurons (control, 2.21 ± 0.15 ; n=20 cells). Ncad Δ E co-expression didn't induce a significant change in the vesicle cluster inducing properties of LRRTM2 as shown by VAMP2 puncta density (5.22 ± 0.36 puncta/10 μ m dendrite, n=22 cells, Fig. 3.23G-I). These results confirmed that the synaptogenic properties of LRRTM2 were not dependent on N-cadherin function.

Both Cre induced conditional knockout of N-cadherin and Ncad Δ E mediated inhibition of N-cadherin function showed that N-cadherin regulates the synaptogenic activity of NLG1 in immature neurons, while LRRTM2 synapse inducing activity was independent of N-cadherin.

3.4.2.3 Effect of N-cadherin knockout on the synaptogenic activity of LRRTM2 in mature neurons (14-15 DIV)

To further confirm the functional independence of LRRTM2 on N-cadherin in mature neurons, dissociated cortical neurons were cultured from homozygous floxed N-cadherin mice and were transfected at 9 DIV with EGFP and LRRTM2 + EGFP. Cre was co-expressed for 5-6 days to knockout postsynaptic N-cadherin and the effect was analyzed using VAMP2 stainings (14-15 DIV).

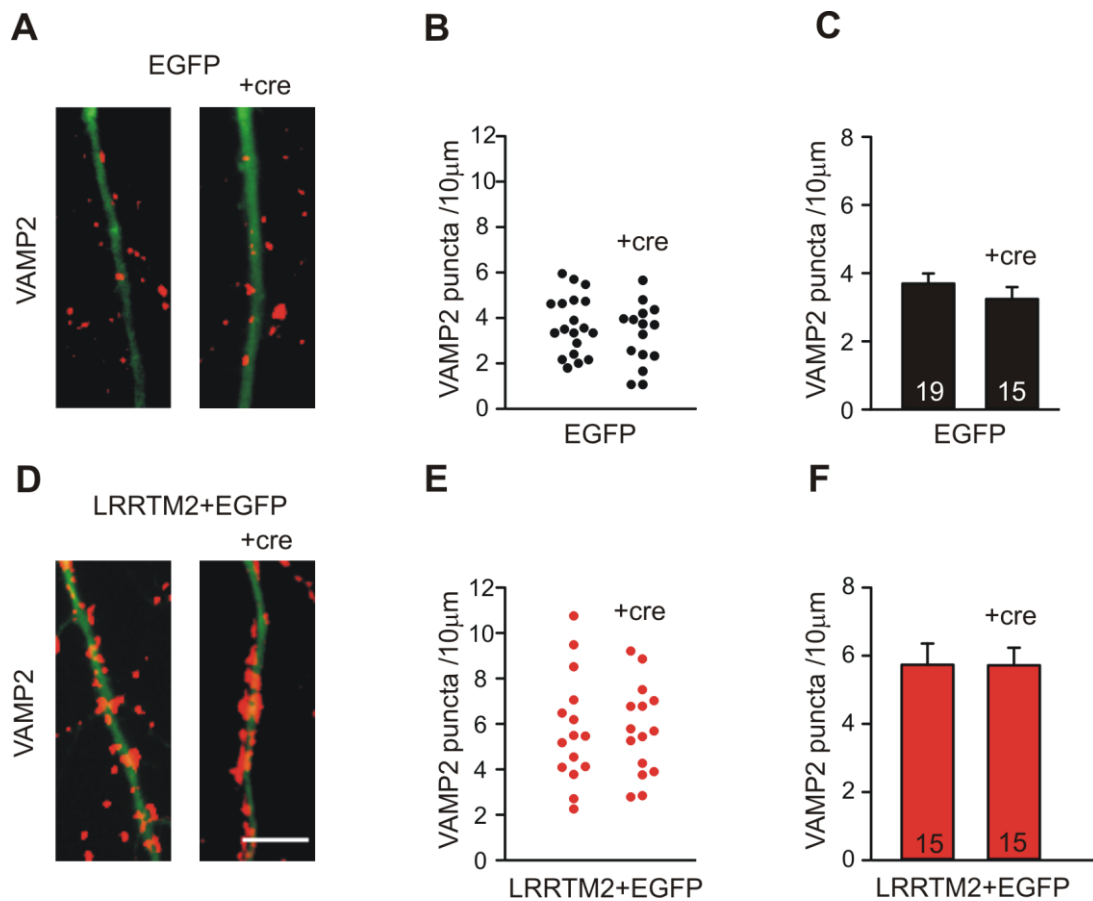


Figure 3.24 LRRTM2 synaptogenic effect is independent of N-cadherin expression in mature neurons (14-15 DIV)

(A-C) VAMP2 puncta density was not altered upon N-cadherin knockout from mature neurons (14-15 DIV). (A) Fluorescence overlay images of VAMP2 immunostained puncta (red) on the dendrites of EGFP expressing cortical neurons. +cre: co-expression of Cre to induce the knockout of N-cadherin (green EGFP; red VAMP2). (B) Quantification of the dendritic density of VAMP2 puncta in individual neurons. (C) Quantification of the average density of VAMP2 puncta (n=19/15 neurons). (D-F) Increased VAMP2 puncta density induced by overexpression of LRRTM2 was not altered significantly by N-cadherin knockout. (D) Fluorescence overlay images of VAMP2 immunostained puncta (red) on the dendrites of LRRTM2 and EGFP co-expressing cells. +cre: co-expression of Cre to induce knockout of N-cadherin (green EGFP; red VAMP2). (E) Quantification of the dendritic density of VAMP2 puncta in individual neurons. (F) Quantification of the average VAMP2 puncta density (n=15/15, n represents the number of neurons). Scale bar 5 μm. Student's t-test.

NLG-1 was excluded from this experiment because it is not synaptogenic in mature neurons (see previous results, Fig. 3.22). Knockout of N-cadherin from mature neurons (+cre, 3.24 ± 0.35 puncta/10 μm dendrite, n=15 cells; Fig. 3.24A-C) didn't change the VAMP2 puncta density as compared to control cells (EGFP, 3.69 ± 0.29

puncta/10 μm dendrite, $n=19$ cells; Fig. 3.24A-C) indicating that once the neurons are mature, N-cadherin did not affect their synapse number.

As expected, postsynaptic overexpression of LRRTM2 led to a strong increase in VAMP2 puncta density (5.73 ± 0.62 puncta/10 μm dendrite, $n= 15$ cells; Fig. 3.24D-F) and this increase was not affected after deletion of N-cadherin (5.71 ± 0.51 puncta/10 μm dendrite, $n=15$ cells; Fig. 3.24D-F), indicating that the synaptogenic activity of LRRTM2 is independent on N-cadherin expression in mature neurons.

These results confirmed that the synaptogenic effects of LRRTM2 were not dependent on N-cadherin expression in mature neurons.

04-

Discussion

4. Discussion

Synapses in the brain communicate via neurotransmission, a process that includes vesicle exo- and endocytosis. Exocytosis involves the fusion of transmitter-filled synaptic vesicles at the presynaptic release sites while the reformation and recovery of these vesicles at the adjacent site (peri-active zone) happens via various modes of endocytosis. Several key proteins are involved in this process and one class among these is homophilic Ca^{2+} dependent cell adhesion protein called N-cadherin. Classical cadherins are among one of the first molecules that has been detected at axon-filopodia contact sites (Jontes et al., 2004). However, the study of the functional role of neural (N)-cadherin at synapses was largely hindered by the embryonic lethality (E10) of N-cadherin null genetic mice (Radice et al., 1997). Therefore, various alternative approaches were used to investigate the role of N-cadherin at synapses. These approaches includes a pan-cadherin block of function by either expressing a dominant-negative truncated cadherin (Togashi et al., 2002; Abe et al., 2004; Bozdagi et al., 2004; Andreyeva et al., 2012), by application of antibodies and peptides that block the interaction of extracellular N-cadherin domains (Tang et al., 1998; Bozdagi et al., 2000), embryonic stem cells (ES) derived N-cadherin knockout neurons (Jüngling et al., 2006; Stan et al., 2010), and cre-mediated conditional knockout approach (van Stegen et al., 2017). N-cadherin has been well known to play an important role in spine stabilization and long-term potentiation (LTP) (Togashi et al., 2002; Bozdagi et al., 2004; Bozdagi et al., 2010). Recent studies have also indicated the role of N-cadherin in synaptic vesicle cycling (Togashi et al., 2002; Jüngling et al., 2006; Viturera et al., 2011; van Stegen et al., 2017).

In this study, selective deletion of N-cadherin using cre-mediated conditional knockout approach was used in combination with SypHy imaging and superresolution microscopy in cortical neurons to gain insights into the functional role of N-cadherin in synaptic vesicle cycling. Furthermore, I investigated the mechanism involved in the regulation of vesicle endocytosis. N-cadherin knockout resulted in reduced vesicle exo- and endocytosis. Both clathrin-mediated and bulk endocytosis were altered in the absence of N-cadherin. Actin polymerizing drug, Jasplakinolide was able to rescue the knockout effects of N-cadherin. During strong release conditions (50 mM K^+), N-cadherin is recruited to the synapses that were previously devoid of it. I

observed a similar recruitment of N-cadherin to the synapses during neuronal development.

4.1 SypHy imaging as a tool to study vesicle exo- and endocytosis

In this study, SypHy imaging was performed using cultured cortical neurons grown in a microisland system. In microisland, 5-8 neurons were grown on the top of a glial cell.

The microisland cultures are important because the growth of the axon is restricted to the glial cell boundary, thereby leading to the formation of a high percentage of autapses (synaptic contacts formed between the axon of a neuron with its dendrites). Autapses are interesting as they have been shown to be present *in vivo* and are not mere the artifact of *in vitro* cultures (Bekkers, 2003). Microisland cultures enable the simultaneous recording from several SypHy puncta within one field of view and autapses allow the deletion of the homophilic cell adhesion molecule N-cadherin on both pre-and postsynaptic site.

The neuronal cultures were transfected using the MagnetofectionTM technique. DsRed2 was used as a transfection marker to visualize the transfected neurons because SypHy signals are quenched in the resting conditions. For analysis, the NH₄Cl-induced maximal SypHy signal was merged with the corresponding DsRed2 signal to differentiate autapses from other axonal contacts (Fig.3.1B). The electrical stimulation led to a fast increase in SypHy fluorescence signal (exocytosis). The decline of SypHy signal post-stimulus corresponds with the speed of vesicle endocytosis and reacidification (Fig. 3.1). As reacidification process is fast compared to vesicle endocytosis, the decline of SypHy signal can be quantified as endocytosis (Atluri and Ryan, 2006; Granseth et al., 2006; Royle et al., 2008).

SypHy fluorescence intensities over time from individual puncta (Fig.3.1E) were averaged to obtain a mean SypHy signal for each cell (Fig.3.1E-F). The combination of SypHy imaging and the autaptic glial microisland culture system is an optimal system for the separate analysis of vesicle exo-and endocytosis.

4.2 Role of N-cadherin in regulating synaptic vesicle exocytosis

Previous studies indicated a role of N-cadherin in synaptic vesicle cycling. N-cadherin deficient neurons have been shown to undergo reduced synaptic vesicle release as shown by FM experiments in N-cadherin deficient neurons (Jüngling et al., 2006). Postsynaptic inhibition of N-cadherin function by the overexpression of a dominant-negative N-cadherin mutant resulted in the reduced recycling vesicle pool and decreased release probability (Vitureira et al., 2011). FM-destaining and SypHy experiments demonstrated a significantly reduced exocytosis in N-cadherin knockout neurons (van Stegen et al., 2017).

However, I did not find any effect of N-cadherin knockout (or mutant N-cadherin overexpression) on vesicle exocytosis as shown by SypHy experiments (Fig. 3.2A-C; Fig 3.3A-C; Fig. 3.5A-C). The change in temperature from room (25°C, Fig. 3.2A-C) to near physiological (34°C, Fig. 3.3A-C) also did not affect the exocytosis.

A possible explanation for this discrepancy in results is because of the variations in the experimental setups used. Firstly, these studies have used FM staining/destaining to study vesicle cycling. FM stainings only provide basic information about the functionality of the presynaptic vesicle cluster and cannot distinguish vesicular exo- and endocytosis. Therefore, a differential analysis of vesicle exocytosis using FM stainings is problematic. Secondly, the electrical stimulation protocols used in these studies were highly different. Jungling et al., 2006 specifically reported impairment in the replenishment of the readily releasable vesicle pool in N-cadherin deficient neurons. van Stegen et al., 2017 used 200 electrical stimulations and 800 stimulations keeping the frequency constant (20 Hz) and showed that vesicle exocytosis was reduced at 200 stimulations while not affected at 800 stimulations. The electrical stimulation used in the current study is 400 stimulations (20 Hz). It is possible that 400 and 800 electrical stimulations might be too strong for the synapses and might result in the depletion of readily releasable vesicle pool. Therefore, these synapses are forced to release vesicles from the other available pools thus masking the exocytosis defect. To test this hypothesis, vesicle release was induced using 100 stimulations (20 Hz) and SypHy experiments were performed to observe the change in exocytosis in N-cadherin knockout neurons.

At this condition, synaptic vesicle exocytosis was reduced in N-cadherin knockout neurons compared to the control cells (Fig. 3.6A-C, F), thus confirming the role of N-cadherin in regulating vesicle exocytosis.

4.3 Role of N-cadherin in regulating synaptic vesicle endocytosis

A role of N-cadherin in synaptic vesicle endocytosis has been suggested previously. N-cadherin overexpressing neurons showed faster vesicle endocytosis (van Stegen et al., 2017) while blocking the functions of N-cadherin resulted in reduced FM uptake (Togashi et al., 2002; Vitureira et al., 2011). However, FM dye uptake is dependent on both vesicle exo- and endocytosis, making it difficult to isolate its effect on one particular process. Recent study from our lab showed the importance of N-cadherin in activity-dependent endocytosis (van Stegen et al., 2017). N-cadherin knockout resulted in a defect in endocytosis only during strong release conditions. However, in this study van Stegen et al., 2017 used an overexpression approach to show enhanced endocytosis at synapses and the experiments were performed at room temperature (van Stegen et al., 2017). N-cadherin knockout did not show any effect on endocytosis during normal release conditions (400 electrical stimuli) at room temperature (Fig. 3.2A, D-G). However, synaptic vesicle endocytosis is known to be temperature sensitive (Watanabe et al., 2014b; Delvendahl et al., 2016; Soykon et al., 2017; Chanaday and Kavalali, 2018). Therefore, SypHy experiments were repeated at near physiological temperature keeping other experimental conditions the same. Interestingly, a defect in endocytosis was observed in N-cadherin knockout cells at near physiological temperature (Fig. 3.3A, D-G) indicating a role of N-cadherin in regulating vesicle endocytosis confirming the previous studies (Togashi et al., 2002; Vitureira et al., 2011). A direct comparison of control data from room temperature experiment with near physiological temperature revealed a clear increase in the speed of the endocytosis with the increase in temperature confirming the temperature sensitivity of this process (Fig. 3.4A, D-G; Watanabe et al., 2013, 2014; Delvendahl et al., 2016). FM1-43 and TMR-dextran co-staining experiments also resulted in a significant reduction in the total density of FM1-43 puncta in N-cadherin knockout cells compared with control cells (Fig. 3.9A-C).

The functions of N-cadherin were inhibited by overexpressing a dominant-negative mutant N-cadherin (Andreyeva et al., 2012) and SypHy results showed a reduction in endocytosis confirming the N-cadherin knockout results (Fig. 3.5A, D-G). There was

a significant decrease in total FM puncta density in dominant-negative mutant N-cadherin overexpressing neurons as compared to control cells again confirming reduced endocytosis (Fig. 3.11A-C).

These results together with the previous studies strengthen the proposed role of N-cadherin in regulating synaptic vesicle endocytosis.

4.4 Role of N-cadherin in regulating clathrin-mediated endocytosis

SypHy experiments demonstrated a role of N-cadherin in vesicle endocytosis. However, synapses have several modes of endocytosis like clathrin-mediated endocytosis (CME) or activity-dependent bulk endocytosis and with the SypHy imaging, it is not possible to differentially study these vesicle retrieval processes. Therefore, FM dye and dextran were used to further study the role of N-cadherin in different modes of endocytosis. FM1-43 is an activity-dependent hydrophobic dye known to label actively cycling vesicles and report all forms of endocytosis (Ryan TA et al., 1996; Gaffield and Betz, 2007; Clayton and Cousin, 2008). Bulk endocytosis was visualized using tetramethylrhodamine-dextran (TMR-dextran, 40 kDa), a high molecular weight fluid phase marker. TMR-dextran is conjugated to a fluorescent molecule and has been shown to label specifically endosomes (bulk endocytosis) (Clayton and Cousin, 2009).

FM1-43 labeled puncta showed a co-localisation with TMR-dextran confirming the specific uptake of dextran at synapses. Uptake of FM1-43 and TMR-dextran at synapses was dependent on the stimulation as well as on temperature. Increase in stimulation (from 200 stimuli to 400 and 2000 stimuli at 20 Hz) at room temperature (25°C) resulted in higher uptake of TMR-dextran indicating that stronger stimulations activate bulk endocytosis (Clayton et al., 2008). Increasing the temperature to near physiological (34°C) also led to an increase in TMR-dextran uptake (Fig. 3.7A-D). These results showed that strong vesicle release and near physiological temperature, both have an enhancing effect on TMR-dextran staining (Fig. 3.7D). These results confirm the previous results from other labs (Clayton and Cousin, 2008; Clayton and Cousin, 2009).

To differentiate CME and bulk endocytosis, two different stimulation conditions were selected. CME was labeled with 200 stimuli at 25°C and bulk endocytosis was observed at 400 stimuli at 34°C. Percentage of FM puncta co-localising with TMR-

dextran was quantified as a change in bulk endocytosis while puncta with only FM staining were measured as change in CME.

N-cadherin knockout neurons were stimulated with 200 stimuli at 25°C in the presence of FM1-43 and TMR-dextran. At this particular condition, most of the synapses were labeled with only FM1-43, thus confirming that clathrin-mediated endocytosis is the main mode of vesicle retrieval. N-cadherin knockout in mature neurons (DIV 14-15) resulted in a significant reduction in FM puncta indicating reduced CME (Fig. 3.8A-C, F-G). To further confirm the N-cadherin knockout results, the dominant-negative N-terminal truncated construct of N-cadherin (Ncad Δ E) was used to inhibit the functions of N-cadherin (Andreyeva et al., 2012). However, inhibiting the functions of N-cadherin did not induce a significant effect on clathrin-mediated endocytosis (Fig. 3.10A-C, F-G; Fig. 3.11F-G). It is possible that Ncad Δ E might induce a weaker inhibition than knockout.

4.5 Role of N-cadherin in regulating activity-dependent bulk endocytosis

To observe the effect of N-cadherin on bulk endocytosis, N-cadherin knockout neurons were stimulated with 400 stimuli at 34°C in the presence of FM1-43 and TMR-dextran. N-cadherin knockout in mature neurons (DIV 14-15) resulted in a significant reduction in the density of FM puncta co-localising with TMR-dextran indicating reduced bulk endocytosis (Fig. 3.9A, D-E). N-cadherin knockout results were confirmed using a dominant-negative N-terminal truncated construct of N-cadherin (Ncad Δ E). Overexpression of Ncad Δ E in the neurons inhibits the functions of N-cadherin (Andreyeva et al., 2012). There was a significant reduction in the density of FM1-43 puncta co-localising with TMR-dextran confirming reduced bulk endocytosis (Fig. 3.11A, D-E). At higher stimulations (400 stimuli as compared to 200 stimuli in the previous experiment), the effect of Ncad Δ E might become more prominent even though the inhibition is still weak.

Watanabe et al., 2013b recently described a novel mode of vesicle endocytosis (ultrafast endocytosis, 100 ms) using an innovative electron microscopy technique. This study used optogenetic stimulations to induce synaptic transmission in hippocampal neurons and the subsequent steps of membrane dynamics were captured by freezing the neurons at defined time intervals. This form of vesicle endocytosis is compensatory and happens at special zones lateral to the site of

exocytosis (peri-active zone). Since N-cadherin is also localized at peri-active zone (Uchida et al., 1996; Elste and Benson, 2006). It may also play an important role during ultrafast endocytosis to remove the extra presynaptic membrane. Synaptic vesicle fusion has been shown to be mandatory for the ultrafast endocytosis. Ultrafast endocytosis is independent of clathrin; however clathrin is required for budding the vesicles from the endosomes (Watanabe et al., 2014).

4.6 Regulation of vesicle endocytosis by actin

Actin polymerization has been shown to enhance vesicle endocytosis (Nguyen et al., 2012; Soykan et al., 2017). The addition of jasplakinolide, an actin polymerization drug to control cells as well as N-cadherin knockout cells did not induce any change in vesicle exocytosis indicating no effect of actin polymerization on vesicle release (Fig. 3.12A-C). However, treatment of control cells with jasplakinolide resulted in a trend towards faster endocytosis as compared to the untreated control cells (Fig. 3.12A2, D-G; Wu et al., 2016; Soykan et al., 2017). This might be because the control cells already have efficient vesicle retrieval. So these synapses might not need to further improve endocytosis, thus show only a slight effect of actin polymerization on vesicle endocytosis. Interestingly, polymerization of actin in N-cadherin knockout cells resulted in faster endocytosis thereby confirming the rescue effect of jasplakinolide (Fig. 3.12A3, D-G). These results indicate that N-cadherin might regulate endocytosis via actin. N-cadherin-mediated homophilic adhesion signals generated at the synaptic sites are probably transmitted to the actin cytoskeleton because the cytoplasmic domain of N-cadherin is known to interact with actin via α -catenin and β -catenin (Bamji et al., 2003; Abe et al., 2004; Dress et al., 2005; Tai et al., 2007; Okuda et al., 2007). For efficient endocytosis to happen, synapses might need a physical force to take up the extra presynaptic membrane added by fused synaptic vesicles (Nguyen et al., 2012; Meunier and Gutiérrez 2016; Wen et al., 2016). This extra membrane might need to first turn inwardly to form invaginations and this inversion of membrane might be derived by N-cadherin/actin mediated force.

4.7 SIM imaging based analysis of the mechanism of regulation of endocytosis by N-cadherin

N-cadherin has been shown to undergo a change in synaptic localization with synapse maturation, initially being present at all synaptic sites but at later stages becoming restricted to a subpopulation of excitatory synapses (Benson and Tanaka, 1998). Furthermore, it has been described that during development, N-cadherin localization undergoes changes. At 5-6 days in culture, when most synapses are newly formed, N-cadherin is uniformly distributed inside the active zone at the synaptic cleft. Whereas when the majority of synapses are rather mature (14 DIV), N-cadherin concentrates in discrete clusters surrounding the synaptic cleft (peri-active zone; Elste and Benson, 2006).

SIM imaging was used to study the spatial localization of N-cadherin during development and results revealed that the majority of the synapses in mature neurons contain N-cadherin in the vicinity of the active zone often flanking one side of the synaptic cleft (peri-active zone; Fig. 3.14A-A1; Fig. 3.15). These findings confirmed the previous studies which showed the presence of N-cadherin at peri-active zone (Uchida et al 1996; Elste and Benson, 2006). However, there was little to no N-cadherin inside the synaptic cleft even in the immature neurons (Fig. 3.14C-C1, Fig. 3.15D). Furthermore, there were a lot of synapses without any N-cadherin associated (Fig. 3.14D-D1). SIM imaging showed that there was an increase in the total fraction of synapses with cleft associated N-cadherin and the fraction of synapses without any N-cadherin goes down during neuronal differentiation (Fig. 3.15D). It is possible that the active zone N-cadherin puncta are only a few in numbers and might be below the detection threshold of our imaging setup. Furthermore, there might be a sensitivity issue of SIM imaging. SIM imaging requires a strong and clear antibody signal and high thresholding was applied for the analysis. This might have led to the disappearance of pure synaptic N-cadherin puncta (active zone; Elste and Benson, 2006).

K⁺ stimulation has been shown to induce N-cadherin dimer formation, induce resistant to trypsin (Tanaka et al., 2000), spine head expansion (Okamura et al., 2004) and movement of beta-catenin into spines (Murase et al., 2002). In addition, Yam et al., 2013 described that KCl depolarization also induces N-cadherin localization change within the synapse. N-cadherin moves out from the central region

of the synaptic cleft (active zone) to the periphery of the synapse (peri-active zone). It has been shown that presynaptic functional impairment in N-cadherin knockout neurons becomes detectable only under high activity conditions when the vesicle pools are used at their maximum capacity, indicating a defective vesicle pool function (Jüngling et al., 2006) and impaired endocytosis (van Stegen et al., 2017). In agreement with these studies, I also found that K^+ stimulation leads to an increase in N-cadherin puncta area (Fig. 3.16A-C, D) and PSD95 puncta were not changed (Fig. 3.16E). Neuronal cultures were stimulated with a high concentration of K^+ and N-cadherin was immunostained. K^+ stimulation led to an increase in the N-cadherin puncta area. Physiologically, K^+ stimulation leads to a massive fusion of synaptic vesicles to the presynaptic membrane leading to an increase in the area of the presynaptic terminal. This increase in N-cadherin area might provide stability to the enlarged presynaptic terminal. In addition, there was an increase in the fraction of synapses with cleft associated N-cadherin or peri-active zone associated N-cadherin (Fig. 3.17A-D). This recruitment of N-cadherin to the peri-active zone might facilitate (enhance) the process of endocytosis.

The peri-active is thought to be the major site for all form of synaptic vesicle endocytosis (clathrin-mediated endocytosis and bulk endocytosis; Gad et al., 1998; Roos and Kelly, 1999; Teng and Wilkinson, 2000; Hua et al., 2011, ultrafast endocytosis; Watanabe et al., 2013b). N-cadherin is also located at peri-active zone (Uchida et al., 1996; Elste and Benson, 2006). Therefore, it is possible that during multiple rounds of exocytosis, ultrafast endocytosis or bulk endocytosis removes the excess presynaptic membrane with the help of N-cadherin. Interestingly, I observed that N-cadherin is recruited to the nascent synapses upon K^+ stimulation (Fig. 3.17D). This N-cadherin might be recruited from the non-synaptic pool of N-cadherin. Therefore, the recruitment of N-cadherin might also represent activity-dependent synapse maturation.

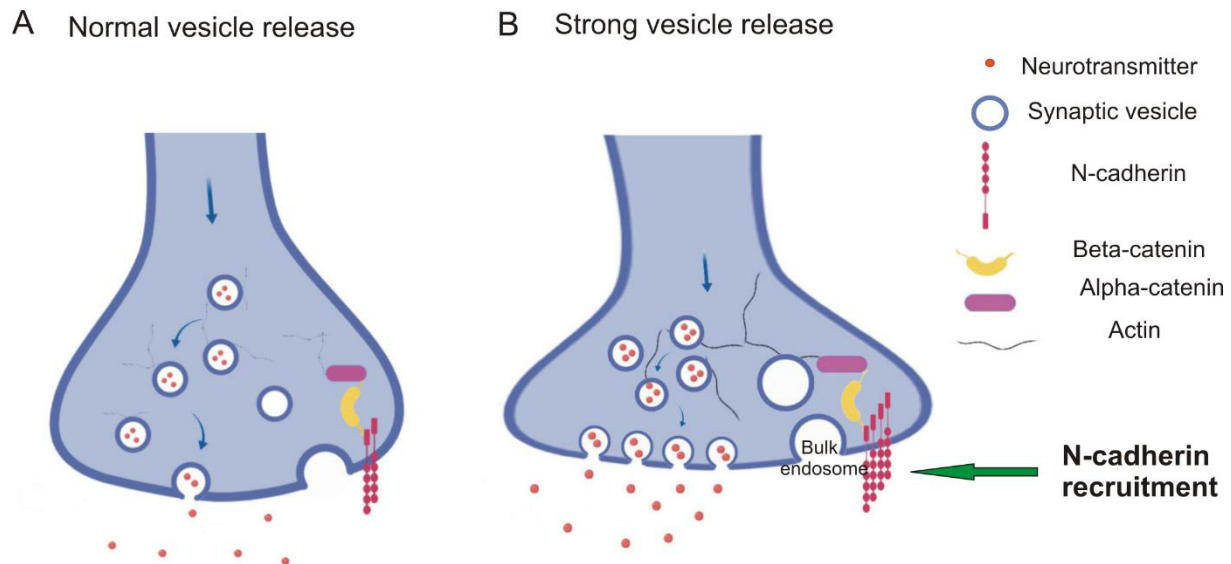


Figure 4.1 Model of N-cadherin involvement in synaptic vesicle cycling

N-cadherin is present at lateral sites (peri-active zone) to the active zone and regulates the retrieval of the presynaptic membrane by playing an important role in various modes of endocytosis. (A) During normal vesicle release, N-cadherin facilitates clathrin-mediated endocytosis, (B) while strong vesicle release recruits additional N-cadherin to the synapses and activates activity-dependent bulk endocytosis.

In summary, the above described results support the role of N-cadherin in vesicle cycling with a particular importance on vesicle endocytosis. Based on the current and previous results, I propose a model explaining the regulation of vesicle cycling by N-cadherin.

During low vesicle release, readily releasable vesicle pool is available for exocytosis and there is an impairment in the replenishment of this pool of vesicles in N-cadherin deficient neurons (Jungling et al., 2006). In line with these results, I also found a reduction in vesicle exocytosis upon knockout of N-cadherin (Fig. 3.6A-C, F). Additionally, vesicle endocytosis is also defective in N-cadherin knockout neurons (Fig. 3.3D-G). During multiple rounds of exocytosis (upon strong stimulations), synapses are forced to release vesicles from recycling pool and reserve pool masking the exocytosis defect in N-cadherin knockout neurons (Fig. 3.2A-C; Fig. 3.3A-C).

Upon strong vesicle release, vesicles fuse with the presynaptic membrane and leads to the enlargement of presynaptic bouton. This results in a bulging of presynaptic

terminal while the postsynaptic region remains the same thus making the synapse unstable. At this point, addition of more vesicular membrane may result in disruption of presynaptic bouton as it needs additional support to remain stable. One possibility is that the non-synaptic N-cadherin molecules are recruited to these synapses which first makes the adhesion more strong to provide stability to the synapses and later activates the actin-mediated signaling to facilitate bulk endocytosis.

Since synaptic vesicle endocytosis is known to occur at peri-active zone (Gad et al., 1998; Teng and Wilkinson, 2000; Watanabe et al., 2013b) and N-cadherin is also localized at the same site (Uchida et al., 1996; Elste and Benson, 2006), it could easily facilitates endocytosis (clathrin-mediated or bulk endocytosis) based on the requirements of the synapse. N-cadherin has been shown to interact with actin cytoskeleton via α -catenin and β -catenin (Bamji et al., 2003; Abe et al., 2004; Dress et al., 2005; Okuda et al., 2007) and polymerization of actin enhances the vesicle endocytosis (Soykan et al., 2017). Therefore, it is possible that N-cadherin regulates endocytosis via interactions with actin cytoskeleton.

4.8 Regulation of the synaptogenic properties of LRRTM2 and Neuroligin1 by N-cadherin

In this study, the synaptogenic activities of LRRTM2 and Neuroligin1 were compared during neuronal differentiation and their dependency on N-cadherin expression and functions was studied. Neuroligin1 has been repeatedly described to induce new presynaptic vesicle clusters in the contacting axon in immature neurons (Scheiffele et al., 2000; Fu et al., 2003; Sara et al., 2005; Ko et al., 2009; Banovic et al., 2010) and our results once again confirm the synapse formation effect of Neuroligin1 in immature neurons (Fig. 3.18B, Fig. 3.19A-C). However, Neuroligin1 is not synaptogenic in mature neurons (Fig. 3.20B, Fig. 3.21A-C). This is in line with previous studies (Wittenmayer et al., 2009; van Stegen et al., 2017) and confirms that Neuroligin1 synaptogenic activity is strongly dependent on neuronal development. In mature neurons, Neuroligin1 is known to enhance synaptic vesicle exocytosis (van Stegen et al., 2017). During neuronal differentiation, there seems to be a switch in Neuroligin1 functions from inducing structural changes in immature neurons to more functional effects in mature neurons. LRRTM2, another postsynaptic cell adhesion molecule has been recently identified as a novel synaptogenic protein when

expressed in non-neuronal cells, capable of inducing vesicle clustering in the contacting axon (Linhoff et al., 2009; de Wit et al., 2009; Ko et al., 2009). Similar to NLG1 and in line with previous studies, I also found that LRRTM2 was able to induce vesicle clustering in immature neurons (Fig. 3.18C, Fig. 3.19A-C). Interestingly, LRRTM2 is synaptogenic even in mature neurons showing that the synaptogenic properties of LRRTM2 were not altered during neuronal differentiation *in vitro* (Fig. 3.20C, Fig. 3.21A-C). These results strongly indicate that both synaptic adhesion molecules behave differently in the molecular context of neurons.

Knockout of N-cadherin from immature neurons led to a reduction in presynaptic vesicle (VAMP2) clusters (Fig. 3.22A-C, Togashi et al., 2002; Stan et al., 2010) while the vesicle clusters were not altered after knockout of N-cadherin from mature neurons (Fig. 3.24A-C). These results were in line with the previously described results in mature N-cadherin deficient neurons (Jüngling et al., 2006; Kadowaki et al., 2007) and mature neurons transfected with a dominant-negative mutant cadherin (Bozdagi et al., 2004). Furthermore, the synaptogenic activity of Neuroligin1 was found to be crucially dependent on the expression and function of the adhesion molecule N-cadherin (Fig. 3.22D-F, Fig. 3.23D-F, Stan et al., 2010; Aiga et al., 2011), whereas LRRTM2 did not require N-cadherin expression or function (Fig. 3.22G-I, Fig. 3.23G-I). These results demonstrate that the requirements to exhibit synaptogenic activity in neurons are rather different for Neuroligin1 and LRRTM2. These results differ from Yamagata et al., 2018. Yamagata et al., 2018 recently described that the synaptogenic properties of both Neuroligin1 and LRRTM2 depend on N-cadherin expression. However, this study used the co-culture of HEK293 cells and presynaptic neurons. This culture system is non-physiological as the presynaptic axons form contacts with postsynaptic HEK293 cells. In our cultures, presynaptic axons make contacts exclusively with other postsynaptic neurons and these neurons have other adhesion molecules which might compensate for the loss of N-cadherin intercellular adhesive activity. Since HEK293 cells are non-neuronal cells, they may not have these extra compensatory synaptic cell adhesion proteins. This might explain the strong dependency of neurite branching and contact formation on N-cadherin in Yamagata et al., 2018. Because intercellular contact formation appears to be an important requirement for vesicle clustering in the presynaptic axon, a defect in contact formation will lead to an apparent loss of synaptogenic activity (Yamagata et

al., 2018). Therefore, the differences in the cell types e.g. HEK293 cells versus cortical neurons, used for overexpression studies can influence the observed functional properties of these adhesion molecules. The lateral mobility of adhesion molecules at synaptic and extrasynaptic sites can also be another determining regulatory factor and might explain the differential dependency of these molecules on N-cadherin (Chamma et al., 2019). Using single-molecule nanoscale imaging, Neuroligin1 has been described to be highly dynamic, dispersed and sensitive to the synaptic stimulations at dendritic spines. In contrast, LRRTM2 is organized in compact and stable synaptic nanodomains (Chamma et al., 2016a, b). N-cadherin is known to control Neuroligin1 activity via SSCAM and this adhesion system might modulate the high lateral mobility of Neuroligin1, thereby potentially regulating its synaptic localization, whereas LRRTM2 might be subsynaptically anchored by other molecular mechanisms and thus might not require N-cadherin for synaptic localization. This might explain the differential requirement for N-cadherin expression of the synaptogenic activities of Neuroligin1 and LRRTM2, respectively.

05-

References

5. References

1. Abe K, Chisaka O, Van Roy F, Takeichi M (2004). Stability of dendritic spines and synaptic contacts is controlled by alpha N-catenin. *Nat Neurosci.* 7(4):357-363.
2. Aiga M, Levinson JN, Bamji SX (2011). N-cadherin and neuroligins cooperate to regulate synapse formation in hippocampal cultures. *J Biol Chem.* 286(1):851-858.
3. Andreyeva A, Nieweg K, Horstmann K, Klapper S, Müller-Schiffmann A, Korth C, Gottmann K (2012). C-terminal fragment of N-cadherin accelerates synapse destabilization by amyloid- β . *Brain.* 135(Pt 7):2140-2154.
4. Arikath J, Reichardt LF (2008). Cadherins and catenins at synapses: roles in synaptogenesis and synaptic plasticity. *Trends Neurosci.* 31(9):487-494.
5. Atluri PP, Ryan TA (2006). The kinetics of synaptic vesicle reacidification at hippocampal nerve terminals. *J Neurosci.* 26(8):2313-2320.
6. Augustine GJ, Burns ME, DeBello WM, Hilfiker S, Morgan JR, Schweizer FE, Tokumaru H, Umayahara K (1999). Proteins involved in synaptic vesicle trafficking. *J Physiol.* 520 Pt 1:33-41.
7. Bamji SX, Shimazu K, Kimes N, Huelsken J, Birchmeier W, Lu B, Reichardt LF (2003). Role of beta-catenin in synaptic vesicle localization and presynaptic assembly. *Neuron.* 40(4):719-31.
8. Banovic D, Khorramshahi O, Oswald D, Wichmann C, Riedt T, Fouquet W, Tian R, Sigrist SJ, Aberle H (2010). Drosophila neuroligin 1 promotes growth and postsynaptic differentiation at glutamatergic neuromuscular junctions. *Neuron.* 66(5):724-738.
9. Bekkers JM (2003). Synaptic transmission: functional autapses in the cortex. *Curr Biol.* 13(11):R433-435.
10. Bembem MA, Shipman SL, Hirai T, Herring BE, Li Y, Badger JD 2nd, Nicoll RA, Diamond JS, Roche KW (2014). CaMKII phosphorylation of neuroligin-1 regulates excitatory synapses. *Nat Neurosci.* 17(1):56-64.
11. Benson DL, Tanaka H (1998). N-cadherin redistribution during synaptogenesis in hippocampal neurons. *J Neurosci.* 18(17):6892-6904.

12. Betz A, Okamoto M, Benseler F, Brose N (1997). Direct interaction of the rat unc-13 homologue Munc13-1 with the N terminus of syntaxin. *J Biol Chem.* 272(4):2520-2526.
13. Bhourri M, Morishita W, Temkin P, Goswami D, Kawabe H, Brose N, Südhof TC, Craig AM, Siddiqui TJ, Malenka R (2018). Deletion of *LRRTM1* and *LRRTM2* in adult mice impairs basal AMPA receptor transmission and LTP in hippocampal CA1 pyramidal neurons. *Proc Natl Acad Sci U S A.* 115(23): E5382-E5389.
14. Bian WJ, Miao WY, He SJ, Qiu Z, Yu X (2015). Coordinated Spine Pruning and Maturation Mediated by Inter-Spine Competition for Cadherin/Catenin Complexes. *Cell.* 162(4):808-822.
15. Blasi J, Chapman ER, Link E, Binz T, Yamasaki S, De Camilli P, Südhof TC, Niemann H, Jahn R (1993a). Botulinum neurotoxin A selectively cleaves the synaptic protein SNAP-25. *Nature.* 365(6442):160-163.
16. Blasi J, Chapman ER, Yamasaki S, Binz T, Niemann H, Jahn R (1993b). Botulinum neurotoxin C1 blocks neurotransmitter release by means of cleaving HPC-1/syntaxin. *EMBO J.* 12(12):4821-4828.
17. Boucard AA, Chubykin AA, Comoletti D, Taylor P, Südhof TC (2005). A splice code for trans-synaptic cell adhesion mediated by binding of neuroligin 1 to alpha- and beta-neurexins. *Neuron.* 48(2):229-236.
18. Bozdagi O, Shan W, Tanaka H, Benson DL, Huntley GW (2000). Increasing numbers of synaptic puncta during late-phase LTP: N-Cadherin is synthesized, recruited to synaptic sites, and required for potentiation. *Neuron.* 28(1): 245-59.
19. Bozdagi O, Valcin M, Poskanzer K, Tanaka H, Benson DL (2004). Temporally distinct demands for classic cadherins in synapse formation and maturation. *Mol Cell Neurosci.* 27(4):509-521.
20. Bozdagi O, Wang XB, Nikitczuk JS, Anderson TR, Bloss EB, Radice GL, Zhou Q, Benson DL, Huntley GW (2010). Persistence of coordinated long-term potentiation and dendritic spine enlargement at mature hippocampal CA1 synapses requires N-cadherin. *J Neurosci.* 30(30):9984-9989.
21. Brasch J, Harrison OJ, Honig B, Shapiro L (2012). Thinking outside the cell: how cadherins drive adhesion. *Trends Cell Biol.* 22(6):299-310.
22. Brigidi GS, Bamji SX (2011). Cadherin-catenin adhesion complexes at the synapse. *Curr Opin Neurobiol.* 21(2):208-214.

23. Brockmann MM, Rosenmund C (2016). Catching Up with Ultrafast Endocytosis. *Neuron*. 90(3):423-424.
24. Brodin L, Löw P, Shupliakov O (2000). Sequential steps in clathrin-mediated synaptic vesicle endocytosis. *Curr Opin Neurobiol*. 10(3):312-320.
25. Brose N, Hofmann K, Hata Y, Südhof TC (1995). Mammalian homologues of *Caenorhabditis elegans* unc-13 gene define novel family of C2-domain proteins. *J Biol Chem*. 270(42):25273-25280.
26. Brose N, Rosenmund C, Rettig J (2000). Regulation of transmitter release by Unc-13 and its homologues. *Curr Opin Neurobiol*. 10(3):303-311.
27. Budreck EC, Scheiffele P (2007). Neuroligin-3 is a neuronal adhesion protein at GABAergic and glutamatergic synapses. *Eur J Neurosci*. 26(7):1738-1748.
28. Burkhardt P, Hattendorf DA, Weis WI, Fasshauer D (2008). Munc18a controls SNARE assembly through its interaction with the syntaxin N-peptide. *EMBO J*. 27(7):923-933.
29. Burré J, Sharma M, Tsetsenis T, Buchman V, Etherton MR, Südhof TC (2010). Alpha-synuclein promotes SNARE-complex assembly in vivo and in vitro. *Science*. 329(5999):1663-1667.
30. Castillo PE, Schoch S, Schmitz F, Südhof TC, Malenka RC (2002). RIM1alpha is required for presynaptic long-term potentiation. *Nature*. 415(6869):327-330.
31. Chamma I, Letellier M, Butler C, Tessier B, Lim KH, Gauthereau I, Choquet D, Sibarita JB, Park S, Sainlos M, Thoumine O (2016a). Mapping the dynamics and nanoscale organization of synaptic adhesion proteins using monomeric streptavidin. *Nat. Commun*. 7:10773.
32. Chamma I, Levet F, Sibarita M, Thoumine O (2016b). Nanoscale organization of synaptic adhesion proteins revealed by single-molecule localization microscopy. *Neurophotonics* 3(4):041810.
33. Chamma I, Thoumine O (2018). Dynamics, nanoscale organization, and function of synaptic adhesion molecules. *Mol. Cell. Neurosci*. 91:95-107.
34. Chamma I, Sainlos M, Thoumine O (2019). Biophysical mechanisms underlying the membrane trafficking of synaptic adhesion molecules. *Neuropharmacology* pii:S0028-3908(19)30076-0.
35. Chanaday NL, Kavalali ET (2018). Optical detection of three modes of endocytosis at hippocampal synapses. *Elife*. 7.pii:e36097.

36. Chanaday NL, Kavalali ET (2018). Time course and temperature dependence of synaptic vesicle endocytosis. *FEBS Lett.* 592(21):3606-3614.
37. Chanda S, Hale WD, Zhang B, Wernig M, Südhof TC (2017). Unique versus Redundant Functions of Neuroligin Genes in Shaping Excitatory and Inhibitory Synapse Properties. *J Neurosci.* 37(29): 6816-6836.
38. Chandra S, Gallardo G, Fernández-Chacón R, Schlüter OM, Südhof TC (2005). Alpha-synuclein cooperates with CSPalpha in preventing neurodegeneration. *Cell.* 123(3):383-396.
39. Chen L, Chetkovich DM, Petralia RS, Sweeney NT, Kawasaki Y, Wenthold RJ, Brecht DS, Nicoll RA (2000). Stargazin regulates synaptic targeting of AMPA receptors by two distinct mechanisms. *Nature.* 408(6815):936-943.
40. Cheung G, Cousin MA (2013). Synaptic vesicle generation from activity-dependent bulk endosomes requires calcium and calcineurin. *J Neurosci.* 33(8):3370-3379.
41. Chih B, Engelman H, Scheiffele P (2005). Control of excitatory and inhibitory synapse formation by neuroligins. *Science.* 307(5713):1324-1328.
42. Chubykin AA, Atasoy D, Etherton MR, Brose N, Kavalali ET, Gibson JR, Südhof TC (2007). Activity-dependent validation of excitatory versus inhibitory synapses by neuroligin-1 versus neuroligin-2. *Neuron.* 54(6): 919-931.
43. Clayton EL, Cousin MA (2008). Differential labelling of bulk endocytosis in nerve terminals by FM dyes. *Neurochem Int.* 53(3-4):51-55.
44. Clayton EL, Evans GJ, Cousin MA (2008). Bulk synaptic vesicle endocytosis is rapidly triggered during strong stimulation. *J Neurosci.* 28(26):6627-6632.
45. Clayton EL, Cousin MA (2009). Quantitative monitoring of activity-dependent bulk endocytosis of synaptic vesicle membrane by fluorescent dextran imaging. *J Neurosci Methods.* 185(1):76-81.
46. Clayton EL, Cousin MA (2009). The molecular physiology of activity-dependent bulk endocytosis of synaptic vesicles. *J Neurochem.* 111(4):901-914.
47. Courtney NA, Bao H, Briguglio JS, Chapman ER (2019). Synaptotagmin 1 clamps synaptic vesicle fusion in mammalian neurons independent of complexin. *Nat Commun.* 10(1):4076.
48. Cousin MA, Robinson PJ (1999). Mechanism of synaptic vesicle recycling illuminated by fluorescent dyes. *J Neurochem.* 73(6):2227-2239.

49. Dai Y, Taru H, Deken SL, Grill B, Ackley B, Nonet ML, Jin Y (2006). SYD-2 Liprin-alpha organizes presynaptic active zone formation through ELKS. *Nat Neurosci.* 9(12):1479-1487.
50. de Wit J, Sylwestrak E, O'Sullivan ML, Otto S, Tiglio K, Savas JN, Yates JR 3rd, Comoletti D, Taylor P, Ghosh A (2009). LRRTM2 interacts with Neurexin1 and regulates excitatory synapse formation. *Neuron* 64(6):799-806.
51. Delvendahl I, Vyleta NP, von Gersdorff H, Hallermann S (2016). Fast, Temperature-Sensitive and Clathrin-Independent Endocytosis at Central Synapses. *Neuron.* 90(3):492-498.
52. Deng L, Kaeser PS, Xu W, Südhof TC (2011). RIM proteins activate vesicle priming by reversing auto inhibitory homodimerization of Munc13. *Neuron.* 69(2):317-331.
53. Drees F, Pokutta S, Yamada S, Nelson WJ, Weis WI (2005). Alpha-catenin is a molecular switch that binds E-cadherin-beta-catenin and regulates actin-filament assembly. *Cell.* 123(5):903-915.
54. El-Husseini AE, Schnell E, Chetkovich DM, Nicoll RA, Brecht DS (2000). PSD-95 involvement in maturation of excitatory synapses. *Science.* 290(5495):1364-1368.
55. Elste AM, Benson DL (2006). Structural basis for developmentally regulated changes in cadherin function at synapses. *J Comp Neurol.* 495(3):324-335.
56. Fannon AM, Colman DR (1996). A Model for Central Synaptic Junctional Complex Formation Based on the Differential Adhesive Specificities of the Cadherins. *Neuron.* 17(3)423:434.
57. Ferguson SM, Brasnjo G, Hayashi M, Wölfel M, Collesi C, Giovedi S, Raimondi A, Gong LW, Ariel P, Paradise S, O'toole E, Flavell R, Cremona O, Miesenböck G, RyanTA, De Camilli P (2007). A selective activity-dependent requirement for dynamin 1 in synaptic vesicle endocytosis. *Science.* 316(5824):570-574.
58. Ferguson SM, De Camilli P (2012). Dynamin, a membrane-remodelling GTPase. *Nat Rev Mol Cell Biol.* 13(2):75-88.
59. Fu Z, Washbourne P, Ortinski P, Vicini S (2003). Functional excitatory synapses in HEK293 cells expressing neuroligin and glutamate receptors. *J Neurophysiol.* 90(6):3950-3957.
60. Fujita Y, Sasaki T, Fukui K, Kotani H, Kimura T, Hata Y, Südhof TC, Scheller RH, Takai Y (1996). Phosphorylation of Munc-18/n-Sec1/rbSec1 by protein

- kinase C: its implication in regulating the interaction of Munc-18/n-Sec1/rbSec1 with syntaxin. *J Biol Chem.* 271(13):7265-7268.
61. Gad H, Löw P, Zotova E, Brodin L, Shupliakov O (1998). Dissociation between Ca^{2+} -triggered synaptic vesicle exocytosis and clathrin-mediated endocytosis at a central synapse. *Neuron.* 21(3):607-616.
 62. Gaffield MA, Betz WJ (2007). Synaptic vesicle mobility in mouse motor nerve terminals with and without synapsin. *J Neurosci.* 27(50):13691-13700.
 63. Gan Q, Watanabe S (2018). Synaptic Vesicle Endocytosis in Different Model Systems. *Front Cell Neurosci.* 12:171.
 64. Gandhi SP, Stevens CF (2003). Three modes of synaptic vesicular recycling revealed by single-vesicle imaging. *Nature.* 423(6940):607-613.
 65. Geppert M, Goda Y, Hammer RE, Li C, Rosahl TW, Stevens CF, Südhof TC (1994). Synaptotagmin I: a major Ca^{2+} sensor for transmitter release at a central synapse. *Cell.* 79(4):717-727.
 66. Graf ER, Zhang X, Jin SX, Linhoff MW, Craig AM (2004). Neurexins induce differentiation of GABA and glutamate postsynaptic specializations via neuroligins. *Cell* 119:1013-1026.
 67. Graf ER, Kang Y, Hauner AM, Craig AM (2006). Structure function and splice site analysis of the synaptogenic activity of the neurexin-1 beta LNS domain. *J Neurosci.* 26(16):4256-4265.
 68. Granseth B, Odermatt B, Royle SJ, Lagnado L (2006). Clathrin-mediated endocytosis is the dominant mechanism of vesicle retrieval at hippocampal synapses. *Neuron.* 51(6):773-786.
 69. Gustafsson MGL (2000). Surpassing the lateral resolution limit by a factor of two using structured illumination microscopy. *J Microsc.* 198:82-87.
 70. Gustafsson MG, Shao L, Carlton PM, Wang CJ, Golubovskaya IN, Cande WZ, Agard DA, Sedat JW (2008). Three-dimensional resolution doubling in wide-field fluorescence microscopy by structured illumination. *Biophys J.* 94(12):4957-4970.
 71. Han Y, Kaeser PS, Südhof TC, Schneggenburger R (2011). RIM determines Ca^{2+} channel density and vesicle docking at the presynaptic active zone. *Neuron.* 69(2):304-316.

72. Harata N, Pyle JL, Aravanis AM, Mozhayeva M, Kavalali ET, Tsien RW (2001). Limited numbers of recycling vesicles in small CNS nerve terminals: implications for neural signaling and vesicular cycling. *Trends Neurosci.* 24(11):637-643.
73. Harata N, Ryan TA, Smith SJ, Buchanan J, Tsien RW (2001). Visualizing recycling synaptic vesicles in hippocampal neurons by FM 1-43 photoconversion. *Proc Natl Acad Sci U S A.* 98(22):12748-12753.
74. Hatta K, Nose A, Nagafuchi A, Takeichi M (1988). Cloning and expression of cDNA encoding a neural calcium-dependent cell adhesion molecule: its identity in the cadherin gene family. *J. Cell Biol.* 106 (3):873-881.
75. Haucke V, De Camilli P (1999). AP-2 recruitment to synaptotagmin stimulated by tyrosine-based endocytic motifs. *Science.* 285(5431):1268-1271.
76. Hayashi M, Raimondi A, O'Toole E, Paradise S, Collesi C, Cremona O, Ferguson SM, De Camilli P (2008). Cell- and stimulus-dependent heterogeneity of synaptic vesicle endocytic recycling mechanisms revealed by studies of dynamin 1-null neurons. *Proc Natl Acad Sci U S A.* 105(6):2175-80.
77. Heuser JE, Reese TS (1973). Evidence for recycling of synaptic vesicle membrane during transmitter release at the frog neuromuscular junction. *J Cell Biol.* 57(2):315-344.
78. Heuser JE, Reese TS, Landis DM (1974). Functional changes in frog neuromuscular junctions studied with freeze-fracture. *J Neurocytol.* 3(1):109-131.
79. Holt M, Cooke A, Wu MM, Lagnado L (2003). Bulk membrane retrieval in the synaptic terminal of retinal bipolar cells. *J Neurosci.* 23(4):1329-1339.
80. Hoopmann P, Punge A, Barysch SV, Westphal V, Bückers J, Opazo F, Bethani I, Lauterbach MA, Hell SW, Rizzoli SO (2010). Endosomal sorting of readily releasable synaptic vesicles. *Proc Natl Acad Sci U S A.* 107(44):19055-19060.
81. Hoopmann P, Rizzoli SO, Betz WJ (2012). Imaging synaptic vesicle recycling by staining and destaining vesicles with FM dyes. *Cold Spring Harb Protoc.* (1):77-83.
82. Hu SH, Christie MP, Saez NJ, Latham CF, Jarrott R, Lua LH, Collins BM, Martin JL (2011). Possible roles for Munc18-1 domain 3a and Syntaxin1 N-peptide and C-terminal anchor in SNARE complex formation. *Proc Natl Acad Sci U S A.* 108(3):1040-1045.

83. Hua Y, Sinha R, Thiel CS, Schmidt R, Hüve J, Martens H, Hell SW, Egnér A, Klingauf J (2011). A readily retrievable pool of synaptic vesicles. *Nat. Neurosci.* 14(7):833-839.
84. Huntley GW, Benson DL (1999). Neural (N)-cadherin at developing thalamocortical synapses provides an adhesion mechanism for the formation of somatotopically organized connections. *J Comp Neurol.* 407(4):453-471.
85. Ichtchenko K, Hata Y, Nguyen T, Ullrich B, Missler M, Moomaw C, Südhof TC (1995). Neuroligin 1: a splice site-specific ligand for beta-neurexins. *Cell.* 81(3):435-443.
86. Ichtchenko K, Nguyen T, Südhof TC (1996). Structures, alternative splicing, and neurexin binding of multiple neuroligins. *J Biol Chem.* 271(5):2676-2682.
87. Irie M, Hata Y, Takeuchi M, Ichtchenko K, Toyoda A, Hirao K, Takai Y, Rosahl TW, Südhof TC (1997). Binding of neuroligins to PSD-95. *Science.* 277(5331):1511-1515.
88. Jahn R, Fasshauer D (2012). Molecular machines governing exocytosis of synaptic vesicles. *Nature.* 490(7419):201-207.
89. Jontes JD, Emond MR, Smith SJ (2004). In vivo trafficking and targeting of N-cadherin to nascent presynaptic terminals. *J Neurosci.* 24(41):9027-34.
90. Jost A, Heitzmann R (2013). Superresolution Multidimensional Imaging with Structured Illumination Microscopy. *Annu Rev Mater Res.* 43:261-282.
91. Jüngling K, Eulenburg V, Moore R, Kemler R, Lessmann V, Gottmann K (2006). N-cadherin transsynaptically regulates short-term plasticity at glutamatergic synapses in embryonic stem cell-derived neurons. *J Neurosci.* 26(26):6968-6978.
92. Kadowaki M, Nakamura S, Machon O, Krauss S, Radice GL, Takeichi M (2007). N-cadherin mediates cortical organization in the mouse brain. *Dev Biol.* 304(1):22-33.
93. Kaeser PS, Deng L, Fan M, Südhof TC (2012). RIM genes differentially contribute to organizing presynaptic release sites. *Proc Natl Acad Sci U S A.* 109(29):11830-11835.
94. Kavalali ET, Jorgensen EM (2014). Visualizing presynaptic function. *Nat Neurosci.* 17(1):10-16.

95. Kittelmann M, Liewald JF, Hegemann J, Schultheis C, Brauner M, Steuer Costa W, Wabnig S, Eimer S, Gottschalk A (2013). In vivo synaptic recovery following optogenetic hyperstimulation. *Proc Natl Acad Sci U S A*. 110(32):E3007-3016.
96. Ko J, Fuccillo MV, Malenka RC, Südhof TC (2009). LRRTM2 functions as a neurexin ligand in promoting excitatory synapse formation. *Neuron*. 64(6):791-798.
97. Ko J, Zhang C, Arac D, Boucard AA, Brunger AT, Südhof TC (2009). Neuroligin-1 performs neurexin-dependent and neurexin-independent functions in synapse validation. *EMBO J*. 28(20): 3244-3255.
98. Ko J, (2012). The leucine-rich repeat superfamily of synaptic adhesion molecules: LRRTMs and Slitrks. *Mol Cells*. 34(4):335-340.
99. Kononenko NL, Haucke V (2012). Molecular mechanisms of presynaptic membrane retrieval and synaptic vesicle reformation. *Neuron*. 85 (3):484-496.
100. Kononenko NL, Puchkov D, Classen GA, Walter AM, Pechstein A, Sawade L, Kaempf N, Trimbuch T, Lorenz D, Rosenmund C, Maritzen T, Haucke V (2014). Clathrin/AP-2 mediate synaptic vesicle reformation from endosome-like vacuoles but are not essential for membrane retrieval at central synapses. *Neuron*. 82(5):981-988.
101. Kostetskii I, Li J, Xiong Y, Zhou R, Ferrari VA, Patel VV, Molkentin JD, Radice GL (2005). Induced deletion of the N-cadherin gene in the heart leads to dissolution of the intercalated disc structure. *Circ Res*. 96(3):346-354.
102. Koushika SP, Richmond JE, Hadwiger G, Weimer RM, Jorgensen EM, Nonet ML (2001). A post-docking role for active zone protein Rim. *Nat Neurosci*. 4(10):997-1005.
103. Lai AL, Huang H, Herrick DZ, Epp N, Cafiso DS (2011). Synaptotagmin 1 and SNAREs form a complex that is structurally heterogeneous. *J Mol Biol*. 405(3):696-706.
104. Lauren J, Airaksinen MS, Saarma M, Timmusk T (2003). A novel gene family encoding leucine-rich repeat transmembrane proteins differentially expressed in the nervous system. *Genomics*. 81(4):411-421.
105. Levinson JN, El-Husseini A (2005). Building excitatory and inhibitory synapses: balancing neuroligin partnerships. *Neuron*. 48(2): 171-174.

106. Linhoff MW, Lauren J, Cassidy RM, Dobie FA, Takahashi H, Nygaard HB, Airaksinen MS, Strittmatter SM, Craig AM, (2009). An unbiased expression screen for synaptogenic proteins identifies the LRRTM protein family as synaptic organizers. *Neuron*. 61(5):734-749.
107. Link E, Edelman L, Chou JH, Binz T, Yamasaki S, Eisel U, Baumert M, Südhof TC, Niemann H, Jahn R (1992). Tetanus toxin action: inhibition of neurotransmitter release linked to synaptobrevin proteolysis. *Biochem Biophys Res Commun*. 189(2):1017-1023.
108. Marambaud P, Wen PH, Dutt A, Shioi J, Takashima A, Siman R, Robakis NK (2003). A CBP binding transcriptional repressor produced by the PS1/epsilon-cleavage of N-cadherin is inhibited by PS1 FAD mutations. *Cell*. 114(5):635-645.
109. McMahon HT, Missler M, Li C, Südhof TC (1995). Complexins: cytosolic proteins that regulate SNAP receptor function. *Cell*. 83(1):111-119.
110. Mendez P, De Roo M, Poglia L, Klausner P, Muller D (2010). N-cadherin mediates plasticity-induced long-term spine stabilization. *J Cell Biol*. 189(3):589-600.
111. Meunier FA, Gutiérrez LM (2016). Captivating New Roles of F-Actin Cortex in Exocytosis and Bulk Endocytosis in Neurosecretory Cells. *Trends Neurosci*. 39(9):605-613.
112. Miesenböck G, De Angelis DA, Rothman JE (1998). Visualizing secretion and synaptic transmission with pH-sensitive green fluorescent proteins. *Nature*. 394(6689):192-195.
113. Miller TM, Heuser JE (1984). Endocytosis of synaptic vesicle membrane at the frog neuromuscular junction. *J Cell Biol*. 98(2):685-698.
114. Mukherjee K, Yang X, Gerber SH, Kwon HB, Ho A, Castillo PE, Liu X, Südhof TC (2010). Piccolo and bassoon maintain synaptic vesicle clustering without directly participating in vesicle exocytosis. *Proc Natl Acad Sci U S A*. 107(14):6504-6509.
115. Murase S, Mosser E, Schuman EM (2002). Depolarization drives beta-Catenin into neuronal spines promoting changes in synaptic structure and function. *Neuron*. 35(1):91-105.
116. Mysore SP, Tai CY, Schuman EM (2007). Effects of N-cadherin disruption on spine morphological dynamics. *Front Cell Neurosci*. 1:1. eCollection 2007.

117. Nagar B, Overduin M, Ikura M, Rini JM (1996). Structural basis of calcium-induced E-cadherin rigidification and dimerization. *Nature*. 380(6572):360-364.
118. Newton J, Murthy V (2006). Measuring exocytosis in neurons using FM labeling. *J Vis Exp*. 30(1):117.
119. Nguyen TH, Maucort G, Sullivan RK, Schenning M, Lavidis NA, McCluskey A, Robinson PJ, Meunier FA (2012). Actin- and dynamin-dependent maturation of bulk endocytosis restores neurotransmission following synaptic depletion. *PLoS One*. 7(5):e36913.
120. Nikitczuk JS, Patil SB, Matikainen-Ankney BA, Scarpa J, Shapiro ML, Benson DL, Huntley GW (2014). N-cadherin regulates molecular organization of excitatory and inhibitory synaptic circuits in adult hippocampus in vivo. *Hippocampus*. 24(8):943-962.
121. Obst-Pernberg K, Medina L, Redies C (2001). Expression of R-cadherin and N-cadherin by cell groups and fiber tracts in the developing mouse forebrain: relation to the formation of functional circuits. *Neuroscience*. 106(3):505-533.
122. Okamura K, Tanaka H, Yagita Y, Saeki Y, Taguchi A, Hiraoka Y, Zeng LH, Colman DR, Miki N (2004). Cadherin activity is required for activity-induced spine remodeling. *J Cell Bio*. 167(5):961-972.
123. Okuda T, Yu LM, Cingolani LA, Kemler R, Goda Y (2007). Beta-Catenin regulates excitatory postsynaptic strength at hippocampal synapses. *Proc Natl Acad Sci U S A*. 104(33):13479-13484.
124. Ozawa M, Kemler R (1990). Correct proteolytic cleavage is required for the cell adhesive function of uvomorulin. *J Cell Biol*. 111(4):1645-1650.
125. Pang ZP, Südhof TC (2010). Cell biology of Ca²⁺-triggered exocytosis. *Curr Opin Cell Biol*. 22(4):496-505.
126. Patel SD, Ciatto C, Chen CP, Bahna F, Rajebhosale M, Arkus N, Schieren I, Jessell TM, Honig B, Price SR, Shapiro L (2006). Type II cadherin ectodomain structures: implications for classical cadherin specificity. *Cell*. 124(6):1255-1268.
127. Pielarski KN, van Stegen B, Andreyeva A, Nieweg K, Jüngling K, Redies C, Gottmann K (2013). Asymmetric N-cadherin expression results in synapse dysfunction, synapse elimination, and axon retraction in cultured mouse neurons. *PLoS One*. 8(1):e54105.

128. Plank C, Schillinger U, Scherer F, Bergemann C, Rémy JS, Krötz F, Anton M, Lausier J, Rosenecker J (2003). The magnetofection method: using magnetic force to enhance gene delivery. *Biol Chem.* 384(5):737-747.
129. Poirier MA, Xiao W, Macosko JC, Chan C, Shin YK, Bennett MK (1998). The synaptic SNARE complex is a parallel four-stranded helical bundle. *Nat Struct Biol.* 5(9): 765-769.
130. Pokutta S, Weis WI (2007). Structure and mechanism of cadherins and catenins in cell-cell contacts. *Annu Rev Cell Dev Biol.* 23:237-261.
131. Prange O, Wong TP, Gerrow K, Wang YT, El-Husseini A (2004). A balance between excitatory and inhibitory synapses is controlled by PSD-95 and neuroligin. *Proc Natl Acad Sci U S A.* 101(38):13915-13920.
132. Radice GL, Rayburn H, Matsunami H, Knudsen KA, Takeichi M, Hynes RO (1997). Developmental defects in mouse embryos lacking N-cadherin. *Dev Biol.* 181(1):64-78.
133. Raimondi A, Ferguson SM, Lou X, Armbruster M, Paradise S, Giovedi S, Messa M, Kono N, Takasaki J, Cappello V, O'Toole E, Ryan TA, De Camilli P (2011). Overlapping role of dynamin isoforms in synaptic vesicle endocytosis. *Neuron.* 70(6):1100-1114.
134. Redies C, Engelhart K, Takeichi M (1993). Differential expression of N- and R-cadherin in functional neuronal systems and other structures of the developing chicken brain. *J Comp Neurol.* 333(3):398-416.
135. Reiss K, Maretzky T, Ludwig A, Tousseyn T, de Strooper B, Hartmann D, Saftig P (2005). ADAM10 cleavage of N-cadherin and regulation of cell-cell adhesion and beta-catenin nuclear signalling. *EMBO J.* 24(4):742-752.
136. Rizo J, Xu J (2015). The Synaptic Vesicle Release Machinery. *Annu Rev Biophys.* 44:339-67.
137. Rizzoli SO, Betz WJ (2005). Synaptic vesicle pools. *Nat Rev Neurosci.* 6(1):57-69.
138. Rizzoli SO, Jahn R (2007). Kiss-and-run, collapse and 'readily retrievable' vesicles. *Traffic.* 8(9):1137-1144.
139. Roos J, Kelly RB (1999). The endocytic machinery in nerve terminals surrounds sites of exocytosis. *Curr Biol.* 9(23):1411-1414.

140. Royle SJ, Granseth B, Odermatt B, Derevier A, Lagnado L (2008). Imaging pHluorin-based probes at hippocampal synapses. *Methods Mol Biol.* 457:293-303.
141. Royle SJ, Lagnado L (2010). Clathrin-mediated endocytosis at the synaptic terminal: bridging the gap between physiology and molecules. *Traffic.* 11(12):1489-1497.
142. Ryan TA, Smith SJ, Reuter H (1996). The timing of synaptic vesicle endocytosis. *Proc Natl Acad Sci U S A.* 93(11):5567-5571.
143. Saglietti L, Dequidt C, Kamieniarz K, Rousset MC, Valnegri P, Thoumine O, Beretta F, Fagni L, Choquet D, Sala C, Sheng M, Passafaro M (2007). Extracellular interactions between GluR2 and N-cadherin in spine regulation. *Neuron.* 54(3):461-477.
144. Saheki Y, De Camilli P (2012). Synaptic vesicle endocytosis. *Cold Spring Harb Perspect Biol.* 4(9):a005645.
145. Sankaranarayanan S, De Angelis D, Rothman JE, Ryan TA (2000). The use of pHluorins for optical measurements of presynaptic activity. *Biophys J.* 79(4):2199-2208.
146. Sankaranarayanan S, Ryan TA (2001). Calcium accelerates endocytosis of vSNAREs at hippocampal synapses. *Nat Neurosci.* 4(2):129-136.
147. Sara Y, Biederer T, Atasoy D, Chubykin A, Mozhayeva MG, Südhof TC, Kavalali ET (2005). Selective capability of SynCAM and neuroligin for functional synapse assembly. *J Neurosci.* 25(1):260-270.
148. Scheiffele P, Fan J, Choih J, Fetter R, Serafini T (2000). Neuroligin expressed in nonneuronal cells triggers presynaptic development in contacting axons. *Cell.* 101(6):657-669.
149. Schermelleh L, Carlton PM, Haase S, Shao L, Winoto L, Kner P, Burke B, Cardoso MC, Agard DA, Gustafsson MG, Leonhardt H, Sedat JW (2008). Subdiffraction multicolor imaging of the nuclear periphery with 3D structured illumination microscopy. *Science.* 320(5881):1332-1336.
150. Schermelleh L, Heintzmann R, Leonhardt H (2010). A guide to super-resolution fluorescence microscopy. *J Cell Biol.* 190(2):165-175.
151. Schiavo G, Benfenati F, Poulain B, Rossetto O, Poverino de Laureto P, DasGupta BR, Montecucco C (1992). Tetanus and botulinum-B neurotoxins

- block neurotransmitter release by proteolytic cleavage of synaptobrevin. *Nature*. 359(6398):832-835.
152. Schikorski T, Stevens CF (1997). Quantitative ultrastructural analysis of hippocampal excitatory synapses. *J Neurosci*. 17(15):5858-5867.
153. Schoch S, Castillo PE, Jo T, Mukherjee K, Geppert M, Wang Y, Schmitz F, Malenka RC, Südhof TC (2002). RIM1alpha forms a protein scaffold for regulating neurotransmitter release at the active zone. *Nature*. 415(6869):321-326.
154. Shan W, Yagita Y, Wang Z, Koch A, Fex Svenningsen A, Gruzglin E, Pedraza L, Colman DR (2004). The minimal essential unit for cadherin-mediated intercellular adhesion comprises extracellular domains 1 and 2. *J Biol Chem*. 279(53):55914-55923.
155. Shapiro L, Fannon AM, Kwong PD, Thompson A, Lehmann MS, Grübel G, Legrand JF, Als-Nielsen J, Colman DR, Hendrickson WA (1995). Structural basis of cell-cell adhesion by cadherins. *Nature*. 374(6520):327-337.
156. Sharma M, Burré J, Bronk P, Zhang Y, Xu W, Südhof TC (2012). CSP α knockout causes neurodegeneration by impairing SNAP-25 function. *EMBO J*. 31(4):829-841.
157. Siddiqui TJ, Pancaroglu R, Kang Y, Rooyakkers A, Craig AM (2010). LRRTMs and neuroligins bind neurexins with a differential code to cooperate in glutamate synapse development. *J. Neurosci*. 30(22):7495-7506.
158. Siddiqui TJ, Craig AM (2011). Synaptic organizing complexes. *Curr Opin Neurobiol*. 21(1):132-143.
159. Soler-Llavina GJ, Fuccillo MW, Ko J, Südhof TC, Malenka RC (2011). The neurexin ligands, neuroligins and leucine-rich repeat transmembrane proteins, perform convergent and divergent synaptic functions in vivo. *Prot Natl Acad Sci U S A*. 108(40): 16502-16509.
160. Soler-Llavina GJ, Arstikaitis P, Morishita W, Ahmad M, Südhof TC, Malenka RC (2013). Leucine-rich repeat transmembrane proteins are essential for maintenance of long-term potentiation. *Neuron* 79(3): 439-446.
161. Söllner T, Whiteheart SW, Brunner M, Erdjument-Bromage H, Geromanos S, Tempst P, Rothman JE (1993). SNAP receptors implicated in vesicle targeting and fusion. *Nature*. 362(6418):318-324.

162. Song JY, Ichtchenko K, Südhof TC, Brose N (1999). Neuroligin1 is a postsynaptic cell-adhesion molecule of excitatory synapses. *Proc Natl Acad Sci U S A.* 96(3):1100-1105.
163. Soykan T, Kaempf N, Sakaba T, Vollweiter D, Goerdeler F, Puchkov D, Kononenko NL, Haucke V (2017). Synaptic Vesicle Endocytosis Occurs on Multiple Timescales and Is Mediated by Formin-Dependent Actin Assembly. *Neuron.* 93(4): 854-866.e4.
164. Stan A, Pielarski KN, Brigadski T, Wittenmayer N, Fedorchenko O, Gohla A, Lessmann V, Dresbach T, Gottmann K (2010). Essential cooperation of N-cadherin and neuroligin-1 in the transsynaptic control of vesicle accumulation. *Proc Natl Acad Sci U S A.* 107(24):11116-11121.
165. Stevens CF, Williams JH (2000). "Kiss and run" exocytosis at hippocampal synapses. *Proc Natl Acad Sci U S A.* 97(23):12828-12833.
166. Sutton RB, Fasshauer D, Jahn R, Brunger AT (1998). Crystal structure of a SNARE complex involved in synaptic exocytosis at 2.4 Å resolution. *Nature.* 395(6700):347-353.
167. Südhof TC (2004). The synaptic vesicle cycle. *Annu Rev Neurosci.* 27:509-547.
168. Südhof TC, Rothman JE (2009). Membrane fusion: grappling with SNARE and SM proteins. *Science.* 323(5913):474-477.
169. Südhof TC, Rizo J (2011). Synaptic vesicle exocytosis. *Cold Spring Harb Perspect Biol.* 3(12). Pii: a005637.
170. Südhof TC (2013). Neurotransmitter release: the last millisecond in the life of a synaptic vesicle. *Neuron.* 80(3):675-690.
171. Tai CY, Mysore SP, Chiu C, Schuman EM (2007). Activity-regulated N-cadherin endocytosis. *Neuron.* 54(5):771-785.
172. Takashima N, Odaka YS, Sakoori K, Akagi T, Hashikawa T, Morimura N, Yamada K, Aruga J (2011). Impaired cognitive function and altered hippocampal synapse morphology in mice lacking *Lrrtm1*, a gene associated with schizophrenia. *PLoS One.* 6(7): e22716.
173. Takei K, Mundigl O, Daniell L, De Camilli P (1996). The synaptic vesicle cycle: a single vesicle budding step involving clathrin and dynamin. *J Cell Biol.* 133(6):1237-1250.

174. Tanaka H, Shan W, Phillips GR, Arndt K, Bozdagi O, Shapiro L, Huntley GW, Benson DL, Colman DR (2000). Molecular modification of N-cadherin in response to synaptic activity. *Neuron*. 25(1):93-107.
175. Tang L, Hung CP, Schuman EM (1998). A role for the cadherin family of cell adhesion molecules in hippocampal long-term potentiation. *Neuron*. 20(6):1165-1175.
176. Teng H, Wilkinson RS (2000). Clathrin-mediated endocytosis near active zones in snake motor boutons. *J Neurosci*. 20(21):7986-7993.
177. Tobaben S, Thakur P, Fernández-Chacón R, Südhof TC, Rettig J, Stahl B (2001). A trimeric protein complex functions as a synaptic chaperone machine. *Neuron*. 31(6):987-999.
178. Togashi H, Abe K, Mizoguchi A, Takaoka K, Chisaka O, Takeichi M (2002). Cadherin regulates dendritic spine morphogenesis. *Neuron*. 35(1):77-89.
179. Trimbuch, T. & Rosenmund, C (2016). Should I stop or should I go? The role of complexin in neurotransmitter release. *Nat. Rev. Neurosci*. 17(2):118–125.
180. Ubach J, Zhang X, Shao X, Südhof TC, Rizo J (1998). Ca²⁺-binding to synaptotagmin: how many Ca²⁺ ions bind to the tip of a C2-domain? *EMBO J*. 17(14):3921-3930.
181. Uchida N, Honjo Y, Johnson KR, Wheelock MJ, Takeichi M (1996). The catenin/cadherin adhesion system is localized in synaptic junctions bordering transmitter release zones. *J Cell Biol*. 135(3):767-779.
182. Uemura K, Kihara T, Kuzuya A, Okawa K, Nishimoto T, Ninomiya H, Suqimoto H, Kinoshita A, Shimohama S (2006). Characterization of sequential N-cadherin cleavage by ADAM10 and PS1. *Neurosci Lett*. 402(3):278-283.
183. Uriu Y, Kiyonaka S, Miki T, Yagi M, Akiyama S, Mori E, Nakao A, Beedle AM, Campbell KP, Wakamori M, Mori Y (2010). Rab3-interacting molecule gamma isoforms lacking the Rab3-binding domain induce long lasting currents but block neurotransmitter vesicle anchoring in voltage-dependent P/Q-type Ca²⁺ channels. *J Biol Chem*. 285(28):21750-21767.
184. van Stegen B, Dagar S, Gottmann K (2017). Release activity-dependent control of vesicle endocytosis by the synaptic adhesion molecule N-cadherin. *Sci. Rep*. 7:40865.
185. Varoqueaux F, Sigler A, Rhee JS, Brose N, Enk C, Reim K, Rosenmund C (2002). Total arrest of spontaneous and evoked synaptic transmission but

- normal synaptogenesis in the absence of Munc13-mediated vesicle priming. *Proc Natl Acad Sci U S A.* 99(13):9037-9042.
186. Varoqueaux F, Jamain S, Brose N (2004). Neuroligin 2 is exclusively localized to inhibitory synapses. *Eur J Cell Biol.* 83(9):449-456.
187. Varoqueaux F, Aramuni G, Rawson RL, Mohrmann R, Missler M, Gottmann K, Zhang W, Südhof TC, Brose N (2006). Neuroligins determine synapse maturation and function. *Neuron.* 51(6):741-754.
188. Verhage M, Maia AS, Plomp JJ, Brussaard AB, Heeroma JH, Vermeer H, Toonen RF, Hammer RE, van den Berg TK, Missler M, Geuze HJ, Südhof TC (2000). Synaptic assembly of the brain in the absence of neurotransmitter secretion. *Science.* 287(5454):864-869.
189. Vituriera N, Letellier M, White IJ, Goda Y (2011). Differential control of presynaptic efficacy by postsynaptic N-cadherin and β -catenin. *Nat Neurosci.* 15(1):81-89.
190. Watanabe S, Liu Q, Davis MW, Hollopeter G, Thomas N, Jorgensen EN (2013a). Ultrafast endocytosis at *Caenorhabditis elegans* neuromuscular junctions. *Elife.* 2:e00723.
191. Watanabe S, Rost BR, Camacho-Pérez M, Davis MW, Söhl-Kielczynski B, Rosenmund C, Jorgensen EM (2013b). Ultrafast endocytosis at mouse hippocampal synapses. *Nature.* 504 (7479):242-247.
192. Watanabe S, Trimbuch T, Camacho-Pérez M, Rost BR, Brokowski B, Söhl-Kielczynski B, Felies A, Davis MW, Rosenmund C, Jorgensen EM (2014). Clathrin regenerates synaptic vesicles from endosomes. *Nature.* 515 (7526):228-233.
193. Watanabe S (2016). Flash-and-Freeze: Coordinating Optogenetic Stimulation with Rapid Freezing to Visualize Membrane Dynamics at Synapses with Millisecond Resolution. *Front Synaptic Neurosci.* 8:24.
194. Watanabe S, Boucrot E (2017). Fast and ultrafast endocytosis. *Curr Opin Cell Biol.* 47:64-71.
195. Wen PJ, Grenklo S, Arpino G, Tan X, Liao HS, Heureaux J, Peng SY, Chiang HC, Hamid E, Zhao WD, Shin W, Näreoja T, Evergren E, Jin Y, Karlsson R, Ebert SN, Jin A, Liu AP, Shupliakov O, Wu LG (2016). Actin dynamics provides membrane tension to merge fusing vesicles into the plasma membrane. *Nat Commun.* 7:12604.

196. Wenzel EM, Morton A, Ebert K, Welzel O, Kornhuber J, Cousin MA, Groemer TW (2012). Key physiological parameters dictate triggering of activity-dependent bulk endocytosis in hippocampal synapses. *PLoS One*. 7(6):e38188.
197. Williams E, Williams G, Gour BJ, Blaschuk OW, Doherty P (2000). A novel family of cyclic peptide antagonists suggests that N-cadherin specificity is determined by amino acids that flank the HAV motif. *J Biol Chem*. 275(6):4007-4012.
198. Wittenmayer N, Körber C, Liu H, Kremer T, Varoqueaux F, Chapman ER, Brose N, Kuner T, Dresbach T (2009). Postsynaptic Neuroligin1 regulates presynaptic maturation. *Proc Natl Acad Sci U S A*. 106(32):13564-13569.
199. Wu W, Wu LG (2007). Rapid bulk endocytosis and its kinetics of fission pore closure at a central synapse. *Proc Natl Acad Sci U S A*. 104(24):10234-10239.
200. Wu Y, O'Toole ET, Girard M, Ritter B, Messa M, Liu X, McPherson PS, Ferguson SM, De Camilli P (2014). A dynamin 1-, dynamin 3- and clathrin-independent pathway of synaptic vesicle recycling mediated by bulk endocytosis. *Elife*. 3:e01621.
201. Wu XS, Lee SH, Sheng J, Zhang Z, Zhao WD, Wang D, Jin Y, Charnay P, Ervasti JM, Wu LG (2016). Actin Is Crucial for All Kinetically Distinguishable Forms of Endocytosis at Synapses. *Neuron*. 92(5):1020-1035.
202. Yam PT, Pincus Z, Gupta GD, Bashkurov M, Charron F, Pelletier L, Colman DR (2013). N-cadherin relocalizes from the periphery to the center of the synapse after transient synaptic stimulation in hippocampal neurons. *PLoS One*. 8(11):e79679.
203. Yamagata M, Duan X, Sanes JR (2018). Cadherins Interact With Synaptic Organizers to Promote Synaptic Differentiation. *Front Mol Neurosci*. 11:142. doi: 10.3389/fnmol.2018.00142.
204. Yap AS, Briehner WM, Gumbiner BM (1997). Molecular and functional analysis of cadherin-based adherens junctions. *Annu Rev Cell Dev Biol*. 13:119-146.

06-

Appendix

6. Appendix

6.1 Abbreviations

ADBE	Activity-dependent bulk endocytosis
AMPA	α -amino-3-hydroxy-5-methyl-4-isoxazole propionic acid)
BFP	Blue fluorescent protein
BME	Basal medium eagle
BSA	Bovine serum albumine
Cadherins	Ca ²⁺ -dependent adhesion molecule
CaMKII	Calcium-calmodulin-dependent proteinkinase II
CAMs	Cell adhesion molecules
CAZ	Cytoplasmic matrix of the active zones
CME	Clathrin-mediated endocytosis
CNR	Cadherin-related neuronal receptors
CNS	Central nervous system
CSP α	cysteine string protein α
DIV	Days in vitro
DL-AP5	DL-2-Amino-5-phosphonopentanoic acid
DNA	Deoxyribonucleic acid
DNQX	6,7-dinitroquinoxalin-2,3-dion
DsRed2	Discosoma <i>sp.</i> red fluorescent protein2
ECD	Extracellular domain
EGFP	Enhanced green fluorescent protein
ES	Embryonic stem cells (ES)
FBS	Fetal bovine serum
FM1-43	<i>N</i> -(3-Triethylammoniumpropyl)-4-(4-(Dibutylamino) Styryl) Pyridinium Dibromide)

GABA	<i>gamma</i> -Aminobutyric acid
GFP	Green fluorescent protein
GTPase	Guanosine triphosphatase
HAV	Histamine, alanine and valine
HEPES	N-2-hydroxyethylpiperazin-N`-2-ethansulfonacid
HSC70	Heat shock cognate 70 kDa protein
Hz	Hertz
ICC	Immunocytochemistry
KD	Knockdown
KO	Knockout
LRRTMs	Leucin-rich repeat transmembrane neuronal proteins
LRRTM2	Leucin-rich repeat transmembrane neuronal protein 2
LTP	Long-term-potentialiation
Munc-18	Mammalian uncoordinated-18
Munc-13	Mammalian uncoordinated-13
NB-media	Neurobasal medium
Ncad ^{flox/flox}	Homozygous floxed N-cadherin mice
N-cadherin	Neural cadherin
Ncad Δ E	N-cadherin lacking extracellular domains
NLG1	Neuroigin1
NMDA	N-methyl D-aspartate
NMDAR	NMDA receptor
NMJ	Neuromuscular junction
NSF	N-ethylmaleimide-sensitive-factor
PBS	Phosphate buffered saline
PFA	Paraformaldehyde

PKC	Protein kinase C
PO	Poly-L-Ornithine
PSD	Postsynaptic density
PSD95	Postsynaptic density of 95 kDa
RIM	Rab3-interacting molecule
RIM-BP	RIM-binding proteins
ROI	Region of Interest
RRP	Readily releasable pool
RT	Room Temperature
SAP102	Synapse-associated protein of 102 kDa
SGT	Glutamate and threonine-rich protein
SIM	Structured illumination microscopy
SM	Sec1/Munc18-like
SNAPs	Soluble NSF-attachment proteins
SNAP-25	Synaptosomal-associated protein 25
SNARE	Soluble N-ethylmaleimide-sensitive-factor-attachment-protein-receptor complex
S-SCAM	Synaptic scaffolding molecule
SVs	Synaptic vesicles
SypHy	Synaptophysin-pHluorin
TMR-dextran	Tetramethylrhodamine-dextran
VAMP2	Vesicle-associated membrane protein 2
VDCC	Voltage-dependent calcium channel
VGLUT1	Vesicular glutamate transporter 1

6.2 List of figures

Figure 1.1	An illustration depicting an overview from brain to synapse	2
Figure 1.2	The presynaptic vesicle cycle	3
Figure 1.3	Different modes of synaptic vesicle endocytosis	7
Figure 1.4	Homophilic adhesion of classical cadherins	10
Figure 1.5	Model of Neuroligin1, LRRTM2 and Neurexin interactions at central synapses	16
Figure 2.1	Formation of glial microisland cultures	30
Figure 2.2	Synaptophysin-pHluorin (SypHy) as a tool to measure synaptic vesicle cycling	35
Figure 2.3	FM1-43 and dextran co-staining to label synaptic vesicle Endocytosis	38
Figure 3.1	Synaptophysin-pHluorin (SypHy) imaging as a measure of synaptic vesicle exo- and endocytosis in autaptic microisland cultures	45
Figure 3.2	Effect of Cre mediated conditional knockout of N-cadherin on synaptic vesicle exo- and endocytosis at room temperature (25°C)	48
Figure 3.3	Reduced Endocytosis in N-cadherin knockout neurons at near physiological temperature (34°C)	50
Figure 3.4	Effect of temperature on synaptic vesicle exo- and endocytosis	51
Figure 3.5	Effects of inhibiting the functions of N-cadherin by NcadΔE overexpression on vesicle exo- and endocytosis	53
Figure 3.6	Release dependent effects of N-cadherin knockout on synaptic vesicle exocytosis	56
Figure 3.7	Differential labeling of clathrin-mediated endocytosis and bulk endocytosis using FM1-43 and tetramethylrhodamine-dextran (TMR-dextran) uptake	59
Figure 3.8	Reduction in clathrin-mediated endocytosis in N-cadherin knockout neurons	62
Figure 3.9	N-cadherin regulates both clathrin-mediated endocytosis and bulk endocytosis	64
Figure 3.10	Effects of NcadΔE-mediated inhibition of N-cadherin functions on clathrin-mediated endocytosis	66
Figure 3.11	Effects of NcadΔE-mediated inhibition of N-cadherin functions on bulk endocytosis	68
Figure 3.12	The F-actin polymerizing drug, Jasplakinolide (Jaspla) reverses the endocytosis defect caused by conditional knockout of N-cadherin	72
Figure 3.13	Comparison of wide field imaging with structured illumination microscopy (SIM) imaging	75
Figure 3.14	Classification of synapses based on N-cadherin localization using SIM imaging	77
Figure 3.15	Recruitment of N-cadherin to synapses during neuronal differentiation as revealed by SIM imaging	80
Figure 3.16	Changes in the distribution of N-cadherin induced by high [K ⁺] stimulation	83
Figure 3.17	Recruitment of N-cadherin to synapses upon strong synaptic release (High [K ⁺] stimulation)	85

Figure 3.18	Overexpression of the synaptic adhesion molecules Neuroligin1 (NLG1) and LRRTM2, respectively in immature neurons (6 DIV)	88
Figure 3.19	Synaptogenic activities of NLG1 and LRRTM2 in immature cortical neurons (6-7DIV)	90
Figure 3.20	Overexpression of the synaptic adhesion molecules Neuroligin1 (NLG1) and LRRTM2, respectively in relatively mature neurons (12-13 DIV)	91
Figure 3.21	Synaptogenic activities of NLG1 and LRRTM2 in mature cortical neurons (12-13 DIV)	93
Figure 3.22	Differential dependence of synaptogenic properties of NLG1 and LRRTM2 on N-cadherin expression in immature neurons (9 DIV)	95
Figure 3.23	Differential dependence of synaptogenic properties of NLG1 and LRRTM2 on N-cadherin function in immature neurons (7 DIV)	97
Figure 3.24	LRRTM2 synaptogenic effect is independent of N-cadherin expression in mature neurons (14-15 DIV)	99
Figure 4.1	Model of N-cadherin involvement in synaptic vesicle cycling	110

6.3 Curriculum vitae

Name: Sushma Dagar
Date of birth: 12th December 1987
Place of birth: Sakatpur, Haryana, India
Marital status: unmarried

Education and Research Experience

2014-2019: PhD, Institute of Neuro- and Sensory Physiology, Heinrich Heine University, Duesseldorf Germany.
2011-2013: Research assistant, National Brain Research Centre, Manesar, India
2008-2010: Masters of Biotechnology, Maharshi Dayanand University, Rohtak, India
2005-2008: Bachelors of Science (Life Science), Maharshi Dayanand University, Rohtak, India

6.4 Publications and Conferences

6.4.1 Publications

- 1) **Dagar S** and Gottmann K. Differential properties of the synaptogenic activities of the neurexin ligands Neuroligin1 and LRRTM2. Manuscript in review.
- 2) Klapper SD, Garg P, **Dagar S**, Lenk K, Gottmann K, Nieweg K. Astrocyte lineage cells are essential for functional neuronal differentiation and synapse maturation in human iPSC-derived neural networks. *Glia*. 2019.
<https://www.ncbi.nlm.nih.gov/pubmed/31246351>
- 3) Van Stegen B, **Dagar S**, Gottmann K. Release activity-dependent control of vesicle endocytosis by the synaptic adhesion molecule N-Cadherin. *Sci Rep*. 2017.
<https://www.ncbi.nlm.nih.gov/pubmed/28106089>
- 4) Krishnamoorthy V, Cherukuri P, Poria D, Goel M, **Dagar S**, Dhingra NK. Retinal Remodeling: Concerns, Emerging Remedies and Future Prospects. *Front Cell Neurosci*. 2016.
<https://www.ncbi.nlm.nih.gov/pubmed/26924962>

- 5) **Dagar S**, Nagar S, Goel M, Cherukuri P, Dhingra NK. Loss of photoreceptors results in upregulation of synaptic proteins in bipolar cells and amacrine cells. PLoS One. 2014.
<https://www.ncbi.nlm.nih.gov/pubmed/24595229>

6.4.2 Conferences and workshops

1. Gordon Research Conference on Excitatory Synapses and Brain Function, June 09-14, 2019 Southern New Hampshire University, Manchester, NH United States.
 Poster: Role of the adhesion molecule N-cadherin in synaptic vesicle exo- and endocytosis.
2. Poster presented in 11th FENS conference of the Federation of European Neuroscience Societies, July 7-11, 2018 Berlin, Germany.
 Poster: Physiological role of the cell adhesion molecule N-cadherin in synaptic vesicle endocytosis.
3. Poster presented in Bonnbrain Meeting “Synapses & Circuits” organized by DZNE Center of Neuroscience, March 27-29, 2018, Bonn, Germany.
 Poster: Regulatory roles of the adhesion molecule N-cadherin in synaptic vesicle exo- and endocytosis.
4. Poster presented in 12th Goettingen meeting of the German Neuroscience Society, March 22-25, 2017 Goettingen, Germany.
 Poster: Regulation of activity-dependent compensatory endocytosis at central synapses by N-cadherin.
5. Poster presented in 10th FENS conference of the Federation of European Neuroscience Societies, July 2-6, 2016, hosted in Copenhagen, Denmark.
 Poster: N-cadherin controls activity-dependent compensatory endocytosis at central synapses.
6. Workshop on Imaging of the synaptic organization hosted by Leibniz Institute for Neuroscience, Magdeburg, Germany, September 26-30, 2016
7. International symposium on Synaptic basis of neuron network dysfunction in brain disorder in Goettingen June 13-14, 2015.

07-

Acknowledgment

7. Acknowledgment

During the journey of this Ph.D. dissertation, I met wonderful people and got opportunities to grow both personally and professionally. I would like to take this opportunity to thank all those people.

First and foremost, I owe my deepest gratitude towards my supervisor *Prof. Dr. Kurt Gottmann, Institut für Neuro- und Sinnesphysiologie*, Heinrich Heine University, Düsseldorf for providing me an opportunity to work in his laboratory. I would like to thank him for critically reviewing my research work at every step and his continued effort in the completion of the thesis. His enthusiasm and love for science have always inspired me to do good work. I have enjoyed all the long and lively discussion during our weekly meetings. He has helped me immensely whether it was interpreting confusing results, troubleshooting, or even sometimes just the basic neuroscience questions. I feel very lucky to have him as my supervisor and I am indebted to him for all the support and guidance. Thank you for always encouraging and supporting me to attend international conferences and scientific workshops. This thesis would not have been complete without his extraordinary guidance and valuable feedback.

I would also like to extend my sincere thanks to *Prof. Dr. Hermann Aberle, Funktionelle Zellmorphologie*, Heinrich Heine University, Düsseldorf for the co-supervision of my Ph.D. project. Thank you for critically evaluating my project during our scheduled meetings and for always encouraging me to try new things. He has always provided me with a new perspective.

I thank the *Center for Advanced Imaging (CAI), HHU*, Düsseldorf for providing the opportunity to use SIM imaging setup, I would like to thank all of my past and present lab members and department colleagues whose help and support made my working experience pleasant. I thank *Dr. Barbara Biermann* for her help with visual basics in Excel. Special thanks to *Sabine Ueberschär-Sahlmann* for providing the technical support and bearing up with my poor German. I would like to thank *Esin Ongun* for always helping me with all sorts of application forms. I am grateful to *iBrain* and *DFG* for financially supporting me throughout my Ph.D. I am highly obliged to *JUNO* for helping me with visa-related issues.

I owe a lot to all my friends who have patiently listened to all my scientific queries and crazy ideas. I am extremely thankful to *Pretty* and *Siva* for their friendship and helping me to adapt to the new living and working environment during my initial days in Düsseldorf. Thank you for making my life easier in Germany.

I would also like to extend special thanks to my friends *Arti, Neha, Parul, Priti, Reema*, and *Renu*. I will be forever grateful for their friendship, love, and support since college

days. I also thank my amazing friends at HHU *Afshin, Arun, Bala, Prashant, Priya, Rizwan, Ruchika, Sarva, and Senthil*, who made my stay memorable. I enjoyed the scientific and non-scientific discussions during our Friday lunch sessions. A huge thanks to *Bala* and *Senthil* for our cooking sessions together (mostly them :)). I would also like to thank *Seema* for saving me from cooking and I have enjoyed our trips throughout Europe. You always provided me the much-needed break. A special thanks to *Prateek, Kuldeep, Priti, and Renu* for their valuable comments on my thesis.

I would like to express my immense gratitude to *Prateek* for his constant support during the writing of the thesis whether it was coming up with the ideas for making explanatory figures or in formatting the text or even proofreading. Thank you for all the support and encouragement.

Words would not be enough but I am and will always be indebted to my entire family, especially my *Maa* and *Papa*. Without their love and unconditional support, I would have never been able to come this far in my life. I would like to especially thank my *Papa* who has always been my role model, for his endless patience and faith in me. Lastly, I would like to thank my nephews and nieces *Aditi, Kuku, Nishu, and Yashu* for constantly nagging me with the same question of when I am going to finish my thesis.

- Sushma Dagar

8. Eidesstattliche Erklärung

Ich versichere an Eides Statt, dass die vorliegende Dissertation von mir selbständig und ohne unzulässige fremde Hilfe unter Beachtung der „Grundsätze zur Sicherung guter wissenschaftlicher Praxis an der Heinrich-Heine-Universität Düsseldorf“ erstellt worden ist. Diese Dissertation wurde keiner anderen Fakultät vorgelegt und es gab bisher keine erfolglosen Promotionsversuche.

Düsseldorf, den 17. Oktober 2019,

Sushma Dagar

8. Declaration

I hereby declare that this thesis is an original work and has not been submitted in whole, or in part, for a degree at this or any other university. Nor does it contain, to the best of my knowledge and belief, any material published or written by any other person, except as acknowledged in the text. This thesis is in compliance with the 'Principles for Ensuring Good Scientific Practice at the Heinrich-Heine-University'. I have not made any unsuccessful promotions.

Düsseldorf

Sushma Dagar

17/10/2019